THE UNIVERSITY OF CALGARY

SOLID-LIQUID PHASE BEHAVIOR OF MIXTURES OF N-ALKANES

by

IRENA PAUNOVIC

A THESIS
SUBMITTED TO THE FACULTY OF GRADUATE STUDIES
IN PARTIAL FULFILLMENT OF THE REQUIREMENTS FOR
THE DEGREE OF MASTER OF SCIENCE
IN CHEMICAL ENGINEERING

DEPARTMENT OF CHEMICAL AND PETROLEUM ENGINEERING

CALGARY, ALBERTA

JUNE, 1999

ABSTRACT

The solid-solid and solid-liquid equilibrium in *n*-alkane systems is a phenomenon of great importance in many industrial fields both directly, as in the study of wax formation in fuels and oils, and indirectly, as a contribution to the understanding of more complex molecules such as polymers (polyethylene), fatty acids and other large molecules with long aliphatic chains.

In this study, the differential scanning calorimeter (DSC) technique was used to investigate the thermal behavior of pure odd- and even-numbered *n*-alkanes and their binary and ternary mixtures. The melting and cooling DSC thermograms of pure *n*-alkanes were measured at several scan rates to study the effect of superheating and supercooling.

The DSC data were used to predict the behavior of mixtures. All mixtures examined in this study have the same pattern, a large difference in chain length between individual components. The analysis of DSC results of binary and ternary mixture indicated that all mixtures examined in this study form eutectic systems. This observation led to the conclusion that large difference in chain length is a governing factor for the immiscibility, as opposed to other factors such as the similarity in crystal structure of pure components and the sample pretreatment.

The experimental results were compared with predictions from existing empirical and semi-theoretical eutectic equilibrium models. Results of prediction of melting

temperature obtained from ideal, regular solution theory and models of Won et al. (1986) and Pedersen et al. (1991) show the presence of non-idealities in all mixtures.

ACKNOWLEDGMENTS

I would like to express my gratitude to the large number of people who contributed to this work in number of different ways.

I wish to express my sincere appreciation and gratitude to my supervisor Professor Dr. A. K. Mehrotra for the opportunity to work on this project, his patience, trust, guidance and support.

I wish to thank to Professor R. A. Heidemann for his support and understanding.

The technical work provided by Bruce Miles, Jake Neudorf, and Claudine Curnow was greatly appreciated. Their dedication and help were precious.

I would like to thank my fellow graduate students for their support during the time at the University of Calgary.

In particular, I would like to thank my husband, Zoran, my daughter Una and son Stevan, my friends Sonja, Nina and Zeljko for encouragement, help, and support. My appreciation also goes to my family across Atlantic, especially to my parents and my sister, for their love and care.

TABLE OF CONTENTS

LIST OF TABLES

LIST OF FIGURES

NOMENCLATURE

A	component A
B	component B
C	component C
ΔC_P	difference in heat capacity between liquid and solid phase
$d_{L,25}^{j}$	liquid-phase density of component j at 25 °C
G	Gibbs free energy
ΔH_m	heat of mixing
$(\Delta H_f^0)_j$	molal heat of fusion of component j
ΔH_{tot}	total transitional enthalpies
ΔH^{∞}	total transitional enthalpies for polyethylene
ΔH_V^j	molar enthalpy of vaporization of pure liquid j
l	molecular chain length
M_w^j	molecular weight of component j
n	carbon number
n_{max}	maximum chain length
n_{min}	minimum chain length
P_S^j	vapor pressure of solid phase for component j
P_L^j	vapor pressure of liquid phase for component j
R	universal gas constant
ΔS_{tot}	total change in entropy

ΔS^{∞}	total change in entropy for polyethylene
s_j	solid phase mole fraction of component j
T	temperature
T_E	eutectic temperature
T_m^0	equilibrium melting temperature for pure component
T_m^{∞}	equilibrium melting temperature for polyethylene
$(T_m^0)_L$	equilibrium liquidus temperature for isomorphous mixture
$(T_m^0)_S$	equilibrium solidus temperature for isomorphous mixture
$(T_m^E)_j$	liquidus temperature of component j in eutectic mixture
$(T_m^E)^*_j$	non-ideal liquidus temperature of component j in eutectic mixture
T_j^{ideal}	ideal liquidus temperature of component j in eutectic mixture (Equation 2.19)
V^j_L	molar volumes of component j in the liquid phase
V^j_S	molar volumes of component j in the solid phase
x_E	eutectic composition
x_j	liquid phase mole fraction of component j

Greek Symbols

α	parameter in Equation 2.50
α-peak	the high temperature peak
β-peak	the low temperature peak
γ_L^j	activity coefficient of component j for liquid phase

γ_S^j	activity coefficient of component *j* for solid phase
δ_L^j	solubility parameter of component *j* for liquid phase
δ_S^j	solubility parameter of component *j* for solid phase
ϕ	melting temperature function in equation 2.50
ϕ_L^j	fugacity of component *j* for liquid phase
ϕ_S^j	fugacity of component *j* for solid phase
φ^j	volume fraction of component *j*
λ	scan rate
Θ	binary parameter in Equation 2.48
ρ_o	empirical interaction parameters
Ω	binary parameter in Equation 2.46
ω_j	mole fraction of component *j*

Superscripts

0	denotes standard state
E	denotes excess properties
Sat	denotes saturation

CHAPTER 1

INTRODUCTION

The appearance of a solid paraffin phase, wax, in hydrocarbon fluids exposed to lower temperatures is a common phenomenon occurring in a diversity of situations from petroleum reservoirs to automobiles in cold mornings. When the temperature falls, heavy hydrocarbon components in the liquid and vapour may precipitate as wax crystals. In the petroleum industry, wax precipitation is undesirable because it may cause plugging of pipelines, reservoirs, and fuel filters and other process equipment. Accumulation of these solid deposits represents a major risk of deterioration of this kind of equipment. This problem has been recognized for many years, and studies have been done to investigate the causes and ways of preventing it. In order to control wax deposition in crude oils, which is linked to changing pressure and temperature conditions and fluid composition, it is essential to be able to predict the phase behavior of reservoir fluids by means of thermodynamic models.

Solid deposits range from almost pure paraffin wax to those that are almost totally asphalt in nature. Most deposits fall between these extremes, and contain paraffin waxes, microcrystalline waxes, asphalt material, resins, oil and silt. Paraffin waxes are a mixture of normal alkanes and constitute about 40 to 60 % of average crude oil deposits. The understanding of this behavior and the ability to model it are fundamental in dealing with the nuisance and problems that the precipitation of waxy phases produce with process equipment.

Paraffin waxes are essentially mixtures of long-chain alkanes with carbon number between 18 and 65 (Srivastava, 1993). Normal paraffins are by far the major components of wax and, therefore, the most important in determining the crystallization behavior of waxy mixtures. In order to successfully formulate the mathematical description of wax melting and solidification, it is important to know exactly how these mixtures melt in relation to the pure components. Binary mixtures of *n*-alkanes serve as important model systems for understanding not only wax solidification, but also as a model for the investigation of the effect of chain-length non-homogeneities on the properties of complex chain-molecules such as polymers and lipid bilayers.

1.1 Scope of the Study

This study follows the previous investigations by Hammami (1994) and Bhat (1996) at the University of Calgary on the thermal behavior and non-isothermal crystallization kinetics of some pure *n*-alkanes, selected binary and ternary mixtures using differential scanning calorimetry. The purpose of the present study is to provide additional phase equilibrium data and improved modeling capabilities on prepared multicomponent mixtures of *n*-alkanes.

Hammami (1994) developed a model for the non-isothermal crystallization of *n*-alkanes, and used this model to predict the behavior of multicomponent systems of paraffins. Bhat (1996) used Hammami's results to extend the mathematical description of phase behavior of multicomponent mixtures. The same differential scanning calorimetry technique is used in this study to investigate the thermal behavior of three *n*-alkanes, with large

differences in the chain length. Thus this study provides an improved understanding of the thermal behavior of pure *n*-alkanes and their multicomponent mixtures.

The main objectives of this work are:

To extend the data presented by Hammami (1994) for pure *n*-alkanes for liquid-solid-solid phase behavior at various scan rates;

To comprehend the thermal behavior of the binary and ternary mixtures forming immiscible systems;

To compare the experimental results with predictions from existing empirical and semi empirical thermodynamic models;

To compile important conclusions from Hammami (1994), Bhat (1996) and the present study related to the thermal behavior of pure *n*-alkanes and their binary and ternary mixtures.

Chapter 2 of this thesis presents a literature review and the background knowledge on *n*-alkanes, their physical and thermodynamic characteristics, and the thermodynamic theories for the multicomponent systems of *n*-alkanes. The theoretical background and applicability of differential scanning calorimetry in studies of thermal behavior of *n*-alkanes and their mixtures are also presented. This chapter also includes a brief summary of the previous studies by Hammami (1994) and Bhat (1996).

Chapter 3 describes the experimental part of the study. This section describes the materials, sample preparations, and instrumentation. The basic principle of differential scanning calorimetry as the analytical tool is also reviewed.

Chapter 4 presents the experimental results obtained for three pure *n*-alkanes and their binary mixtures. The results for pure *n*-alkanes are analyzed for determining the effects of

supercooling and superheating. For all binary mixtures, comparisons are made between the experimental equilibrium results and the values predicted by existing thermodynamic models.

Chapter 5 presents the thermal behavior of the different concentration of the ternary mixture. The discussion of the differences between the experimental equilibrium results and the values predicted by existing thermodynamic models is also presented in this chapter.

Chapter 6 summarizes the results from the present study. The important characteristics of thermal behavior of *n*-alkanes and their multicomponent systems are highlighted.

Chapter 7 presents the important conclusions of this study along with the suggested recommendations for future studies in this area.

CHAPTER 2

LITERATURE REVIEW

Chemists have recognized the varied and complex composition of crude oils for many years. Regardless of this complexity numerous attempts have been made to classify petroleum.

From the viewpoint of the petroleum refiner of crude oil, it is of two general classes or types: those petroleum which carry practically no asphalt and which yield solid hydrocarbons of paraffin series and are termed "paraffin base"; and those which yield practically no solid paraffins, but are rich in asphalt, the "asphalt base". A drawback in this classification system resides in the fact that crude oils vary from asphaltic to the light crude oils and that between these two extremes is a virtually continuous range of characteristics. Even a very "simple" crude oil has all categories of hydrocarbons (n-paraffins, cycloalkanes, isoparaffins, indans, aromatics, napthalenes, biphenyls), nitrogen, sulfur, oxygen compounds (Smith,1968).

In the present study the nature and occurrence of paraffin deposit will be emphasized. The paraffin deposit problems occur in almost every oil-producing area. The problems range from year-around depositions in formation, down-hole equipment, surface lines, separators and storage tanks to seasonal problems which occur only in the winter months. Compositions of paraffin deposit vary between two extremes; pure paraffin waxes and asphaltic materials.

Paraffin waxes constitute about 40 to 60 % of an average crude paraffin deposit. They can be described as long-chain compounds with 21 to 50 carbon atoms. Microcrystalline waxes account for less than 10 % of the crude paraffin deposits. They are long chain hydrocarbons with branched-chain and cyclic-ring molecules. Asphaltic materials are sticky, dark semi-solid amorphous substances. The amount present in crude oil deposits has been reported to range from 10 to 50 %. The asphaltenes are made up of condensed aromatic rings with few side chains (Bucaram, 1967).

The precipitation of paraffin waxes from crude oil is a commonly observed phenomenon in the production of petroleum products. If the wax content of the crude oil is low to moderate (0-10%), these problems are periodically handled on "as needed" basis. When wax contents is above 10%, these crudes experience severe deposition and flow problems necessitating constant treatment to ensure continued production.

A variety of mechanical ("pigging"), thermal ("heat tracing") and chemical ("pour point depressants") treatments have evolved over the years to alleviate the problems associated with wax depositions and pumping problems including heating-cooling cycles, water emulsions and crystal modification chemicals. Solid deposition mechanisms must be more generally recognized and understood to make better economic decisions concerning the modern approach to petroleum reservoir development, production system design for primary production, and enhanced recovery (Matlach, 1983).

Paraffin deposition is an example of fluid-solid phase equilibrium, which is a result of changes in the "solvent capacity" of lighter ends to dissolve heavy "solute" molecules resulting from temperature changes in wellbore, pressure and temperature changes in the

equipment and pipelines, and supercritical solvent phenomenon in the reservoir (Norman, 1989).

Different experimental techniques and different principles have been used to study the crystallization behavior of paraffin waxes. Thermal behavior, kinetics of crystallization, rheological properties, structural characteristics have been investigated using differential scanning calorimetry (DSC), infrared spectroscopy, X-ray diffraction, dilatometry, electron crystallography, thermomicroscopy, nuclear magnetic resonance (NMR) and gas chromatography (Gimzewski et al., 1993; Maroncelli et al., 1982; Ungar et al., 1985; Asbach et al., 1991; Denicolo et al., 1984; Nyburg et al., 1992; Challa et al., 1968; Dorset et al., 1990; Letoffe et al., 1995; Pedrersen et al., 1991; Zhao et al., 1996).

A new, microscopic procedure was suggested by Srivastava et al. (1997). The measurement of wax solubility, wax appearance (also known as the wax appearance point and/or cloud point) and gel formation temperatures of *n*-alkanes and petroleum waxes in organic solvents can be measured in a single experiment.

Coutinho (1997) developed a new experimental technique for measuring the composition of the phase equilibrium and amount of paraffins precipitating from a hydrocarbon mixture. The new technique measures the equilibrium data below the cloud point temperature (wax appearance temperature). The results foster the understanding of hydrocarbon solid phase formation from solution. They provide strong evidence for the formation of multiple solid phases in alkane crystals.

2.1 Normal Alkanes

Normal alkanes are among the most fundamental of molecular series. A homologous series is a family of compounds with molecular formulas that are obtained by repeatedly inserting a given group (most commonly $-CH_2-$) into a parent structure. The normal alkanes are a homologous series of aliphatic hydrocarbons that are derived from C_2H_6 by inserting $-CH_2-$ groups and having a molecular formula C_nH_{2n+2} (hereafter denoted by C_n). The alkanes were once called the paraffins from the Latin words for "little affinity" because they are not very reactive.

These simple molecular chains are important constituents of many molecules in organic, biological and polymer systems. The normal alkanes or normal paraffins are widely distributed in nature, in waxy coatings associated with leaves, fruits, and nuts of many different plants; in coating and secretions of various forms of animal life. In addition, the normal alkanes themselves are important components of petroleum, shale oils, tars and coals, and thus play important role in many products such as fuels and lubricants.

The simple structure and the complex phase behavior of these compounds make them a desirable medium for investigation. In addition, knowledge of alkane physical properties and thermodynamic functions have brought a better understanding of the behaviour of wax formation in fuels and oils directly, and indirectly, as a contribution to the understanding of more complex molecules such as polymers (polyethylene), fatty acids and other large molecules with long aliphatic chains.

The repetitive nature of chemical constitution of the alkane series permits treatment of their physical properties as dependent not only on pressure and temperature but also on

their carbon number. Some physical properties, such as liquid density and boiling points, change fairly regularly as the molecular weight increases; others involving the solid state, such as melting point, show a variation among the lower members of series according to whether the number of carbon atoms in the molecule is odd or even. The number of carbon atoms is an important factor in determining their complex phase behavior (Turner, 1971).

2.1.1 Carbon Chain Structure

In *n*-alkanes, since each carbon atom (except at the two ends) is bonded to two others and to two hydrogen atoms, the arrangement giving the minimum energy is the one in which the chain takes the form of zigzag of carbon atoms (Kitaigorskii, 1965). The carbon-carbon bond angle is about 112°, and the intermolecular carbon-carbon distance is 15.3 nm. Carbon-carbon bond lengths and bond angles are maintained by strong forces. On the other hand, rotation can occur readily about single bonds, opposed by weak forces only, since neither a change of bond length nor angles is involved (Daniel, 1953). As a result of rotation about single bonds, the carbon-hydrogen units of chain can assume a variety of positions differing in energy. One conformation, however, represents minimal potential energy and results from the competing forces arising from the tendency of bond angles to assume ideal values and of the nonbonded atoms to be situated at an equilibrium distance. In the case of normal alkanes, the arrangement giving minimum energy is one in which the chain takes the form of flat zigzag of carbon atoms (Woodward and Sauer, 1965). When a normal alkane molecule is said to have a "straight" chain, the reference is

actually being made to zigzag arrangement of carbon atoms in the position of least energy, the form in which the molecule is usually in solid state and at temperatures just above the melting point.

2.2 Crystal Structures of n-Alkanes

The crystalline structures of *n*-alkanes have been investigated by a number of workers, and there is some disagreement on many aspects of crystallinity. The crystalline phase of alkanes is characterised by a compact stacking of chain molecules, which is normal to the stacking planes in odd-numbered and tilted in even-numbered paraffins. In the lowest-temperature phase, the carbon skeleton of the alkane molecule is planar zigzag (all trans); this arrangement corresponds to the minimal potential energy (Daniel, 1953; Woodward and Sauer, 1965).

Pure alkanes are known to crystallize in at least four distinct forms: hexagonal, orthorhombic, monoclinic and triclinic. These four solid forms are sufficient to characterize the structures of all *n*-alkanes above C_9 containing odd number of carbon atoms in the molecules, and the structure of all *n*-alkanes above C_4.

The odd *n*-alkanes with carbon atoms of 9 up to 21 have a primitive orthorhombic structure at low temperature. With increasing temperature, up to 15 °C of their melting point, this structure transforms, before melting occurs, into a face-centered orthorhombic one, the so-called rotator form (Espeau et al., 1996). This form has a large degree of rotational freedom; the molecules are supposed to oscillate around their longitudinal axis, an effect that increases with temperature (Stolk et al.,1998; Sirota, 1993).

Crystallographic analyses show that the rotator phase can be roughly described as a layered structure formed by hexagonal packing of aliphatic chains rotating as rigid rods around their long axis. Studies have presented a somewhat more complex behavior but the idea of the hexagonal packed rods by Ungar (1983) remains accurate enough.

The even paraffins from C_6 through C_{18} are triclinic at all temperatures up to the melting point. The rotator form for this group is metastable. In mixing with other alkanes, however, it can become stable, which can be seen as the stabilization of an orientations disorder by a compositions one (a mixture of molecules with different chain lengths) (Stolk et al., 1998; Espeau et al., 1996).

The orthorhombic structure is the stable structure for all even alkanes from C_{22} to C_{40}. The hexagonal form is stable just below the freezing point in even paraffins from C_{22} to C_{44}. Even-numbered paraffins above C_{24} are preferentially in the monoclinic configuration at ambient temperatures. The orthorhombic phase is stable for odd paraffins above C_{40} (Broadhurst, 1962b; Srivastava et al., 1993; Turner, 1971).

2.2.1 Phase Transition

There has been considerable interest in the study of crystallization habits of *n*-alkanes and other long chain hydrocarbons. Polymorphism has been found to be common in such compounds, and crystalline transitions frequently occur in the solid phase. Alkanes with carbon number between 18 and 40 are polymorphic; hence, they assume more than one crystalline form stable at different temperatures and with different crystal habits. Normal hydrocarbons with chain lengths between 21 and 40 carbon atoms are known to exhibit a

transition from an orthorhombic to a hexagonal crystal structure upon heating, while hydrocarbons with chain lengths outside this range crystallize directly into orthorhombic structure and a transition is not seen. The high temperature solid phase, known as the rotator phase due to the capacity of the chain molecules to rotate around their axis, has hexagonal crystalline structure and exists within a few degrees below the freezing point. Upon further cooling, the molecules rearrange themselves in more orderly, stable, crystalline structures, developing a low temperature solid phase, orthorhombic. The transition points of hydrocarbons with even number of carbon atoms are much closer to the melting points than those with an odd number (Schaerer, 1955).

The phase transition can be detected by several methods; nearly all are based on observation of a sudden change in physical properties of the solid. The transitions are accompanied by a change in refractive index, in specific gravity, and in the absorption in infrared region. A large heat of transition is necessary to convert the orthorhombic modification, which is stable at lower temperatures, into the hexagonal modification, which is stable at higher temperatures up to the melting point. Thermal methods such as differential thermal analysis (DTA) and differential scanning calorimetry (DSC) are capable of detecting the existence of new phase in polymorphic alkanes. However, the corresponding phase transitions emerge as very small peaks in the DSC traces, and are usually visible only in high-sensitive recordings (Ungar, 1983). Investigations of the rotator phase have established the existence of several new phases (Denicolo, 1984).

2.2.2 Equilibrium Melting Temperature

Equilibrium melting temperature, T_m^0, is an important macroscopic quantity used to characterise a given crystal of flexible, linear molecules. There have been numerous reported sets of pure paraffin melting temperatures (Dorset, 1990; Etessam and Sawyer, 1939; Garner et al., 1931; Gray, 1943; Maroncelli et al., 1982; Mazee, 1948; Royaud et al., 1990; Schaere et al., 1955, 1956; Seyer et al., 1944. Snyder et al., 1981). Recently, Hammami, (1994) reported melting temperatures of ten pure paraffins from C_{23} to C_{50}.

The discrepancies between the reported values arise primarily from superheating effects, which depend on the experimental technique and the heating rate used to measure the melting point. Superheating occurs when heat is supplied to a crystal faster than it can melt so that the inner portions of the crystals get heated above T_m^0 before actually melting (Prime and Wunderlich, 1969). Prime and Wunderlich (1969) also pointed out that in order to maintain the sample at equilibrium during a melting experiment, it is necessary to proceed practically at zero heating rate.

Many relationships, $T_m=T_m(n)$, between the melting temperatures, T_m, of paraffins and the corresponding numbers, n, of carbon atoms in the molecule (or equivalently the molecular length or weight) have been proposed. For most of those equations there exists an asymptotic value, T_m^∞, defined as:

$$T_m^\infty = \lim_{n\to\infty} T_m(n) \qquad 2\text{-}1$$

T_m^{∞} is constant which represents the equilibrium melting point of polyethylene; the melting point of a large, infinite molecular weight crystal of -CH_2- chains.

Broadhurst (1962a) proposed an empirical equation to calculate T_m^0 as a function of the number of carbon atoms , n, in the paraffin molecule. His equation is of the form:

$$T_m^0 = T_m^{\infty} \cdot \left(\frac{n-1.5}{n+5} \right) \qquad 2\text{-}2$$

where T_m^{∞}, equals 414.3 K.

It is important to note that Equation 2-2 was derived from melting points of fourteen paraffins from C_{44} to C_{100}. They have orthorhombic crystal structure up to the melting point; it has the underlying assumption that the heat and entropy of fusion change linearly with the number of carbon atoms.

Flory and Vrij (1963) modified Equation 2-2 so as to include extrapolated melting points of alkanes that have a low-temperature orthorhombic crystal structure, but undergo a solid-solid transition before final melting. By adding a logarithmic term to account for the disordering of the methyl layers during melting, Wunderlich (1980) presented a more flexible melting equation, which he attributed to Flory and Vrij (1963):

$$T_m^0 = T_m^{\infty} \cdot \left(\frac{n-3.478}{n+\ln(n)-0.452} \right) \qquad 2\text{-}3$$

From Equation 2-3, T_m^{∞} is predicted to be 419.6 K.

Alternatively, Pechhold et al. (1966) suggested that $1/T_m^0$ varies linearly with $1/n$. They found that most of the reported literature data on the melting temperatures of alkanes follow the simple relation:

$$\frac{1}{T_m^0} = \frac{1}{T_m^\infty} \cdot \left(1 + \frac{6.86}{n}\right) \qquad 2\text{-}4$$

As such, T_m^∞ is found to be 414.6 K, which compares well with the value predicted by Broadhurst (1962a).

There are several important aspects to the problem of calculating a value for T_m^0, which must be considered:

1. The validity of the equation must be established not only over the range of chain lengths covered by experimental data but also up to the limit of infinite chain length;
2. The *n*-alkane melting points used in fitting the function and correctly evaluating the constants therein must themselves be accurate temperatures of equilibrium between the liquid and crystal phases;
3. These liquid and crystal phases must be the ones that persist up to the very long chain limit. That is, the extrapolated melting points of one phase would obviously not predict the melting points of some different phase (Broadhurst, 1962).

2.2.3 Enthalpy and Entropy Changes

Garner et al. (1926) reported that, beyond the first few members of the homologous series, the heats and entropies of fusion increase linearly with molecular weight for a given group of alkanes (i.e. odd- or even-numbered). Schaerer et al. (1954), however, found that the increase in the heats of fusion of pure paraffins from C_{17} to C_{36} is linear regardless of n being odd or even. However, their measured values of the heats of transition and, in turn, the total enthalpy change ΔH_{tot} (i.e. the sum of heat of fusion and heats of transition) between crystal and melt show a clear odd/even effect within the same range of n.

Dollhopf et al. (1981) noticed that when the experimental data of ΔH_{tot} are plotted versus $1/n$, straight lines are generated which can be described as:

for even n:

$$\Delta H_{tot} = \Delta H^{\infty}\left(1-\frac{3}{n}\right) \qquad 2\text{-}5$$

For odd n:

$$\Delta H_{tot} = \Delta H^{\infty}\left(1-\frac{4.4}{n}\right) \qquad 2\text{-}6$$

where ΔH^{∞} is the melting enthalpy of polyethylene, extrapolated from the linear plots of the experimental data for odd- and even-numbered paraffins, and it is 4.12 kJ/mol CH_2 (or 984 cal/mol CH_2).

A combination of Equations 2-4 with 2-5 and 2-6 was used to formulate the dependence of ΔS_{tot} on the chain-length using the thermodynamic relation:

$$\Delta S_{tot} = \frac{\Delta H_{tot}}{T_m^{\infty}} \qquad 2\text{-}7$$

which for even n becomes:

$$\Delta S_{tot} = \Delta S^{\infty} \cdot \left(1 + \frac{3.8}{n} + \frac{20.6}{n^2}\right) \qquad 2\text{-}8$$

and for odd n:

$$\Delta S_{tot} = \Delta S^{\infty} \cdot \left(1 + \frac{2.5}{n} + \frac{30.2}{n^2}\right) \qquad 2\text{-}9$$

From these equation Dollhopf et al. (1981) predicted ΔS^{∞} to be 9.94 J/K mol CH_2 for polyethylene.

2.3 Systems of Alkanes

A number of studies have been devoted to binary mixtures of alkanes due to their importance in understanding the physical behaviour of various polydisperse linear chain molecules such as lipid bilayers and polymers (Maroncelli et al., 1985). In solid state solubility often is not continuous throughout the entire range of compositions and temperatures.

When two members of the same homologous series of compounds are blended together, they may form systems representative of two extreme cases in which they show either complete solubility (solid solution) or nearly complete insolubility. In addition, these members may form many systems having behaviours intermediate of these extremes, where complete mutual solubility may occur only over certain ranges of temperature and composition. Hence, the miscibility behaviour of paraffin mixtures is of importance, i.e., whether they form a simple eutectic system, a solid solution or possibly both.

Kitaigorodskii (1961) has compiled, from the extensive literature published by Mnyukh (1960), the rules and conditions favouring the formation of stable solid solutions. He has concluded from numerous calorimetric and diffraction studies that the cosolubility of alkanes in the solid state is sensitive to:

1) the relative molecular volumes of the two components making up the binary mixture

2) their respective crystal structure symmetries

Matheson and Smith (1985) proposed an empirical rule, which defines the boundary conditions for continuous solid solutions in alkanes, when conformational influences are

least important. The boundary conditions for continuous solid solution have been stated empirically to be:

$$n_{max} = 1.244\, n_{min} - 0.411 \qquad 2\text{-}10$$

where n_{max} and n_{min} denote the maximum and minimum chain lengths in such binary mixtures.

Using the Gibbs free energy analysis, Bhat (1996) developed a new relationship for miscibility limits:

$$n_{max} = 1.16\, n_{min} + 2.07 \qquad 2\text{-}11$$

Dorset (1985, 1986, 1987) used an electron diffraction technique to investigate microphase separation in binary solid solutions as well as the role of symmetry in the formation of paraffin mixed crystals. The main findings of his studies were:

Fractionation occurs at room temperature in melt crystallised samples of C_{30}+C_{36} on a time scale of days.

There exists no continuity of space group symmetry, but only a continuum of methylene subcell symmetry and type of layer packing for the chain axes (i.e. rectangular or oblique).

These limitations in the tendency to form solid solutions give rise to complex phase behaviour among binary mixtures of certain members of the homologous series.

Hammami (1994) studied the thermal behaviour of some selected binary mixtures using differential scanning calorimetry (DSC).

Recently, Dirand et al. (1996) published results of a study, which presents the more complex behaviour of binary mixtures forming solid solution. In spite of what is generally found in the literature (Mazee, 1960; Turner, 1971; Denicolo et al., 1984; Marconelli et al., 1985; Dorset, 1990), two consecutive even-even or odd-odd *n*-alkanes do not form a continuous homogeneous solid solution. This study shows the existence of terminal solid solutions, which have the pure *n*-alkane structure and many intermediate solid solutions. These intermediate phases have an orthorhombic cell as the odd-numbered *n*-alkanes, but they are not isostructural with pure *n*-alkanes or with their terminal solid solutions.

Dirand et al. (1996) assumed that same behavior occurs in other binary systems of consecutive *n*-alkanes. In all cases, below the rotator phases temperature, these binary systems do not form a continuous solid solution and it is probably not possible with the binary mixtures of *n*-alkanes whose carbon number difference is greater than two. The existence of the intermediate solid solution accounts for the anomalies in these binary systems, and can be associated with a particularly remarkable phenomenon, detected by Goghoumu et al. (1990), that addition of one long *n*-alkane to a shorter one increases the solubility of the latter in organic solvents.

Chevallier et al. (1998) studied structural behavior of eight commercial and industrial waxes and a heavy crude oil by X-ray diffraction. According to the experiment results, each multicomponent paraffin wax (from 20 to 33 *n*-alkanes), which has a continuous distribution of consecutive *n*-alkanes ($19 < n < 53$), forms a single orthorhombic solid

solution. The structure of this multi *n*-alkane phase of 23 and 33 *n*-alkanes is identical to the one of the two orthorhombic intermediate solid solutions, which has been observed in binary and ternary mixtures of consecutive alkanes.

The molecule packing identity period along the long c-axis of this solid solution corresponds to a chain length of a hypothetical orthorhombic *n*-alkane, whose carbon number is equal to the average carbon number of *n*-alkanes contained in each multicomponent paraffin wax.

In the orthorhombic structure of the 'low temperature' multi- *n*-alkane solid solution, the chains, whose carbon atom numbers are higher than that of this hypothetical C_n, must bend to insert themselves between the molecule layer stacking crystallographic planes. For these bent molecules it is difficult to undergo the orientational oscillations around their long axis as described in the pure C_{23}. Only the small molecules, which are rigid, may freely turn around their long axis. That is the reason why the expected rotator state is not seen in these mixtures. This multicomponent phase was observed in the deposit of the heavy crude oil with the presence of an amorphous solid (Chevallier et al., 1998).

2.3.1 Application of Mixtures of Alkanes as an Energy Storage

Owing to their considerable heats of melting and the large temperature range of their melting point, the *n*-alkanes and their mixture are excellent substances for the storage of energy and for thermal protection. The *n*-alkanes with 11 to 50 carbon atoms have melting points from -25°C to +92°C, which is in the range where many applications are found.

In practice, for storage and protection purposes, mixtures of *n*-alkanes are used rather than the pure substances themselves, especially if their "thermal windows" (temperature difference between liquidus and solidus at a certain composition) are narrow. First of all, mixtures offer the opportunity to tune in on the desired temperature level. For example, by combining *n*-pentadecane and *n*-hexadecane, mixtures with thermal windows less than 2°C can be designed that range from about 10°C to about 16°C. Secondly, the use of mixtures is favored because they are less expensive than their pure components (Stolk et al, 1997).

Espeau et al. (1996) showed that molecular alloys of alkanes could provide suitable materials to work as MAPCMs (Molecular Alloys Phase Change Materials) in the field of energy storage and/or thermal protection, if two conditions are respected. The first is to choose the right composition(s) in the right alkane system(s) to obtain the melting of the alloy at the required level of temperature. The second one is to choose alloys having a narrow thermal window. Reliability tests have been performed on different kinds of binary mixtures of *n*-alkanes.

C_{15}-C_{21} system was chosen for investigating the eutectic systems as a MAPCMs. A material having a thermal window significantly higher than the norms was intentionally chosen. Thermal behavior of that mixture was investigated far from the eutectic point. Depending on the selected standard procedure there were significant differences between the results of the two cases. In the first case, the final state was the liquid state. In the second case, the melting was not complete; this situation may be encountered in some applications due to the high value of the thermal window.

2.3.2 Typical Isobaric Phase Diagrams

Mazee (1957) and Turner (1971) have discussed the isobaric phase diagrams of various alkane mixtures; some of these are presented schematically in Figure 2.1. The first type of binary system exhibits no solution in the solid state, so there are three phases involved: liquid, the solids of pure A and pure B. A temperature versus composition diagram of this type is illustrated in Figure 2.1a. The binary system exhibits a single liquid phase and two completely immiscible components in the solid state. These three phases (i.e. the isotropic liquid, pure solid A and pure solid B) will be in equilibrium at a point, the eutectic, of fixed temperature T_E and fixed composition x_E. This system is known as the eutectic mixture.

The expected behaviour for binary mixtures of *n*-alkanes selected in this study is eutectic, according to the empirical formula found by Matheson and Smith (1985), Equation 2.10. From a practical point of view, eutectic appears whenever the difference in chain length exceeds a critical limit beyond which the formation of solid solution does not occur to appreciable extent.

In general, studies on binary eutectic mixtures of alkanes have indicated that the eutectic melts within one degree of the pure hydrocarbon of shorter chain length; the eutectic mixtures usually contain 90-95% of the shorter paraffin (Mazee, 1949, 1957; Butler and MacLeod, 1961).

The next binary mixture is the isomorphous (solid solution) type. This binary system of *n*-alkanes is one in which the two components of the mixture exhibit complete miscibility in both liquid and solid phases. For this to be likely, the two pure components would be

Figure. 2.1 Some possible *T*-*x* diagrams of binary systems of alkanes (Mazee, 1957)

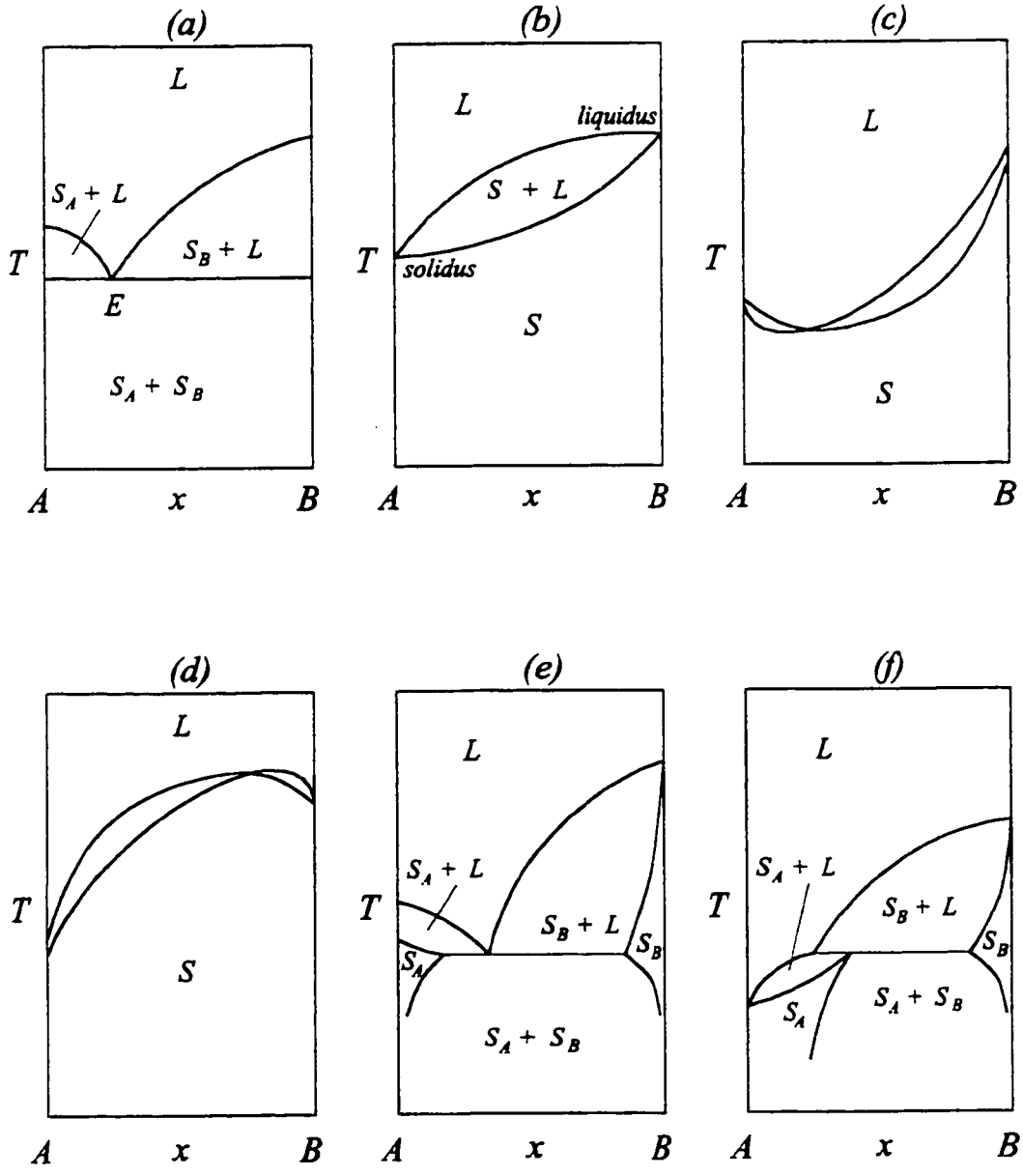

expected to be similar in chain length and crystalline structure, so as to be able to adopt identical crystal structure in solid state. The requirement follows from the fact that as the composition of the mixture varies, molecules of component B have to substitute directly for the molecules of component A in the solid, as the composition varies from mole fraction of B from 0 to 1. This is only likely if the structures adopted by A and B in the solid are identical. This system is depicted in Figures 2.1b through 2.1d. The "azeotropic" solid-liquid systems in Figures 2.1c and 2.1d exhibit a minimum and a maximum, respectively, a fact pointing to a less ideal behavior of the components. In Figures 2.1e and 2.1f, the temperature-composition diagram is given for complete miscibility in the liquid state but only partially miscibility in the solid phase.

2.3.3 Ternary Mixture

When three components are present, mixtures can exhibit a wealth of phase behaviors including equilibrium among solid, gas and multiple liquid phases. Some phase behaviors as well as methods of presentation will be briefly described.

2.3.3.1 Triangular Diagram

The phase behavior of ternary mixture is conventionally presented on an equilateral triangular diagram, such as in Figure 2.2. Any position on the diagram represents a ternary mixture of a particular composition. The compositions are usually given in mole fractions, but weight fractions can also be used.

Figure 2.2 Standard equilateral triangle for representing ternary mixture at constant temperature and pressure

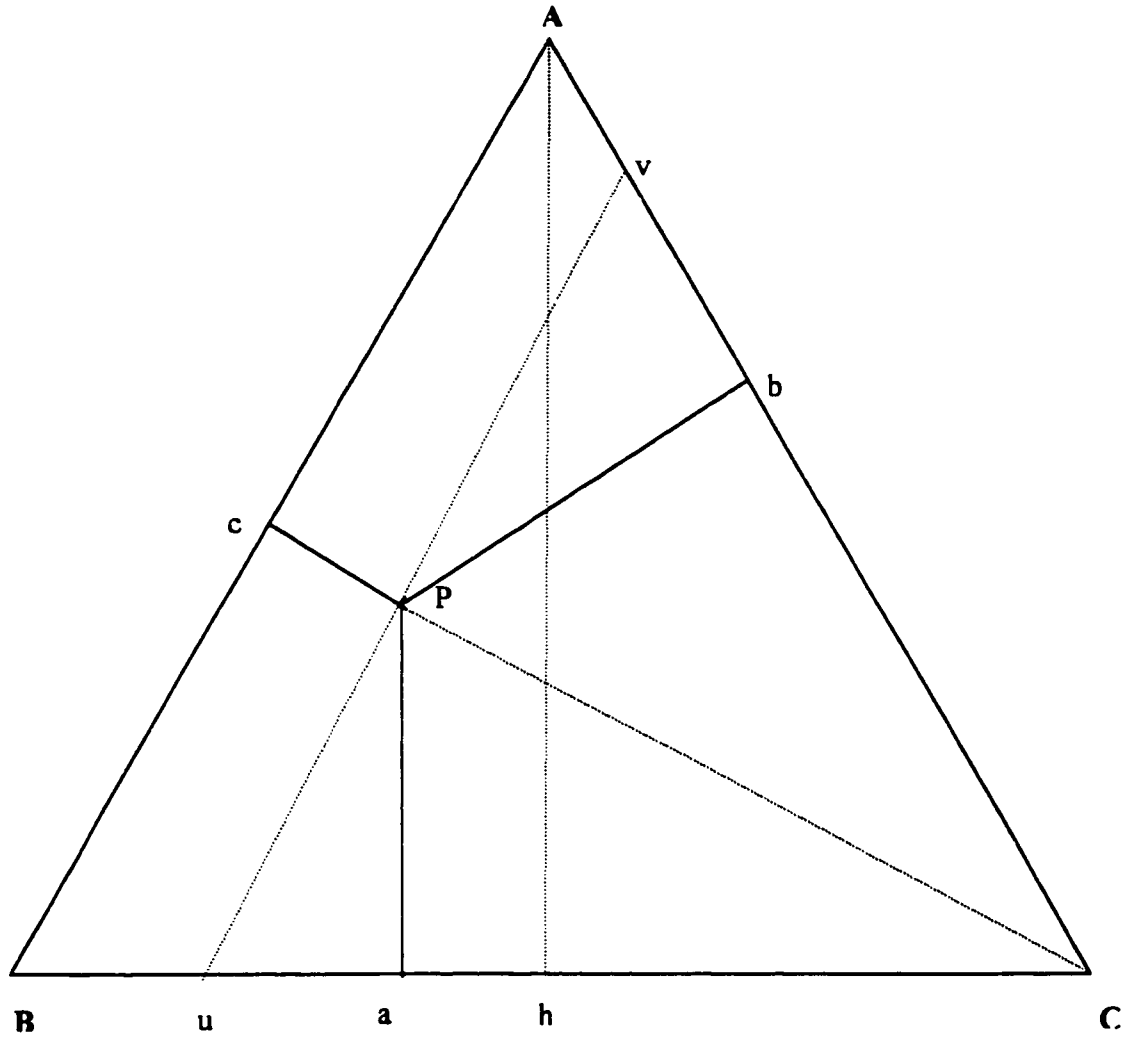

On a triangular diagram, the vertices represents pure components; as shown in Figure 2.2 pure A, B and C .Then each of the triangle represents the binary mixture formed by two of the three components; for example edge AC represents all mixtures of components A and C. A particular point on an edge divides the edge into two segments and is simply related to the composition of the binary represented by the point. Any point of the interior of the triangle, such as point P in the Figure 2.2, represents a ternary mixture. Since the mole fractions must always sum to unity, the composition is determined by giving values for any two independent mole fractions.

The symmetry of equilateral triangles imposes invariant on certain lines that represent particular classes of mixtures. One set is composed of lines that are parallel to an edge. Every mixture on that line has the same fraction in the component represented by the opposite vertex. The line *uv* in Figure 2.2 is parallel to edge AB and every mixture on *uv* has the same value for the C component mole fraction: $x_c=cP/hA$. A second set of invariant lines on which every point has the two perpendiculars to adjacent edges in the same ratio, and therefore every mixture on the line has the same relative amounts in those components. The line PC in the figure 2.2 passes through vertex C and mixture on PC has the same ratio of mole fractions for components A and B: $x_A/x_B=aP/bP$.

In general the diagram shown in Figure 2.2 applies to mixtures of different components, but in some cases it may apply to one mixture at different conditions of temperature and pressure or both. Such changes in the diagram of one ternary mixture can be explained by changes in the miscibility of its component binaries.

2.3.4 Effects of Non-Equilibrium Solidification

In order to experimentally construct equilibrium phase diagrams such as those discussed previously, it is necessary that the change in temperature take place very slowly, because a relatively long time is required at each decrement of temperature for the compositions of the two phases to readjust. This readjustment requires not only the diffusion of A and B in both phases, but also the exchange of molecules across the liquid-solid interface. Since molecular diffusion proceeds slowly, especially in the solid state, true equilibrium is difficult to maintain during cooling (Askeland, 1984). The effects of rapid cooling (non-equilibrium solidification) on typical isomorphous phase diagram is discussed below with reference to Figure 2.3, which is based on the work of Lee (1977).

When a binary melt of composition x^* is cooled, it will start to solidify at the temperature T_1 corresponding to the liquid and solid compositions L_1 and x_1. By T_2 the liquid composition will have shifted to L_2, so the formed crystal is relatively enriched in higher melting component. However, if the cooling rate is too fast, then the formed solid will not have enough time to change its composition from x_1 to equilibrium x_2, and thus solid will have some intermediate, average composition represented by x_2'. As the temperature continues to drop to T_3, the average solid composition x_3' departs more and more from its corresponding equilibrium value x_3. Eventually the last drop of liquid would not disappear at the equilibrium temperature T_5, but instead at a lower temperature T_n where the average solid composition reaches the bulk composition x^*. The actual shape and location of the non-equilibrium line and the final non-equilibrium solidus temperature

Figure 2.3 The effect of fast cooling on the phase diagram (Lee, 1977)

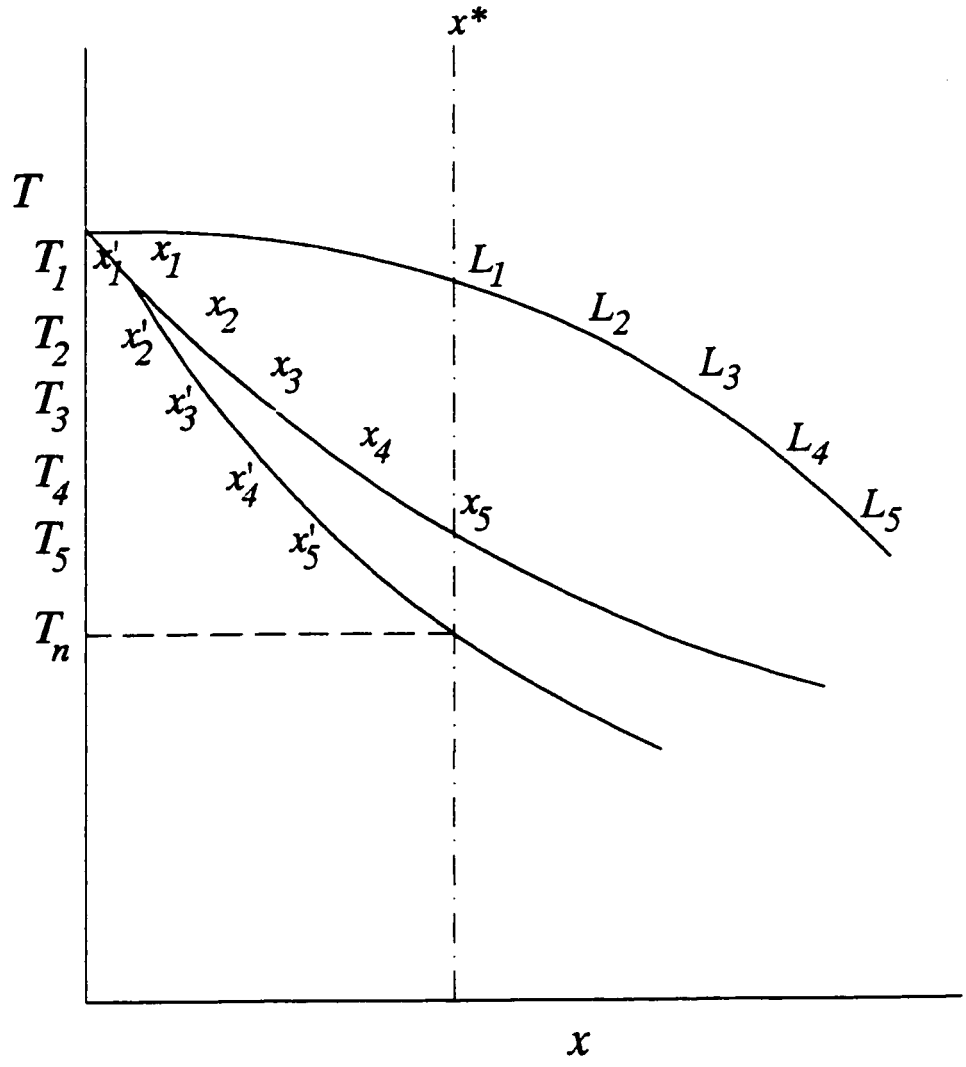

depend on the rate of change of temperature; faster cooling rates cause greater departures from equilibrium (Lee, 1977).

When a liquid is cooled, it may not start to crystallize at the freezing point, but at a lower temperature, at which first crystals spontaneously appear. It has been established that, at the same rate of temperature change, the amount of superheating during melting is considerably less severe than the amount of supercooling during the crystallization.

Supercooling occurs when the heat is withdrawn from the crystal faster than it can solidify. Consequently, melting points are usually accepted as being a much better measure of the equilibrium solid-liquid temperature. Ideally, the onset of crystallization will occur at exactly the same temperature as the termination of melting process if the cooling/heating rates are sufficiently slow. However, even at the scan rate of 0.01°C/min the disparity is found to be significant (Gimzewski and Audley, 1993).

2.4 Differential Scanning Calorimetry, DSC

Thermal analysis is the measurement of changes in physical properties of a substance as a function of temperature while the substance is subjected to a controlled temperature program (Wunderlich, 1992). Thermal systems capable of providing quantitative data using dynamic calorimetric techniques are often classified as differential scanning calorimeters in order to differentiate these devices from those that provide only qualitative data (David, 1970). Giavarani and Pchetti (1973) noted that DSC is relatively quicker than most conventional experimental techniques and, foremost, it needs very small quantities of the test sample. The applications of DSC are varied, e.g. estimation of

purity, measurement of transition temperatures and identification of materials.

A sample and the reference are both maintained at the temperature pre-determined by the program even during a thermal event in the sample. The amount of energy that has to be supplied to or withdrawn from the sample to maintain zero temperature differential between the sample and the reference is an experimental parameter which displayed as the ordinate of the thermal analysis curve.

The sample and the reference are placed in identical environments, metal pans on individual bases thermally isolated from each other. Each base contains a thermocouple and a heater. The thermal mass of the holders is minimized so that the response of the resistance thermometers is rapid. The temperatures of the two thermocouples are compared, and the electrical power supplied to each heater adjusted so the temperatures of both the sample and the reference remain equal to the programmed temperature. In this way any temperature difference which would result from thermal event in the sample is neutralized.

A DSC curve is a plot of differential power against temperature or time. The ordinate signal is proportional to the specific heat of sample since the specific heat at any temperature determines the amount of thermal energy necessary to change the sample temperature by given amount. Any transition accompanied by a change in specific heat produces a discontinuity in power signal, and exothermic or endothermic enthalpy changes give peaks whose areas are proportional to the total enthalpy change.

The obvious advantage of thermal analysis over the traditional melting point methods is that the entire melting or crystallization curve is observed. The interesting feature of the

plots is that the melting and cooling curves can be extrapolated to nearly the same temperature at zero heating or cooling rates.

However, the main problem in applying DSC is the choice of the cooling rate. If too low, the test takes a long time; if too high, there is considerable supercooling. Obviously there must be a compromise, but there is a little information on what it should be and what errors are likely (Gimzewski and Audley, 1993). It was confirmed experimentally by Onoe et al. (1997) that both melt temperature and cooling speed affect thermal properties, such as transition points. Results of this study give useful information about the criteria of operational conditions for DSC.

2.4.1 Applications of DSC to the Study of Binary Systems

Srivastava et al. (1993) reviewed the various analytical methods applied to the study of phase transitions in pure alkanes, their binary mixtures and paraffin waxes. Among these, the DSC has been recognised as an invaluable tool for analysing and characterising petroleum products. In the petroleum field, DSC is a useful technique both for research and for product analysis. Despite the fact that thermodynamic equilibrium is not usually established, DSC provides much valuable information about phase transitions of samples and enables a relatively accurate quantification of their related energies and thermodynamic parameters (Wesolowski, 1981). Hammami (1994) used the DSC technique to evaluate the melting and the crystallization behaviour of ten pure odd- and even-numbered *n*-alkanes at various cooling and heating rates and under quiescent

conditions. He also studied the melting and solidification characteristics of binary, and ternary mixtures of *n*-alkanes and multicomponent waxy mixtures.

DSC can be used to study the melting processes, as well as such associated properties as melting points, heat and entropy of fusion, and degree of crystallinity. Because DSC analysis can detect the transition temperatures of individual components in a mixture, the effect of a diluent on the melting behaviour of a crystalline sample can be conveniently studied.

2.4.1.1 Application of DSC on Binary Solid Solution System

Maroncelli et al. (1985) studied the phase behaviour of polymorphic odd-numbered paraffins, C_{19} and C_{21} by using DSC technique. The DSC thermogram for that mixture exhibits two major transitions and three distinct phases for such a mixture. They have linked the unusually small melting ranges of 0.5-0.8 K, observed in the cases of the pure C_{19} and C_{21}, to instrumental effects, which are believed to contribute up to ±1 K uncertainty in temperature. Phillips et al. (1970) suggested that transition regions be defined as the difference between the onset temperature on heating and cooling at the same scan rate. Nevertheless, their method is found to give a melting range less than 1 K for pure lecithin, which is of the same order as that obtained using the convention of Maroncelli et al. (1985).

2.4.1.2 Application of DSC to Binary Eutectic System

Smith and Pennings (1974, 1976, 1977) explored the possibility of constructing binary eutectic phase diagrams using a DSC. Most thermogram for polymer-diluent mixtures, except those for the pure components and for a polymer volume fraction of 0.8, exhibit two peaks; the position of the low temperature peak (i.e. around 115°C) is independent of the overall polymer composition. These important observations led Smith and Pennings (1974) to believe that the invariant low temperature and the 0.8 volume fraction as the eutectic temperature and composition, respectively. They also noted that the eutectic composition is insensitive to kinetic factors within the tested range of cooling rates. This finding seems to point to a favourable liquid structure in the eutectic mixture (Smith and Pennings, 1976).

Dorset et al. (1989) have adopted the convention of Smith and Pennings (1974) to construct binary phase diagrams of paraffin-diluent eutectic from both heating and cooling experiments. They found that the cooling curve for the binary melt resembles the phase diagram constructed from heating scans, except for the observed more or less consistent supercooling of the melt prior to crystallization and the shift of the eutectic point toward the diluent-rich side.

Coutinho (1998) presented a new experimental technique, using DSC measurements to establish solid-liquid equilibrium phase diagrams of binary systems of organic compounds with complete immiscibility in solid phase. The technique measures the changes on the relative size of the liquid phase during the fusion of a mixture, which is later converted into phase diagrams using the lever rule. The technique is much faster and

cheaper, but it has limited applicability and lower accuracy than other methods currently used.

2.5 Hammami's Study

Since the present study is an extension of the work by Hammami (1994), it is worthwhile to summarise briefly the work carried out by Hammami (1994) and Hammami and Mehrotra (1992, 1993, 1994, 1995a, 1995b). Hammami (1994) used the DSC technique to study the melting and the crystallization behaviour of high-purity even-numbered and odd-numbered alkanes (Hammami and Mehrotra, 1992, 1993) at various cooling and heating rates.

2.5.1 Non-isothermal Crystallization Kinetics

Hammami (1994) investigated the thermal behaviour of ten pure *n*-alkanes, at various cooling and heating rates, viz.

a) Even numbered *n*-alkanes: C_{28}, C_{30}, C_{34}, C_{44}, and C_{50}

b) Odd numbered *n*-alkanes: C_{23}, C_{25}, C_{33}, C_{37}, and C_{41}

Hammami also developed a model for the non-isothermal crystallization of *n*-alkanes. The model was derived based on the fundamental equation of Ozawa for non-isothermal crystallization, the surface nucleation theory, and the growth rate theory for extended chain crystals. The DSC data were treated in terms of Ozawa theory, utilising for the first time a semi-empirical formulation for the so-called Ozawa cooling crystallization function. The model is found to be equally efficient and reliable in simulating the

experimental data for both, even and odd-numbered *n*-alkanes at low supercooling. The crystallization exotherms and the model parameters for odd and even *n*-paraffins were compared.

Hammami (1994) noted that even- and odd-numbered *n*-paraffins might not necessarily show the same crystallization behaviour under non-isothermal conditions. This is because the difference is detectable by DSC only when a paraffin, odd-or even-numbered, crystallises in either the monoclinic or triclinic form or when a solid-solid transition is involved. However, the proposed non-isothermal model described the crystallization behaviour of *n*-paraffins at cooling rates of up to 10°C/min.

2.5.2 Multicomponent Systems

Hammami (1994) also studied the thermal behaviour of mixtures of *n*-alkanes and proposed a non-isothermal model, based on the model developed for pure *n*-alkanes, to predict the kinetic behaviour of mixtures. In the case of C_{28}+C_{25} system, both the melting and crystalliazation thermograms exhibit two major peaks, corresponding to the liquid-solid and solid-solid transitions. Hence, he classified that mixture as isomorphous. Hammami used Pedersen et al.'s (1991) modified Regular Solution Theory successfully to model the thermodynamic behaviour of the isomorphous system. The mixture of C_{44}+C_{50} was found to form either isomorphous or eutectic systems dependent on the thermal history of the prepared mixture. Once formed, however, eutectic or isomorphous system was found to be stable over long periods of time. Hammami and Mehrotra (1995a, 1995b) have published the results for these systems.

Bhat (1996) used Hammami's experimental results for binary mixtures to develop a better model to predict the phase behaviour of multicomponent mixtures. He extended Hammami's mathematical description of liquid-solid phase transformation kinetics derived for pure components to the case of binary mixtures. An improved approach to Hammami's model for non-isothermal crystallization was presented, which gives better comparison with the experimental data.

2.6 Crystallization Theories for Binary Systems

A number of studies in the literature deal with the thermodynamic and kinetic behaviour to simulate the equilibrium crystallization behaviour of binary systems. A brief summary is presented below.

2.6.1 Thermodynamic Approach

Various workers (Asbach et al., 1982: Butler and MacLeod, 1961; Holder and Winkler, 1965; Lee, 1977; Mazee, 1949) have developed the mathematical descriptions of solidification and/or melting for different binary systems using a thermodynamic approach.

2.6.2 The Ideal Isomorphous System

The equilibrium between a liquid phase L and solid phase S is described by the isofugacity criterion:

$$\phi_S^j = \phi_L^j \qquad 2\text{-}12$$

where ϕ^j denotes the fugacity of pure component j. In terms of the solid and liquid vapour pressures of j, Raoult's law gives:

$$s_j P_S^j = x_j P_L^j \qquad 2\text{-}13$$

where s_j and x_j are the mole fractions of j in the solid and liquid phases, respectively. For a pure substance, the vapour pressures of solid and liquid phases have one and the same value, which can be expressed using the Clausius-Clapeyron equation:

$$\frac{d\ln\left(P_S^j / P_L^j\right)}{dT} = \frac{\left(\Delta H_f^0\right)_j}{RT^2} \qquad 2\text{-}14$$

where R is the universal gas constant, and $(\Delta H_f^0)_j$ is the molal heat of fusion of component j evaluated at the melting point. Equation 2-14 may be readily integrated if $(\Delta H_f^0)_j$ is assumed constant to yield:

$$\ln\left(\frac{P_S^j}{P_L^j}\right) = \ln\left(\frac{x_j}{s_j}\right) = \frac{\left(\Delta H_f^0\right)_j}{R}\left[\frac{1}{\left(T_m^0\right)_j} - \frac{1}{\left(T_m^0\right)_L}\right] \qquad 2\text{-}15$$

where $(T_m^0)_L$ is the temperature at which the last traces of mixed crystals just become liquid, also called the liquidus temperature. Rearranging Equation 2-15 becomes:

$$s_j = x_j \exp\left\{-\frac{\left(\Delta H_f^0\right)_j}{R}\left[\frac{1}{\left(T_m^0\right)_j} - \frac{1}{\left(T_m^0\right)_L}\right]\right\} \qquad 2\text{-}16$$

The mole fractions s_j are restricted by the following condition:

$$\sum_{j=1}^{2} x_j \exp\left\{-\frac{\left(\Delta H_f^0\right)_j}{R}\left[\frac{1}{\left(T_m^0\right)_j} - \frac{1}{\left(T_m^0\right)_L}\right]\right\} = 1 \qquad 2\text{-}17$$

Setting the liquid composition equal to the bulk mole fractions, the liquidus temperature can be determined iteratively by varying the solid mole fractions and vice versa (Butler and MacLeod, 1961).

A similar procedure can be adopted to evaluate the solidus temperature $(T_m^0)_S$, at which the last traces of liquid freeze, and can also be calculated using the following constraint where the solidus mole fractions are now set equal to the bulk composition, and either the liquidus temperature or mole fractions are varied iteratively until Equation 2-18 is satisfied.

$$\sum_{j=1}^{2} s_j \exp\left\{-\frac{\left(\Delta H_f^0\right)_j}{R}\left[\frac{1}{\left(T_m^0\right)_S}-\frac{1}{\left(T_m^0\right)_j}\right]\right\}=1 \qquad 2\text{-}18$$

2.6.3 The Ideal Eutectic System

Hsu and Johnson (1974) derived the freezing point depression of the liquid solution of two compounds assuming an ideal eutectic mixture in the solid state, i.e. assuming no heat of mixing and no change in volume. Thus, the equation describing ideal eutectic behaviour for binary mixtures is:

$$\ln x_j = -\frac{\left(\Delta H_f^0\right)}{R}\left[\frac{1}{\left(T_m^E\right)_j}-\frac{1}{\left(T_m^0\right)_j}\right] \qquad 2\text{-}19$$

where $(T_m^E)_j$ is the liquidus temperature of component j in the eutectic mixture, and the other terms are as previously defined. Simultaneous solution of the two freezing point depression equations with $x_j = x_E$ and $(T_m^E)_j = T_E$ permits the calculation of eutectic temperature, T_E, and the eutectic composition, x_E, for the simple eutectic binary system.

Lee (1977) noted that non-ideal behaviour, particularly in the solid state, is the rule rather than the exception for most organic solutions. In the specific case of alkane mixtures, the molecules are sufficiently alike in size and shape to be interchangeable in a lattice, but the configurational energy is not quite independent of mutual disposition of two or more chain molecules (Guggenheim, 1952). The non-ideality of this type of mixture can be

formulated using the concept of regular solution or alternatively in terms of the lattice model, such as the Flory-Huggins theory.

2.6.4 Regular Solutions

When mixtures deviate from the ideal behaviour, mainly due to the non-zero heat of mixing, the non-ideal behaviour can be accounted for by using the relation $\Delta H_m = \rho_o x_1 x_2$, here ρ_o is an empirical interaction parameter. For the case of eutectic binary systems, Lee (1978) derived the following expression:

$$\frac{\rho_0 (1-x_j)^2}{\left(\Delta H_f^0\right)_j} = \frac{\left(T_m^E\right)_j^*}{T_j^{ideal}} - 1 \qquad 2\text{-}20$$

where $(T_m^E)^*_j$ is the non-ideal liquidus temperature of component j in the eutectic binary system; T_j^{ideal} is the ideal liquidus temperature predicted from Equations 2-19.

2.7 Crystalliazation Theories of Multicomponent Mixtures

In order to successfully formulate the mathematical description of wax melting and/or solidification, it is important to know exactly how these paraffin solid solutions melt in relation to the pure component.

The melting temperature of mixed crystals can be calculated from the rule of Küster (Küster, 1890),

$$\left(T_m^0\right)_L = \sum_j \omega_j \left(T_m^0\right)_j \qquad 2\text{-}21$$

where ω_j is the mole fraction of component j. Empirical model of Küster usually overpredicts the melting temperatures of mixture. Out of nineteen of paraffin solid solutions examined in the literature (Mazee, 1957, 1960; Nechitailo et al., 1960; Piper et al., 1931; Smith, 1932), thirteen melt lower (up to 4°C) and only one melts higher (about 0.5°C), a fact pointing to the non-ideal behaviour of these waxy mixtures.

Despite the evidence cited, a few authors (Butler and MacLeod, 1961; Dorset, 1990; Holder and Winkler, 1965) have used the ideal solution theories as defined in Equations 2-17 and 2-19 to predict the melting behaviour of isomorphous mixtures and eutectic systems of alkanes, respectively. Computational methods based on regular solution theory of mixtures as well on equation on state have been proposed to model wax precipitation (Won, 1986, 1989; Hansen et al., 1988; Pedersen et al., 1991; Pedersen, 1993; Erickson et al., 1993). All of these methods assume that all compounds that precipitate from liquid or vapor form solid solution. However, recent spectroscopic and calorimetric studies by Snyder et al. (1992, 1993, 1994) and Pedersen et al. (1991) suggest that large hydrocarbons are mutually insoluble in the solid state.

Won (1985, 1986, 1989) has used regular solution theory to describe the non-idealities in the oil (liquid) and wax (solid) phases. The basis of his model is the isofugacity criterion at thermodynamic equilibrium between the two phases:

$$\phi_S^j = \phi_L^j \qquad 2\text{-}22$$

Fugacity for liquid phase is defined by:

$$\phi_L^j = x_j \gamma_L^j \left(\phi_L^j\right)^0 \exp\left(\int_0^P \frac{V_L^j dP}{RT}\right) \qquad 2\text{-}23$$

For solid phase, the fugacity is similarly defined by:

$$\phi_S^j = s_j \gamma_S^j \left(\phi_S^j\right)^0 \exp\left(\int_0^P \frac{V_S^j dP}{RT}\right) \qquad 2\text{-}24$$

where most of the terms are as defined earlier; the superscript "*0*" denotes the standard state.

The standard state fugacity for the liquid phase $(\phi_L^j)^0$ is related to the pressure:

$$\left(\phi_L^j\right)^0 = \left(\phi_L^j\right)^{Sat} \exp\left[\int_{\left(P_L^j\right)^{Sat}}^0 \frac{V_L^j}{RT} dP\right] \qquad 2\text{-}25$$

Similary, for solid phase:

$$\left(\phi_S^j\right)^0 = \left(\phi_S^j\right)^{Sat} \exp\left[\int_{\left(P_S^j\right)^{Sat}}^0 \frac{V_S^j}{RT} dP\right] \qquad 2\text{-}26$$

Substitution of Equations 2-24 to 2-26 into Equation 2-22 yields,

$$\gamma_S^j \cdot s_j \cdot (\phi_S^j)^0 = \gamma_L^j \cdot x_j \cdot (\phi_L^j)^0 \exp\left[\int_0^P \frac{V_L^j - V_S^j}{RT} dP\right] \quad 2\text{-}27$$

The relation between standard state fugacity of component *j* in the solid phase, and in the liquid phase, can be derived by calculating the Gibbs energy change of pure component *j* from solid to liquid:

$$\ln\left(\frac{(\phi_L^j)^0}{(\phi_S^j)^0}\right) = \frac{(\Delta H_f^0)_j}{R(T_m^0)_L} \cdot \left(1 - \frac{(T_m^0)_L}{(T_m^0)_j}\right) + \frac{\Delta C_P}{R}\left(1 - \frac{(T_m^0)_j}{(T_m^0)_L} + \ln\frac{(T_m^0)_j}{(T_m^0)_L}\right) \quad 2\text{-}28$$

The solid-liquid equation is then derived:

$$\frac{s_j}{x_j} = \frac{\gamma_L^j}{\gamma_S^j} \exp\left[\frac{(\Delta H_f^0)_j}{R(T_m^0)_L} \cdot \left(1 - \frac{(T_m^0)_L}{(T_m^0)_j}\right) + \frac{\Delta C_P}{R}\left(1 - \frac{(T_m^0)_j}{(T_m^0)_L} + \ln\frac{(T_m^0)_j}{(T_m^0)_L}\right) + \int_0^P \frac{V_L^j - V_S^j}{RT} dP\right] \quad 2\text{-}29$$

The first term on the right side of Equation 2-29 represents the ratio of liquid activity coefficient to that in the solid, which are mixture properties depending mainly on the compositions and also on temperature. The exponential term contains only pure properties, and it depends on temperature and pressure.

Assuming that the liquid and solid-phase molar volumes are independent of pressure, and at low to moderate pressures, this order of magnitude will have a minor effect on the

liquid-solid equilibrium so the pressure term is approximated by unity, and can be dropped out of equation 2-29 (Pedersen et al., 1991).

In the models of Won (1985, 1986) and Hansen et al. (1988), it is assumed that the contributions that arise from the heat capacities between liquid and solid phase are nearly equal. Consequently Equation 2-29 becomes:

$$\frac{s_j}{x_j} = \frac{\gamma_L^j}{\gamma_S^j} \exp\left[\frac{\left(\Delta H_f^0\right)_j}{R}\left(\frac{1}{\left(T_m^0\right)_L} - \frac{1}{\left(T_m^0\right)_j}\right)\right] \qquad 2\text{-}30$$

Equation 2-30 maintains the same general form of Equation 2-16 for ideal solution, but has an additional pre-exponential factor, namely the activity coefficient ratio, to account for the non-ideal behaviour.

In Won's work, the activity coefficient ratios are estimated by regular solution theory:

$$\ln \gamma_L^j = \frac{V_L^j\left(\overline{\delta_L} - \delta_L^j\right)^2}{RT} \qquad \ln \gamma_S^j = \frac{V_S^j\left(\overline{\delta_S} - \delta_S^j\right)^2}{RT} \qquad 2\text{-}31$$

$$\overline{\delta_L} = \sum_j \varphi_L^j \cdot \delta_L^j \qquad \overline{\delta_S} = \sum_j \varphi_S^j \cdot \delta_S^j \qquad 2\text{-}32$$

$$\varphi_L^j = \frac{x_j V_L^j}{\sum_j x_j V_L^j} \qquad \varphi_S^j = \frac{s_j V_S^j}{\sum_j s_j V_S^j} \qquad 2\text{-}33$$

The solubility parameter of component j in liquid solution is defined and given in many standard textbooks (e.g., Reid et al., 1977):

$$\delta_L^j = \left(\frac{\Delta H_V^j - RT}{V_L^j} \right)_j^{1/2} \qquad 2\text{-}34$$

where ΔH_V^j is the molar enthalpy of vaporisation of pure liquid j at temperature T. On the other hand, the solubility parameter of component j in solid solution is evaluated, based on a modified cohesive energy, using the relation (Won, 1986):

$$\delta_S^j = \left(\frac{\Delta H_V^j - \left(\Delta H_f^0\right)_j - RT}{V_S^j} \right)_{j,s}^{1/2} \qquad 2\text{-}35$$

Won (1986) determined the required properties at 25°C. He used the following expression for the liquid and solid molar volumes in cm^3/mol:

$$V^j = V_L^j = V_S^j = \frac{M_w^j}{d_{L,25}^j} \qquad 2\text{-}36$$

where M_w^j is the molar mass of component j, $d_{L,25}^j$ is the liquid-phase density (in g/cm^3) of component j at 25°C, for which the following relation was used:

$$d_{L,25}^j = 0.8155 + 0.6272 \cdot 10^{-4} M_W^j - \frac{13.06}{M_W^j} \qquad 2\text{-}37$$

After combining Equations 2-30 and 2-31 and rearranging, Won (1986) arrived at the following simplified form of the equation for non-ideal equilibrium melting of paraffin mixed crystals

$$\frac{s_j}{x_j} = \exp\left[\frac{\left(\Delta H_f^0\right)_j}{R\left(T_m^0\right)_L}\cdot\left(1-\frac{\left(T_m^0\right)_L}{\left(T_m^0\right)_j}\right)+\frac{V^j}{RT}\left[\left(\overline{\delta_L}-\delta_L^j\right)^2-\left(\overline{\delta_S}-\delta_S^j\right)^2\right]\right] \qquad 2\text{-}38$$

where the molar enthalpy of melting, $(\Delta H_f^0)_j$ in cal/mol, is estimated using the following correlation:

$$\left(\Delta H_f^0\right)_j = 0.1426 M_W^j \left(T_m^0\right)_j \qquad 2\text{-}39$$

And the equilibrium melting temperature (in K) of pure component j is predicted from:

$$\left(T_m^0\right)_j = 374.5 + 0.02617 M_W^j - \frac{20172}{M_W^j} \qquad 2\text{-}40$$

Won (1986) pointed out that the values of $(\Delta H_f^0)_j$ are approximately equal to the sum of heat of fusion and one half of heats of transitions for paraffins heavier than C_{22}.

In 1989, Won used his method to calculate the solubility of C_{28} and C_{36} solids in C_5 and C_{12} at atmospheric pressure. He modified his earlier model by:

1) Incorporating an extended regular solution expression for activity coefficients in liquid phases

2) Assuming a pure solid phase for heavier hydrocarbon component

3) Including the heat capacity effect on the fugacity ratio.

Hansen et al. (1988) observed that Won's model (1986) was not satisfactory for calculation of the cloud-point temperature of 17 oil mixtures. These authors proposed to use the polymer solution theory of Flory (1953) for describing non-idealities in the liquid state. Three adjustable parameters in the proposed model were estimated from the measured cloud-point data.

Extensive data on cloud-point temperature and amount of wax deposition became available in 1991. Pedersen et al. (1991) evaluated the performance of Won's (1986) and Hansen et al. (1988) models with data. These models significantly overestimated the amount of wax deposition and cloud-point temperature. To obtain an improved representation, Pedersen et al. (1991) proposed to modify Won's model by:

1) Using solubility parameters δ_S^j and δ_L^j with one adjustable parameter for each of the solid and liquid phases

2) Incorporating the paraffinic/naphthenic/aromatic split for each pseudocomponent of C_{7+} fraction

3) Modifying the melting enthalpies by one adjustable parameter

4) Incorporating the effect of heat capacity difference with two adjustable parameters.

To account for the expected higher non-ideality of solutions, Pedersen et al. (1991) have suggested the following empirical correlations for calculating the liquid- and solid-phase solubility parameters [in $(cal/cm^3)^{1/2}$]:

$$\delta_L^j = 7.41 + a_1 \ln\left(\frac{n}{7}\right) \qquad 2\text{-}41$$

$$\delta_S^j = 8.50 + a_2 \ln\left(\frac{n}{7}\right) \qquad 2\text{-}42$$

The following values for a_1 and a_2 were reported by Pedersen et al. (1991):

$a_1 = 0.5914$ (cal / cm^3)$^{1/2}$

$a_2 = 5.763$ (cal / cm^3)$^{1/2}$

Both models yield fairly similar results for liquid-phase solubility; they clearly produce different values of solid-phase solubility parameters, especially for the higher hydrocarbons.

While Pedersen's model provided an improvement representation of wax precipitation over previous procedures because it took into account highly non-ideality of solution, it requires abundant experimental data for determining various model parameters.

2.8 Chain Delta Lattice Parameter Model

Coutinho et al. (1996) developed a model that can describe the non-ideality of the high temperature solid phase of alkanes. The Chain Delta Lattice Parameter model (CDLP) is developed allowing a successful description of the solid-liquid equilibrium of *n*-alkanes ranging from C_{20} to C_{40}.

A true thermodynamica equilibrium exists between the two solid phases. The thermodynamic modeling of solid-liquid equilibrium is based on Equation 2-29, assuming that the liquid-and solid-phase molar volumes are independent of pressure.

The challenge in the description of solid-liquid equilibrium lies in the capacity to describe the non-ideality of the phases. Coutinho et al. (1996) found the Flory-free volume to be a good model for the description of a liquid mixture of saturated hydrocarbons in equilibrium with a solid phase.

Molecules of *n*-alkanes differ only in the chain length; therefore the interaction energy for the different pairs should only be dependent on their differences in size. A method to equate the variation of interaction energy with molecular size is used in the Delta Lattice Parameter model. This model first presented for inorganic compounds like alloys and semiconductors relates the interaction energy with the crystal lattice parameters. A similar procedure, but applied to long chain molecules, was followed.

Coutinho et al. (1996) assumed zero excess volume and entropy. Since the temperatures and heats of melting of *n*-alkanes are asymptotic functions of the chain length, an assumption is made that the heat of melting can be related with the molecular size *l* by an equation with the form:

$$H_m = \frac{k \cdot l}{l + b} \qquad 2\text{-}43$$

The excess enthalpy of the solid phase is related to the heats of melting by:

$$H^E = x_l \cdot H^0_{ms} \cdot l_l + x_s \cdot H^0_{ms} \cdot l_s - H^{mix}_m \cdot l^{mix} \qquad 2\text{-}44$$

where l_l and l_s are lengths of the long and short alkane molecules in the rotator phase, respectively, calculated using the following correlation by Broadhurst (1962):

$$l_i = 1.27 \cdot n + 1.98 \qquad 2\text{-}45$$

The cell length parameter for the mixture is presumed to follow Vegrard's law:

$$l^{mix} = x_l \cdot l_l + x_s \cdot l_s \qquad 2\text{-}46$$

The parameter Ω in the following equation may be obtained comparing the results from Equations 2-43 to 2-46 with the formulation of excess Gibbs energy, for x=0.5

$$G^E = \Omega \cdot l_l \cdot l_s \qquad 2\text{-}47$$

$$\Omega = \frac{2 \cdot k \cdot l}{l_l + b} + \frac{2 \cdot k \cdot l_s}{l_s + b} - \frac{4 \cdot k \cdot (l_l + l_s)}{(l_l + l_s) + 2 \cdot b} \qquad 2\text{-}48$$

The above implies that Ω is only a function of the pure components chain length. Expanding Equation 2-48 in series around *ls* and neglecting of higher order terms yields for *ls* larger than *b*:

$$\Omega = \Theta \frac{(l_l - l_s)}{l_s^3} = \Theta \cdot \Psi \qquad 2\text{-}49$$

By introducing this result in Equation 2-47, a model for excess enthalpies and/or Gibbs free energies for *n*-alkane mixtures is obtained.

$$G^E = H^E = \Theta \frac{(l_l - l_s)^2}{l_s^3} \cdot x_l \cdot x_s \qquad 2\text{-}50$$

Using just one parameter, Θ, it should then be possible, according to this model, to describe the non-ideality of the high temperature solid phase in the entire range of chain lengths for *n*-alkane molecules. The Θ parameter is estimated by a linear correlation of database of solid-liquid equilibrium for *n*-alkane systems, and a value of Θ=2317 kJ Å/mol was obtained.

The CDLP model presented above is based in the hypothesis of negligible excess entropy. If the hypothesis does not hold, both the S^E and H^E will be wrongly estimated in spite of the capacity of the model in what relates to G^E. A wrong value for H^E leads to poor temperature dependence. In the liquid phase, the possibility of an incorrect excess enthalpy is not likely because generally its value is not very large and thus a model can be used within a fair temperature range without problems. The solid phase models have to be able to cover large temperature ranges. As a result a model with poor temperature dependence will perform poorly at temperatures removed from its validity domain.

Comparisons with experimental data show that the hypothesis of negligible S^E is not valid, and assert the importance of a correct H^E description in the alkane solid phase.

The proper description of the excess Gibbs free energy, as the comparison of the calculations with experimental data suggests, does not imply that S^E=0 and G^E=H^E as was assumed, but that TS^E=H^E. This indicates that an equation similar to Equation 2.49 can be used to describe the solid-liquid equilibrium but cannot be applied to temperatures different from those around the melting point of the pure components; therefore, it is of limited interest.

The experimental data show a symmetric behavior for H^E. The phase equilibrium data require a similar trend for G^E implying that S^E should be approximately symmetrical given the narrow temperature range in these phase diagrams. It should thus be possible to represent the three excess properties by Margules type equations and based on statistical thermodynamic considerations, for solids:

$$\frac{H^E}{G^E} = \alpha \frac{T_{ms} \cdot T_{ml}}{T_{ms} + T_{ml}} = \alpha \cdot \phi \qquad 2\text{-}51$$

where α should be approximately constant for similar systems. Each family of compounds is presenting a characteristic value of α. If it holds also for *n*-alkanes it should then be possible to represent G^E, S^E and H^E simultaneously by:

$$G^E = \Theta' \frac{(l_l - l_s)^2}{l_s^3} \cdot \left(1 - \frac{T}{\alpha \cdot \phi}\right) \cdot x_l \cdot x_s \qquad 2\text{-}52$$

where ϕ represents the melting temperature function.

There are two approaches that can be followed in the calculation of α; the first relies on H^E experimental data and on the experimental phase diagram. The other uses Equation 2-52 and estimates the parameters α and Θ' through a procedure similar to that previously described using the new model for the solid phase. The value of α obtained by the two methods is remarkably similar, α=2.05. Value of Θ' in Equation 2-52 is 6714 kJ Å/mol.

The introduction of temperature dependence in the model using Equation 2-51 improves the temperature-independent version using Equation 2-50. In the small temperature range present in the phase diagrams the improvement is not always very significant. The temperature-dependent version should provide a much better description of the phase equilibrium at temperatures far from the melting temperatures of the pure components, such as in multicomponent mixtures.

The thermophysical properties of n-alkanes have been measured up to 300 000 kPa. The data indicate that the effect of pressure on both thermophysical properties and non-ideality of solid phase is small at moderate pressure.

The analysis of solid-liquid phase behavior shows that it is almost pressure independent thus pressure dependence of this model has also been studied and found to be valid up to 10 MPa.

CHAPTER 3

EXPERIMENTAL

3.1 Materials

Precipitation of paraffin solids is a well-recognized production problem. Accurate compositional analysis of whole crude oil, especially the C_{7+} fraction is used to predict solid deposition.

The composition of a typical crude oil is shown in the Figure 3.1. Figure 3.1 shows a semilogarithmic distribution of molecular weight (expressed as carbon number, in this example). The semilogarithmic distribution of carbon numbers is typical of many naturally occurring petroleum fluids (Carnahan, 1989).

The aim of this study is to extend a series of study done by Hammami (1994). Hammami investigated the thermal behavior of solid *n*-alkanes. The present study deals with the thermal behavior of three *n*-alkanes and their binary and ternary systems. Compositions of the binary and ternary mixtures are much better controlled, comparing to the composition of crude oil. The present study examined effects of lighter alkane on the solid paraffins. All *n*-alkanes are with large difference in chain length, which blocks the formation of a complete solid solution.

A low molecular weight component, C_{16}, was selected to investigate the effect of liquid *n*-alkane to the solid paraffins, one even numbered alkane C_{28}, and one odd, C_{41}.

Figure 3.1 Typical oil composition versus carbon number (Carnahan, 1989)

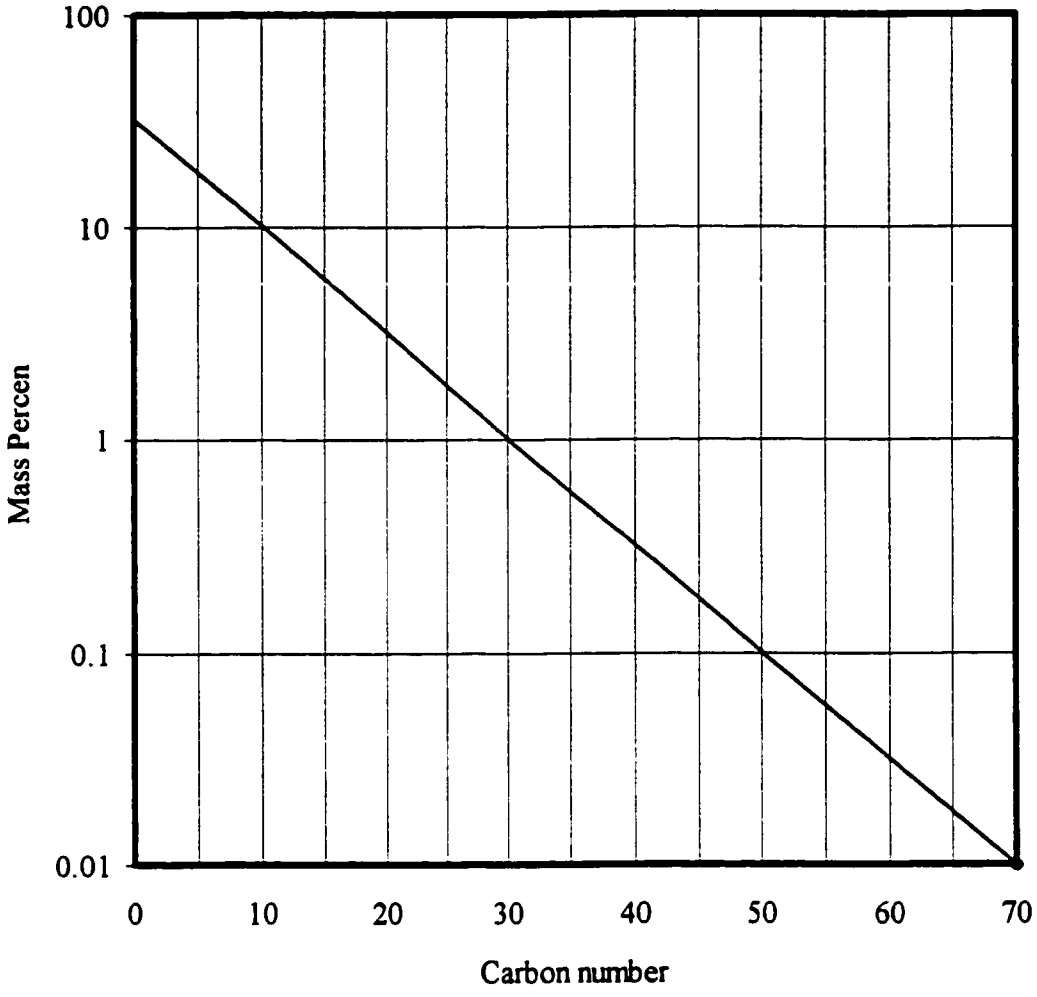

3.1.1 Pure Components

The samples of three alkanes studied in this work were obtained from Aldrich Chemical Milwaukee, WI, (USA) and Fluka Chemie AG, New York, (USA). The purities as well as the measured transition enthalpies and equilibrium melting temperatures of these *n*-alkanes are reported in Table 3.1.

Hexadecane, $C_{16}H_{34}$, is liquid at the room temperature; octacosane, $C_{28}H_{58}$, a is fine white powder; and hentetracontane, $C_{41}H_{84}$, is coarse transparent flakes. C_{28} and C_{41} are the results of crystallization from solution, and no further purification of the samples was performed. The melting points, T_m^0, reported in Table 3.1 do not correspond to the peak melting points but rather to the return to the baseline temperatures (Hammami, 1994). Melting temperatures determined by DSC are compared to values calculated using the Wunderlich (1980) empirical formula. Melting temperatures are found to agree reasonably well for C_{28} and C_{41}, but for C_{16} the difference is more then 5°C. Good agreement is not found when experimentally determined transition enthalpies are compared to values predicted by Dollhopf et al. (1981). The experimentally determined transition enthalpies are consistently lower than theoretical values. The calculated from DSC measurements are nearly independent of chain length, yielding a mean value 233.33 ± 6.66 J/g. Dorset (1990) and Hammami (1994) have also found similar results and concluded that the alkane samples were not perfectly crystalline.

Table 3.1 Melting temperatures and transition enthalpies for selected *n*-alkanes

	C_{16}	C_{28}	C_{41}
Source	Aldrich	Aldrich	Fluka
Purity	99%	99%	>97%
T_m^0 (°C) exp[1]	18.2	62.9	84.3
T_m^0 (°C) calc[2]	13.6	60.1	82.6
ΔH_{tot} (J/g) exp[3]	228	240	323
ΔH_{tot} (J/g) calc[4]	236.9	261.6	271.8

[1] Experimental values

[2] Values calculated using Equation 2-3

[3] Experimental values using Metter Graphware TA89E package

[4] Values calculated by Equation 2-5 and 2-6 (Dollhopf et at., 1981)

3.2 Sample Preparation

3.2.1 Pure Components

About 4-8 mg of each alkane was weighed to 0.001 mg on a Mettler microbalance Model UMT2 directly into the aluminium crucible (sample container). Aluminium is the standard material for the crucibles because of its low cost compared to other metals with high heat transfer properties. The crucibles were then cold-welded (mechanically sealed) to their special covers using a mechanical crucible sealer. A crimp-sealed empty aluminium crucible was used as a reference in all measurements. In this study, it has been implicitly assumed that the physical properties of the sample and reference are identical, except for the thermal phenomenon occurring on the sample side.

3.2.2 Binary Mixtures

Samples of three binary pairs were prepared by sealing together pairs of alkanes in the same crucible. The total mass of alkane pairs did not exceed 8 mg. For each binary mixture of pure paraffins, at least seven mole fractions (approximately 0.10, 0.25, 0.40, 0.50, 0.75, 0.92 and 0.95) were considered. Table 3.2 lists the various prepared binary mixtures along with their molar compositions.

Table 3.2 Molar compositions of the binary mixtures tested in this study

C_{16}+C_{28}		C_{16}+C_{41}		C_{28}+C_{41}	
S_{16}	S_{28}	S_{16}	S_{41}	S_{28}	S_{41}
0.0	1.00	0.00	1.00	0.00	1.00
0.03	0.97	-	-	-	-
0.10	0.90	0.11	0.89	0.09	0.91
0.24	0.76	0.25	0.75	0.23	0.77
0.41	0.59	-	-	0.40	0.60
0.45	0.55	-	-	-	-
0.51	0.49	0.49	0.51	0.50	0.50
0.61	0.39	-	-	0.59	0.41
0.74	0.26	0.75	0.25	0.77	0.23
0.81	0.19	-	-	-	-
0.90	0.10	-	-	0.89	0.11
0.93	0.07	0.925	0.075	0.92	0.08
0.947	0.053	0.965	0.035	0.95	0.05
1.0	0.00	1.00	0.00	1.00	0.00

3.2.3 Ternary Mixtures

Samples of ternary mixtures were prepared by sealing together predetermined masses of pure paraffins, three at a time, in the same crucible. In this case, the total mass was also kept to 8 mg or less. The molar compositions of the prepared ternary mixtures are reported in Table 3.3.

3.3 Instrumentation

The results described in this study were obtained using a Mettler differential scanning calorimeter Model DSC-12 E interfaced with a PC for automatic data acquisition. Mettler System Software TA89E package allows the computer to control the microcontroller of this DSC, thereby enabling the calorimetric signals to be recorded stored and eventually analyzed off-line. The DSC measuring cell is shown schematically in Figure 3.2.

During all measurements, the DSC measuring cell was continuously purged with dry nitrogen. DSC was calibrated for temperature and heat flow measurements using the melting point and enthalpy of fusion of high purity indium according to the standard procedures described in the user's manual. The calibration was run between 150°C and 160°C with the heating rate of 1°C/min. In this calorimeter, it was possible to melt and recrystallize a paraffin specimen many times without apparent thermal degradation. Therefore, the same sample was used for a whole series of experiments improving the reproducibility of the DSC measurements.

Table 3.3 Ternary mixture and its molar compositions

S_{16}	S_{28}	S_{41}
0.24	0.25	0.51
0.25	0.49	0.26
0.50	0.24	0.26
0.34	0.32	0.34

Figure 3.2 Representation of the DSC measuring cell

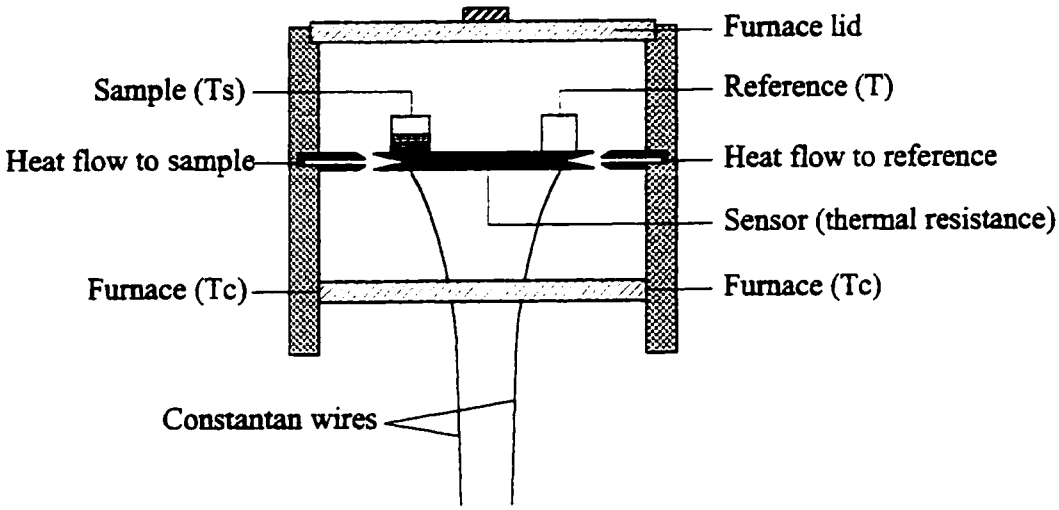

TOP VIEW

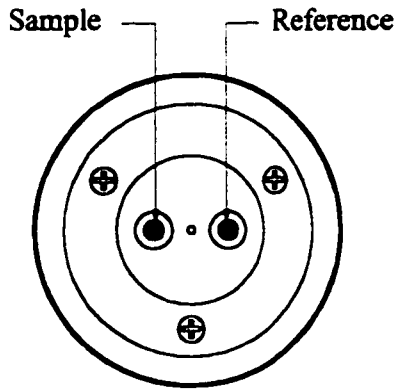

All thermograms presented in this study are plots of heat flow versus temperature, because the DSC does not have their ordinates calibrated in actual units. The vertical axis can be easily converted to enthalpy or specific heat. The exothermic changes are displayed in the positive ordinate directions, and endothermic changes in negative directions. For each scan rate, the measured heat rates have been divided by temperature and the mass of sample, and this allows a comparison between DSC curves obtained for different samples.

3.3.1 New Refrigeration System

To maintain the same temperature rate during the measurements the DSC is connected to the refrigerating bath. The temperature in the refrigerating bath is predetermined depending on the desired temperature and scan rate to accept the correct amount of energy. The maximum cooling rates as well as the lowest desired temperature in the measurements depend on the temperature difference between coolant and the furnace of the DSC.

Hammami (1994) measured the thermal behavior of 10 different n-alkanes, with their melting temperatures as low as 50 °C. The coolant in the refrigerating bath was ethylene glycol. For the new set of *n*-paraffins the temperature of the furnace is set to be as low as 5°C. The maximum flow rate of ethylene glycol was not sufficient to achieve the desired temperature because of very high viscosity at the low temperature.

The first decision was to choose the refrigeration liquid capable of handling the low temperature requirement. To perform measurements below the room temperature a new

cooling liquid, silicon based polymer liquid, was selected. The new coolant satisfied several conditions:

- nonflammable,
- low viscosity at the low temperature
- low freezing point.

3.3.2 Data Processing

Once DSC analyses have been obtained the apparatus software presented the data in the graphical form, and data files were in machine language format. Each measurement file contained information about the mass of the sample, calorimetric sensitivity, temperature and measured signal.

Complete description of data processing is given in Appendix.

3.3.3 Thermal Behavior

3.3.3.1 Temperature Programs

Three different thermal treatments were employed for each sample in the study. First, to erase the thermal histories of the as-received alkanes, each prepared sample of paraffins was annealed initially at 120°C for at least two minutes.

To examine whether vaporisation occurs at the temperature of 120°C, the total mass of the C_{16} sample and crucible was measured. There was no difference in mass before and

after the thermal treatment. Thus, the isothermal step does not cause any vaporisation of C_{16} paraffin.

After the 2-min isothermal step, the sample was cooled, at the rate of 1°C/min, to a temperature 30°C below the melting point of the paraffin, for pure component sample, or 20°C below the melting point of the shorter paraffin in the binary and the ternary mixtures. The third temperature treatment applied to the sample was the heating step. Each sample was heated at a rate of 1°C/min, to a temperature 30°C above the melting point, for pure component sample, or 20°C above the melting point of the heavier paraffin in the binary and the ternary mixtures.

3.3.3.2. Effects of Temperature Program Rates

DSC conveniently studies the effect of various temperature program rates on melting and crystallisation phenomena. The standard temperature rate of 10°C/min has been adopted by the ASTM Standards for wax and alkanes. The scan rate adopted by ASTM was chosen for many reasons. A decrease in the scan rate brings a reduction in the DSC peak areas, accompanied by a reduction of the temperature range over which the peak occurs; hence, the high scan rate was chosen partly for convenience (time to complete one experimental run). A slower rate would be more accurate in terms of measuring the equilibrium melting point. The greater the temperature program rate the greater will be the displacement from an equilibrium condition, because at the fast program rates the sample temperature cannot keep pace with the DSC platform temperature.

In this study, the equilibrium melting temperatures of pure alkanes as well as their binary and ternary mixtures were evaluated from the 1°C/min melting traces to avoid the effects of supercooling and superheating. For the pure components, additional DSC thermal traces were measured at various scans rates (1, 3, 5 and 7°C/min) to study the effects of superheating and supercooling.

3.3.3.3 Equilibrium Melting Temperature

Various workers (Evans et al., 1950; Flory et al., 1951; Mandelkern and Flory, 1951; Mandelkern et al., 1952, 1953; Roberts and Mandelkern, 1955) have demonstrated that when many crystalline polymers are heated slowly, the temperature at which the last traces of crystallinity disappear is well defined, reproducible and independent of any previous thermal history of the sample. It is believed that this temperature is the one of thermodynamic significance, for it is the temperature at which the most perfect crystallites are unstable relative to the pure melt. Hence, it can be identified as the equilibrium melting temperature of the crystalline material.

Figure 3.3 shows evaluation of the equilibrium melting temperature of C_{41} from the 1°C/min scan rate, as the endset temperatures. For the binary mixture thermal traces obtained by 1°C/min melting thermograms were used to evaluate the equilibrium melting temperature. For the eutectic binary mixture the convention of Smith and Pennings (1974) was adopted; the peak value of the lower melting component and the return to the baseline temperature for the higher melting component.

The recorded temperatures were corrected for a small thermal lag between the sample and the calorimeter. This temperature lag is the sum of the thermal gradient inside the sample and of the temperature lag between the sample bottom and calorimeter furnace. Hammami (1994) calculated the thermal gradient by calibrating the DSC with an indium standard at various rates of temperature change. The relation is a function of mass of the sample and was used by Hammami to correct for the effect of scan rate on the non-isothermal measurements:

$$T_{real} = T_{disp} - 0.02\lambda \qquad 3\text{-}1$$

where λ, in °C/min, is the rate of changing the temperature, negative during cooling.

The same correlation was used in the present study only for calculating the actual temperature for pure sample measurements. For binary and ternary mixtures, the thermal lag was not calculated since only one scan rate (1°C/min) was used. The maximum difference between sample and the furnace would be ±0.02 °C.

Figure 3.3 Graphical evaluation of the equilibrium melting temperature of C_{41} from 1°C/min scan rate

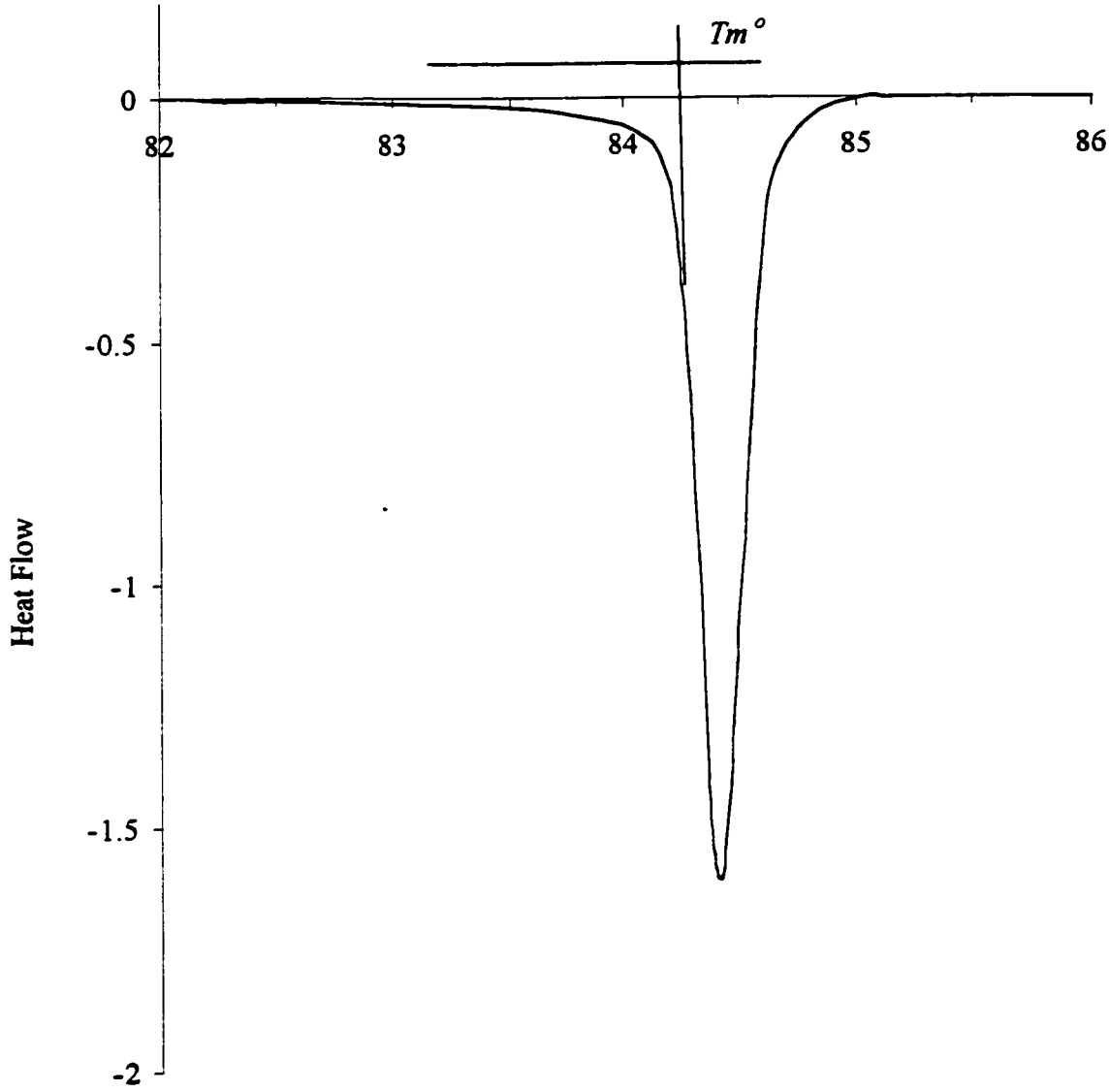

CHAPTER 4

RESULTS AND DISCUSSION

4.1 Pure Component

4.1.1 Analysis of DSC Thermograms

Melting and crystallization thermogram curves for the three pure paraffins were obtained at scan rates of 1, 3, 5, and 7°C/min. A set of heating scans for C_{16} is shown in Figure 4.1. All thermograms, melting temperature versus scan rate, have the same shape. It can be seen for all measurements that the baseline is the continuation of straight lines observed on thermograms before and after the thermal event. Figure 4.2, where cooling thermograms for C_{16} are presented, shows that the crystallization peaks are essentially mirror images of the melting peaks, except that the cooling curves are shifted to slightly lower temperatures. Crystallization during the cooling rate of 1°C/min occurs at a temperature 2-3 °C lower than the melting scan at the same rate. There is only one major peak representing liquid-solid transition upon cooling and/or heating regardless of the scan rate.

The peaks for the low scan rate are small, but sharp. The melting or crystallization range for the scan rate of 1°C/min is found to be very narrow, less than 1°C. An increase in the scan rate brings about an increase in the peak height, accompanied with an enlargement

Figure 4.1 DSC heating endotherms for C_{16} at different scan rates (in °C/min)

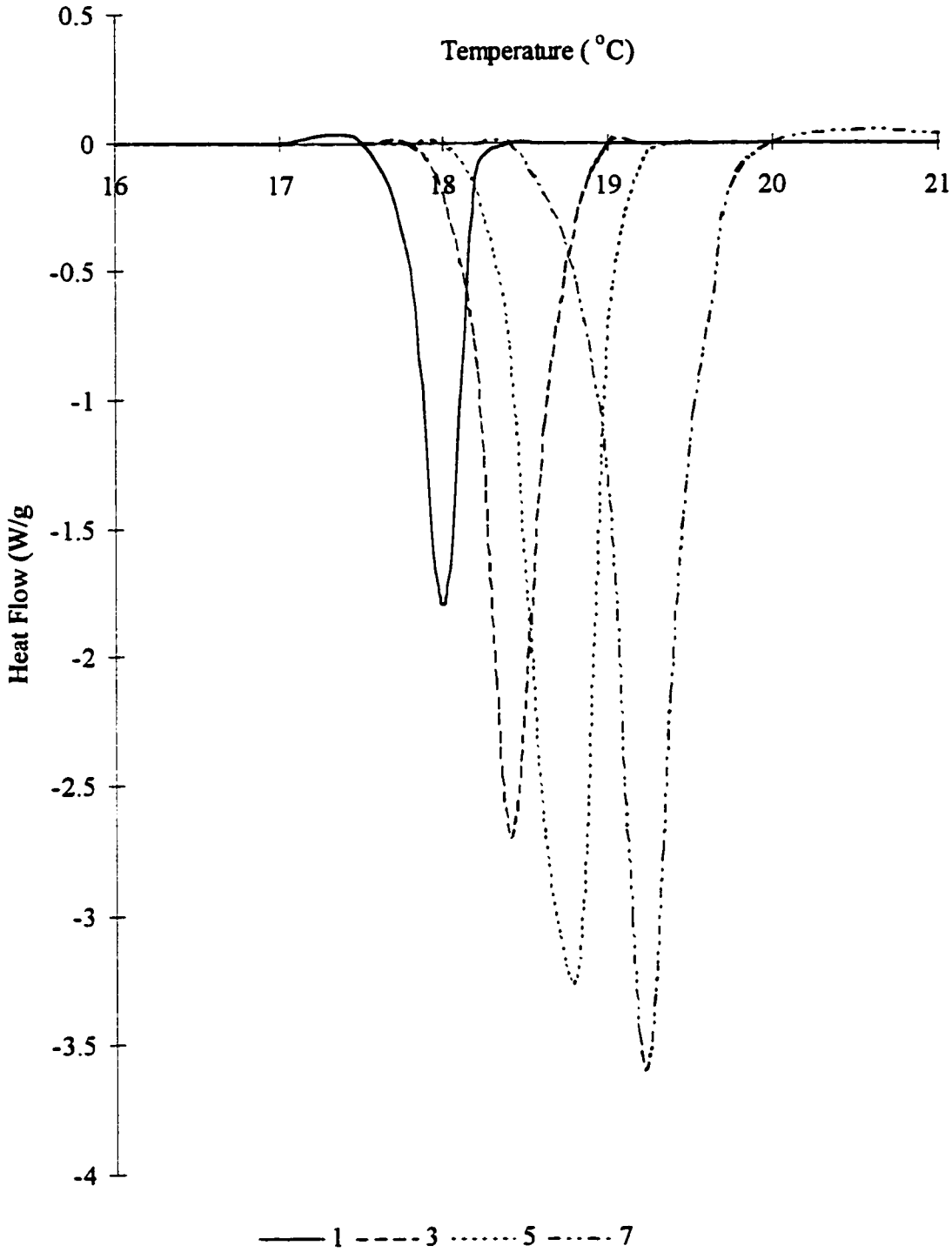

Figure 4.2 DSC cooling exotherms for C_{16} at different scan rates (in °C/min)

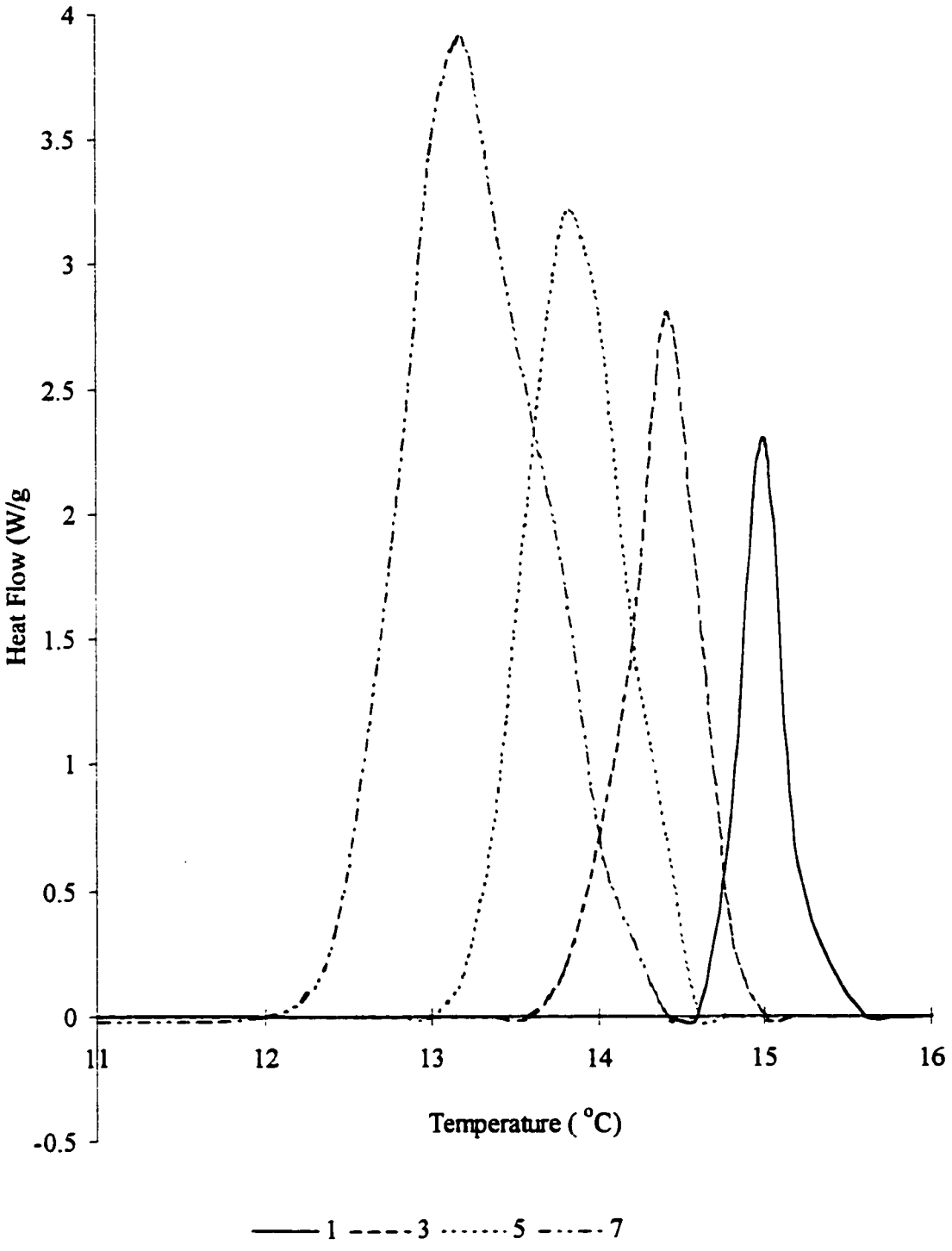

range is due to the moving away from thermodynamic solid-liquid equilibrium and for the scan rate of 7°C/min the temperature range becomes 2°C. Similar behavior was observed for C_{41}, where also just one major peak is observed. The C_{41} only undergoes an orthorhombic-to-liquid transitions, as shown in Figures 4.3 and 4.4.

Typical DSC measurements of different heating scans for C_{28} are presented in Figure 4.5. Figure 4.6 represents the cooling thermograms for C_{28} for thermograms quite different from those obtained of C_{16} and C_{41}. The thermograms show the existence of two major peaks. The high temperature peak represents the hexagonal-to-melt transition and the low temperature peak stands for the orthorhombic-to-hexagonal transition. The solid-solid transition is an orthorhombic to hexagonal crystalline rearrangement, involving a rotational motion at the molecular level (Ungar et al., 1985). The transition involves a rotational motion from rotator solid phase α to the denser, low temperature, non-rotating solid phase β. The phase α is a highly disordered phase, which exists in a narrow temperature range below and up to the melting point. The observed double peak is a clear indication of the polymorphic nature of this alkane. From a practical aspect, the transition is important since a substantial amount of latent heat is involved.

The melting and crystallization peaks involve a relatively narrow temperature range as can be seen from the Figure 4.5 and 4.6, the peak width is less the one half of the peak height for low scans rate. Again, as the scan rate increases, the peak areas also increase. The rotator transition peak is shorter than the melting transition peak under all heating and cooling rates. The observed dependence of the relative magnitudes of the peaks is not fully understood.

Figure 4.3 DSC heating endotherms for C_{41} at different scan rates (in °C/min)

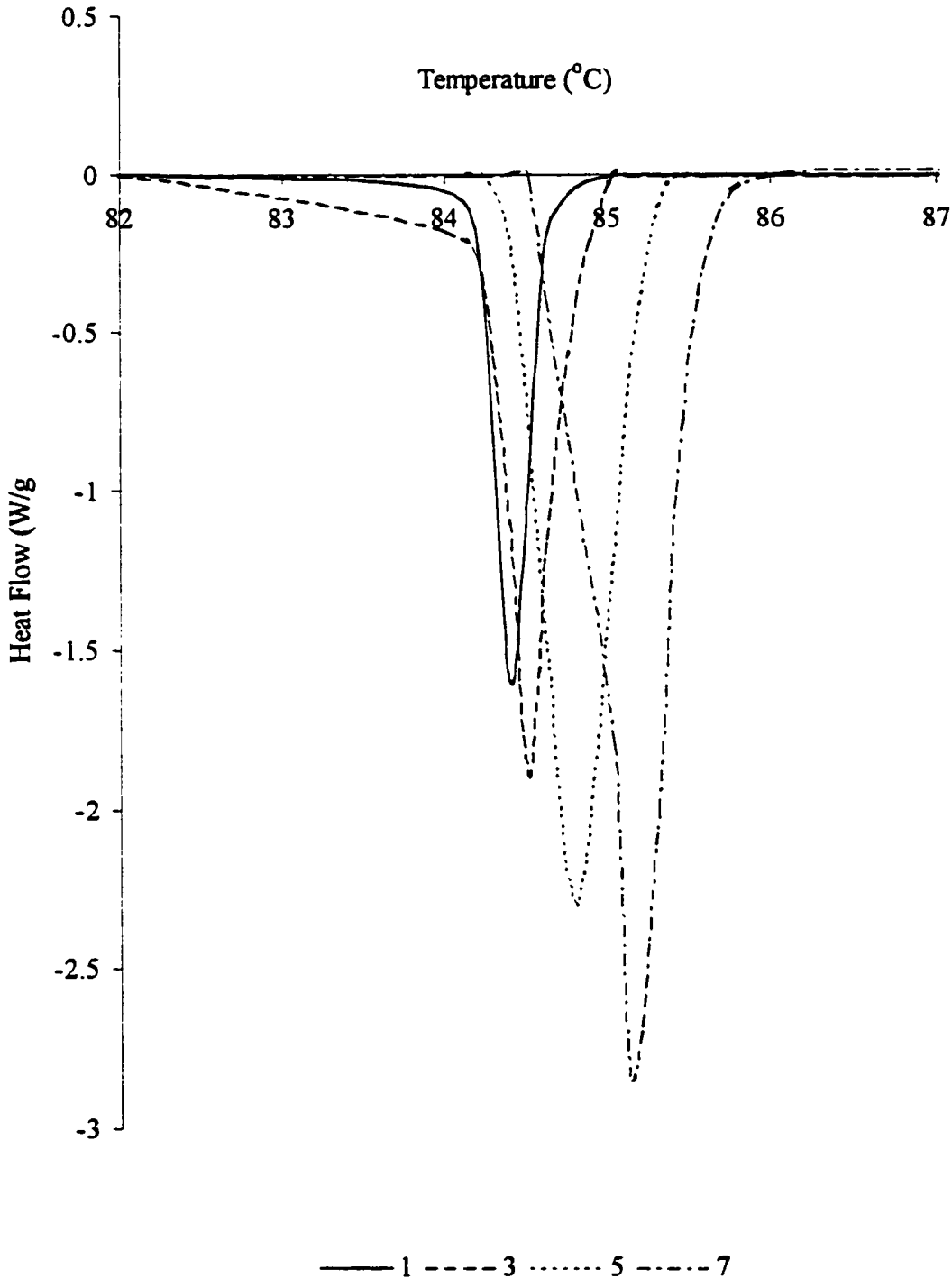

Figure 4.4 DSC cooling exotherms for C_{41} at different scan rates (in °C/min)

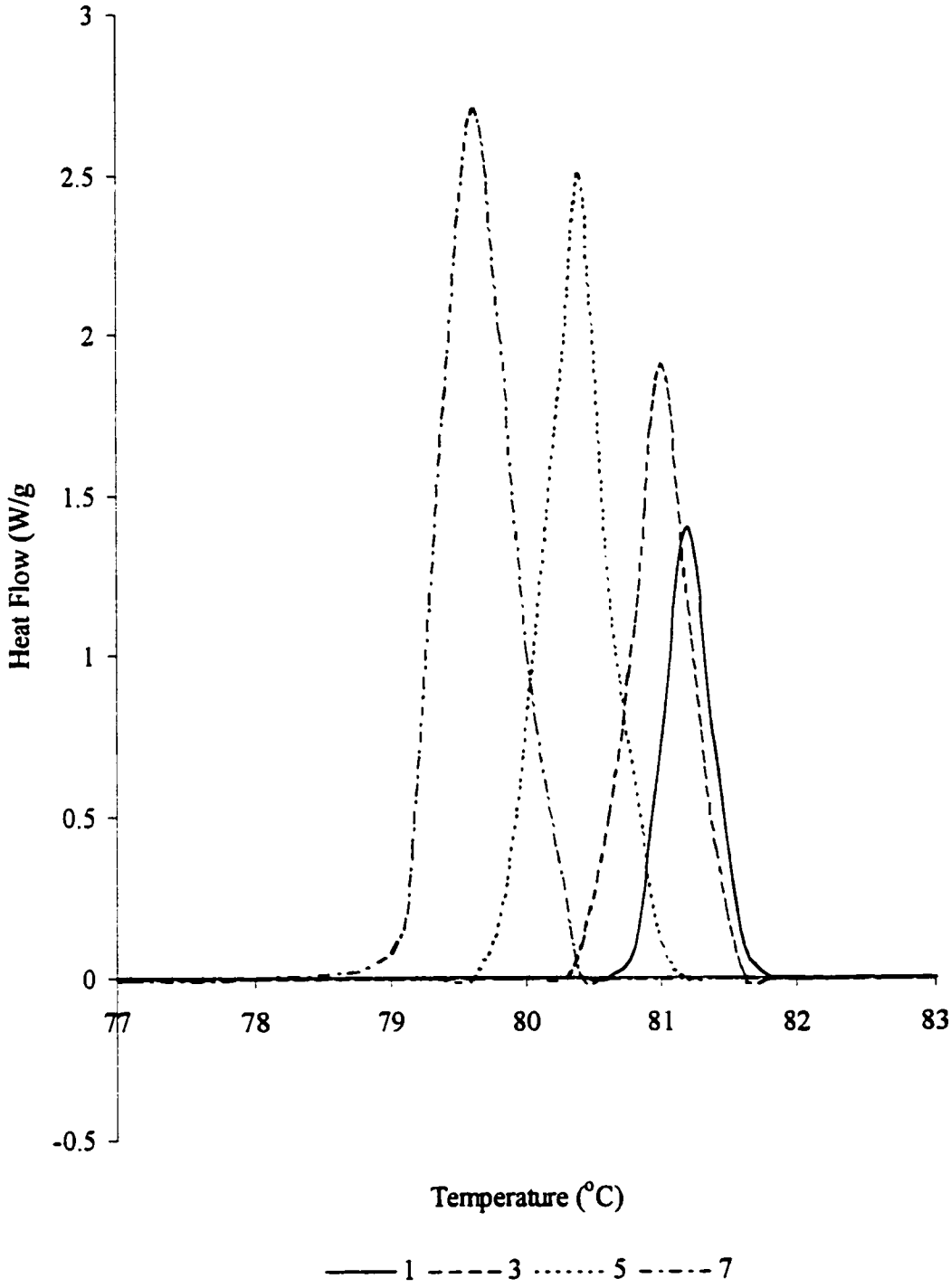

Figure 4.5 DSC heating endotherms for C_{28} at the different temperature rates (in °C/min)

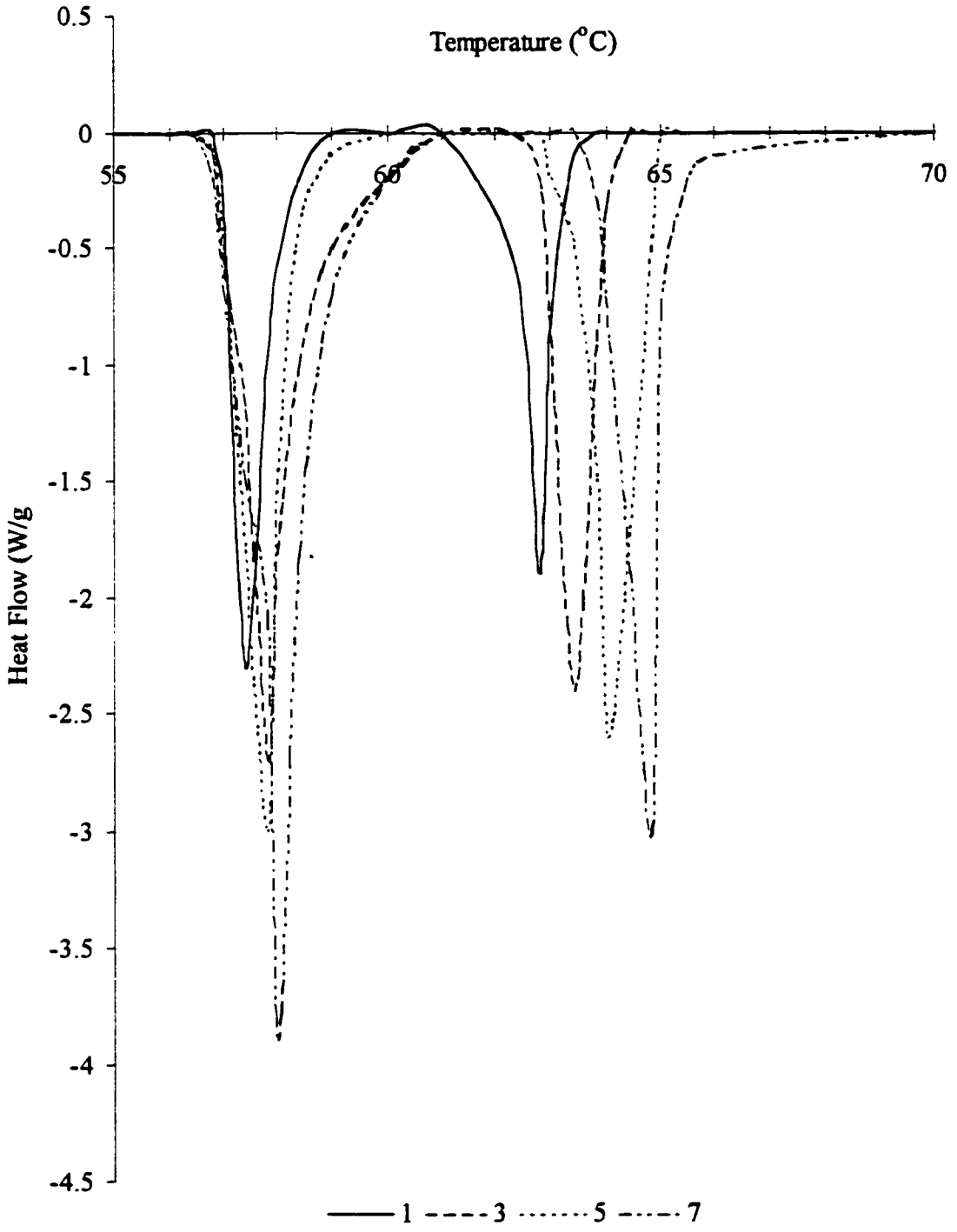

Figure 4.6 DSC cooling exotherms for C_{28} at different cooling rates (in °C/min)

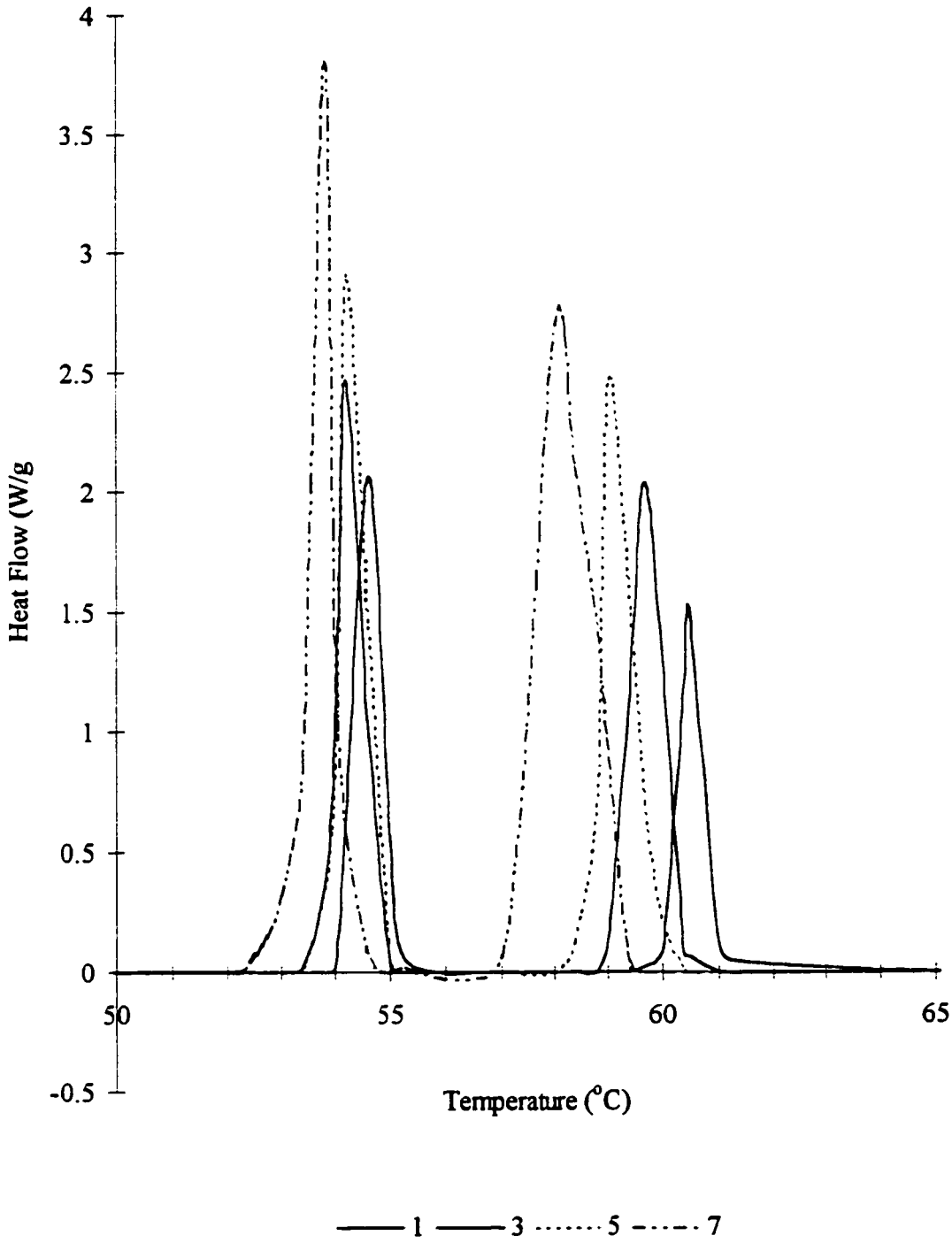

There is only a slight difference in DSC traces and temperatures for pure C_{28} and C_{41} obtained in the present study and results presented by Hammami (1995). The difference in the value of melting temperature for pure C_{28} is 0.4°C and for pure C_{41} is 0.2°C. Such a good agreement between results is confirmation of proper use of apparatus and correct measuring procedure (Flyn, 1993).

4.1.2 Effect of Scan Rates on the Peak Temperature

The effect of the scan rate can be demonstrated by comparing the DSC thermogram curves in the Figures 4.1, 4.2, 4.3, 4.4, 4.5 and 4.6 These scans were obtained on the identical samples of C_{16}, C_{41} and C_{28} at the heating and cooling rates of 1, 3, 5, and 7°C/min, respectively. The DSC thermograms show shifts to the higher temperature as the heating rate increases. Effect of supercooling can be seen as the temperature peaks shift noticeably to lower temperature with the cooling rate. From Figures 4.5, and 4.6, it can been seen that the solid-solid transitions were found to occur without much supercooling or superheating.

The results of various scan rates on the melting and crystallization temperatures for the three paraffins are summarized in Tables 4.1 and 4.2, respectively. As expected, there is a significant effect on the peak temperature due to supercooling or superheating. In general, the higher the rate of change the temperature, the greater will be the shift from equilibrium conditions. Basically, at the high scan rate the sample can not keep up with platform temperature. This is caused by thermal resistance between sample and

Table 4.1 Melting temperature (in °C) for selected *n*-alkanes under different heating rates

Heating rates	1 °C /min	3 °C /min	5 °C /min	7 °C /min
T_m^0 C_{16}	18.2	18.5	18.8	19.1
T_m^0 C_{28}	62.9	63.2	63.4	63.7
T_m^0 C_{41}	84.3	84.6	84.8	85.2

Table 4.2 Melting temperature (in °C) for selected *n*-alkanes under different cooling rates

Cooling rates	1 °C /min	3 °C /min	5 °C /min	7 °C /min
T_m^0 C_{16}	15.1	14.3	13.8	13.3
T_m^0 C_{28}	60.3	59.7	59.3	59.0
T_m^0 C_{41}	81.1	80.6	80.2	79.8

and the DSC platform (Faust, 1978).

The experimental melting temperatures versus scan rate from Table 4.1 and 4.2 are plotted in Figure 4.7, 4.8, and 4.9 for C_{16}, C_{28}, and C_{41}, respectively. The linear trend corresponds to the given set of experimental points of a chosen temperature rate. The equation for each line is given in the same plot, along with its correlation coefficient "R^2". The correlation coefficients indicate good fits for all of the data.

This observation is in agreement with Gimzewski and Audley (1993) who found that at a scan rate lower than 1°C/min the curve rises steeply for cooling experiments, and falls steeply for heating runs. Because of that phenomenon equilibrium condition can not be reached even at the scan rate of 0.01°C/min.

An interesting feature of Figures 4.7 to 4.9 is that the melting and cooling curve extrapolated to the zero cooling or heating rate were found not to correspond to the same temperature for a particular *n*-alkane. The extrapolated melting temperature at the zero heating rate for pure C_{16}, C_{28}, and C_{41} is 18.1°C, 62.8°C and 84.2°C, respectively. The difference in melting temperatures obtain by extrapolating the heating and cooling curves to the zero scan rate is for C_{16}, C_{28}, and C_{41} is 3.1°C, 2.4°C and 2.9 °C, respectively.

The DSC used in this study is limited to the lowest scan rate of 1°C/min, due to this and foundlings of Gimzewski and Audley (1993), the extrapolation of the phase change temperature to the zero scan rate would be only approximate. The non-linearity of the curve describing the effects of supercooling and superheating is perhaps the main reason why the values of extrapolated phase change temperature at the zero scan rate are

Figure 4.7 Variation of the melting temperature (in °C) for C_{16} with different heating and cooling rate (in °C/min)

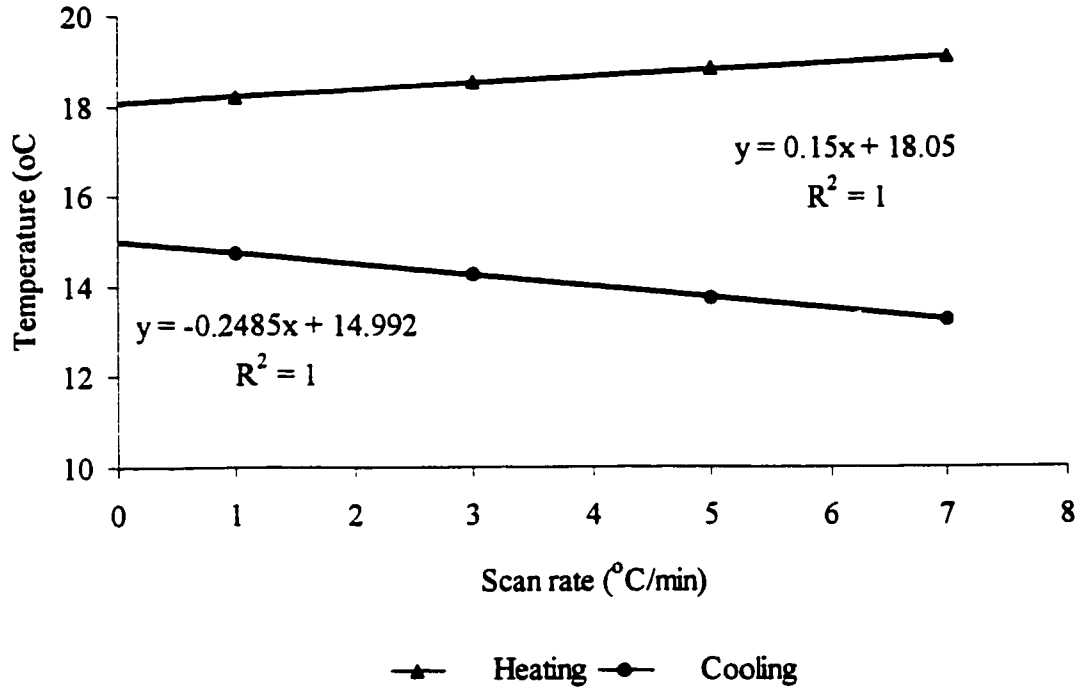

Figure 4.8 Variation of the melting temperature (in °C) for C_{28} with different heating and cooling rate (in °C/min)

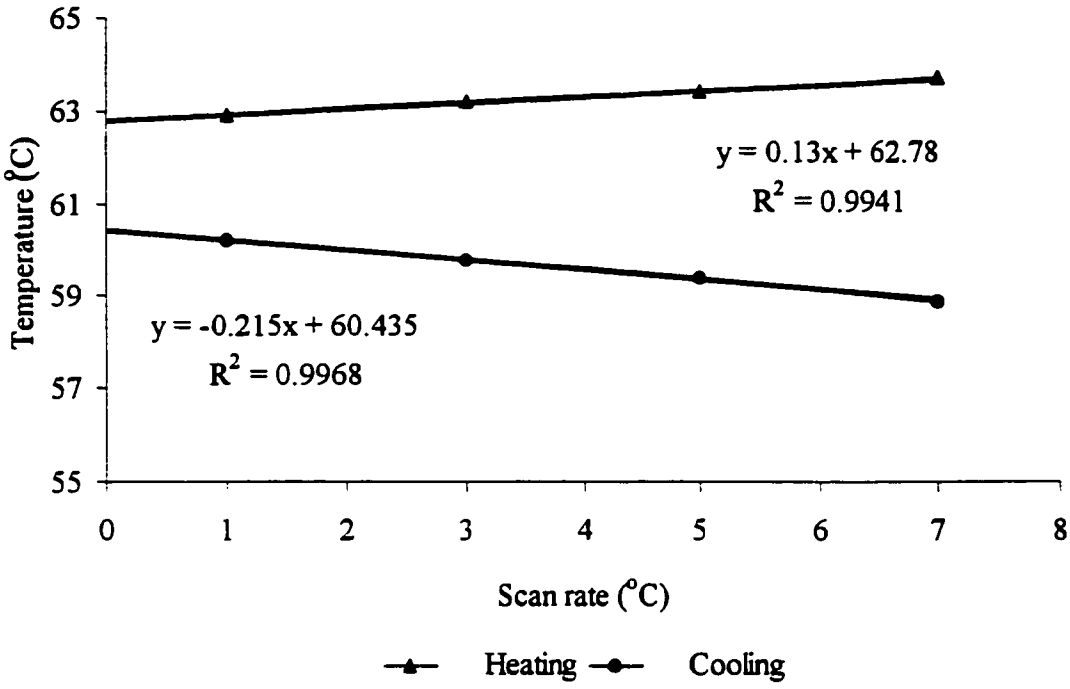

Figure 4.9 Variation of the melting temperature (in °C) for C_{41} with different heating and cooling rate (in °C/min)

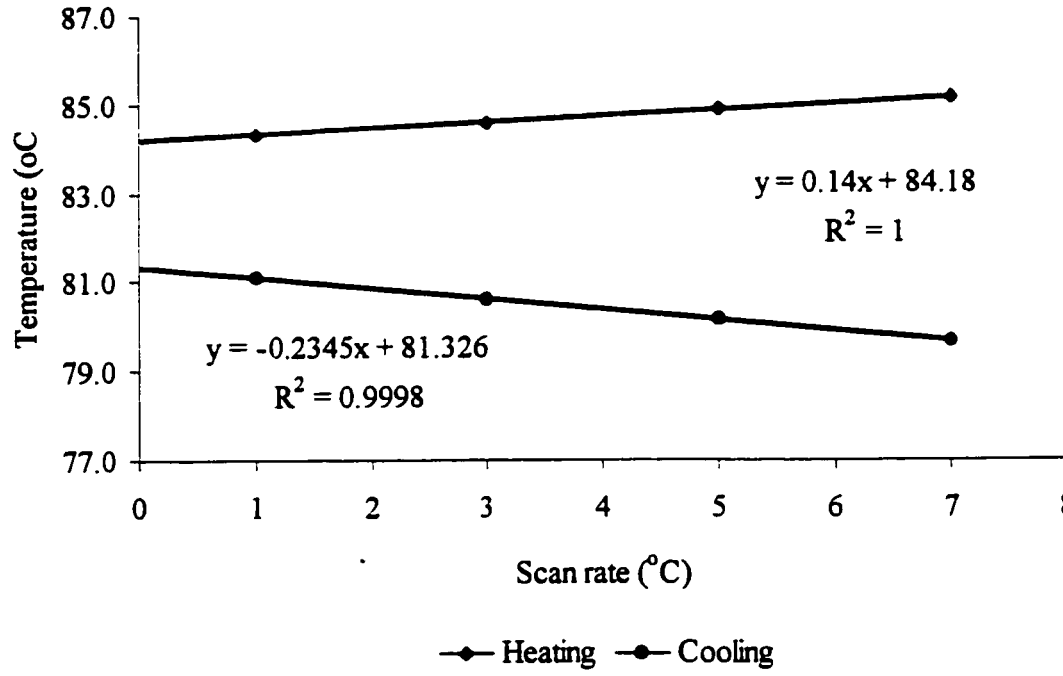

different for cooling and heating experiments.

The slope for each line can be used as a measurement of the amount of supercooling or superheating. For each *n*-alkane, as can be seen in Figures 4.7, 4.8 and 4.9, the amount of superheating is less severe than the amount of supercooling. A lower slope of the line indicates better equilibrium conditions even at higher scan rates.

4.1.2.1 Effect of Cooling Rate on Rotator Transition Temperature and the Melting Transition Temperature of C_{28}

The effect of varying the scan rate on the double peaks for C_{28} is summarized in the Table 4.3, which contains the measured values of T_α and T_β peaks for C_{28} at different cooling and heating rates. Figure 4.10 shows the difference in the peak temperatures versus cooling and heating rates. It can be seen that both T_α and T_β vary linearly with heating and cooling rates. The temperature difference between two peaks was found to be independent of cooling or heating rates and remained constant. The average peak-to-peak temperature difference for the heating thermograms is 5.5 °C, and for cooling is 5.4 °C. Value of standard deviation for the mean value in both cases is $< \pm 0.15$°C. Figure 4.8 confirms the work done previously by Hammami (1994) and Hammami and Mehrotra (1995), who had similar results for several *n*-alkanes.

Table 4.3 Experimental values of the transition temperatures for C_{28} under different scan rates

	1 (°C/min)	3 (°C/min)	5 (°C/min)	7 (°C/min)
T_α Heating (°C)	62.9	63.2	63.4	63.7
T_β Heating (°C)	57.5	57.7	57.8	58.0
T_α Cooling (°C)	60.2	59.8	59.4	58.9
T_β Cooling (°C)	54.7	54.4	54.1	53.7

Figure 4.10 Variation of the peak temperatures (in °C), T_α and T_β, for C_{28} with different heating and cooling rates (in °C/min)

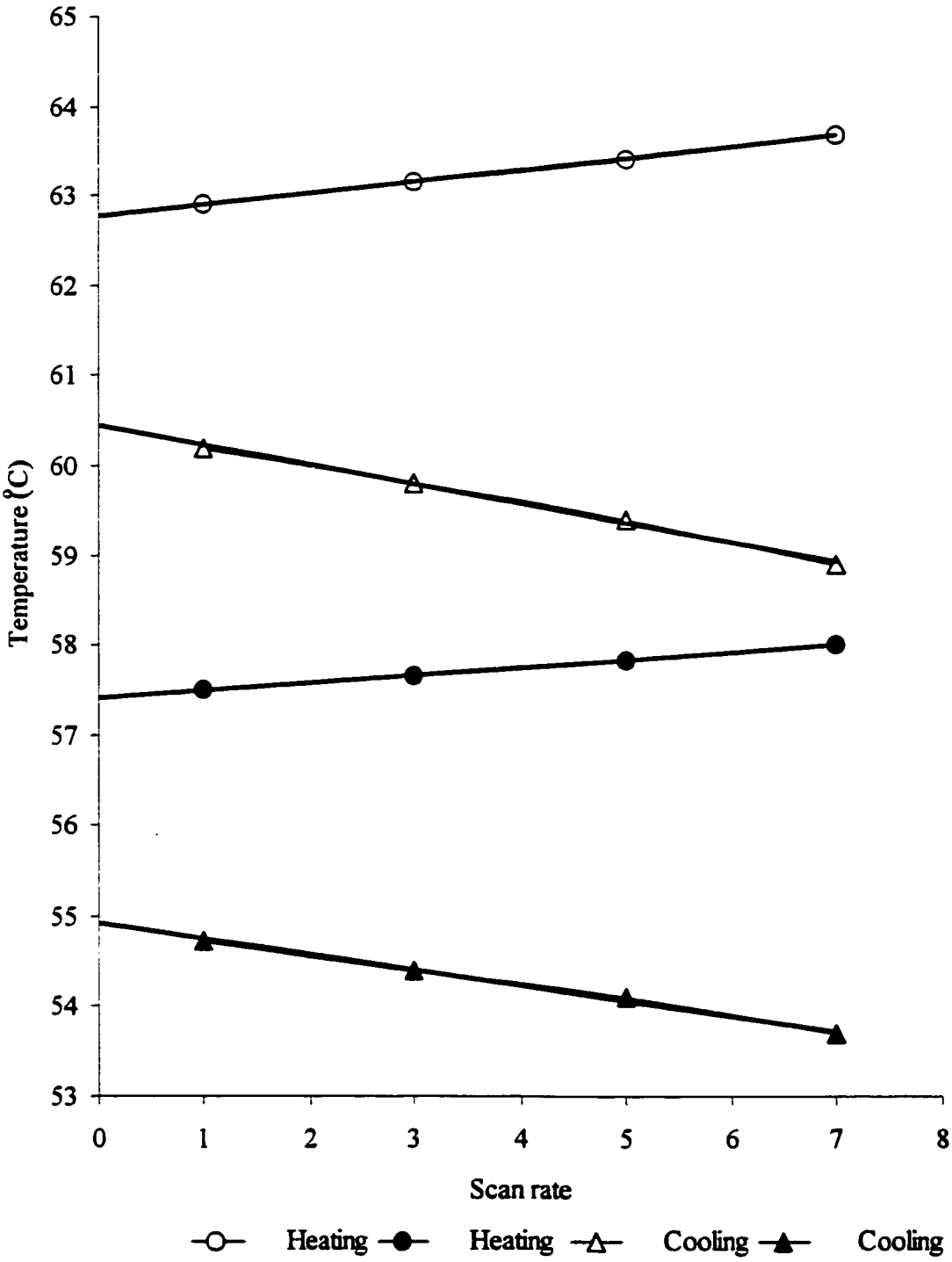

4.2 Binary Mixture

As mentioned previously DSC measurements were made on three binary *n*-alkane systems: C_{16}+C_{28}, C_{16}+C_{41} and C_{28}+C_{41} with the scan rate of 1°C /min.

4.2.1 Gibbs Energy Analysis

The miscibility behavior of a binary mixture can be predicted using the Gibbs free energy analysis. At the fixed temperature and pressure, a stable state is that which has the minimum Gibbs energy. Thermodynamic stability analysis indicates that mixture splits into two separate phases if Gibbs energy can be lowered. A decrease in the Gibbs energy of binary a mixture due to formation of another phase can occur if a plot of the Gibbs energy change of mixing against mole fraction is concave downward.

Values of Gibbs energy were calculated for the three binary mixtures according to the temperature independent version of Coutinho et al. (1996), the CDPL model, Equation 2-50. A plot of values of Gibbs energy versus composition is shown in the Figure 4.11.

As can be seen from the plots all three mixtures are concave downward, which suggests completely immiscible behavior of the binary mixtures (Bhat, 1996).

4.2.2 Comparison between Models

Pauly et al. (1998) performed measurements at atmospheric pressure on mixtures made up of decane and various distributions of heavy normal paraffins from octadecane to

Figure 4.11 Gibbs free energy curve for three binary mixtures

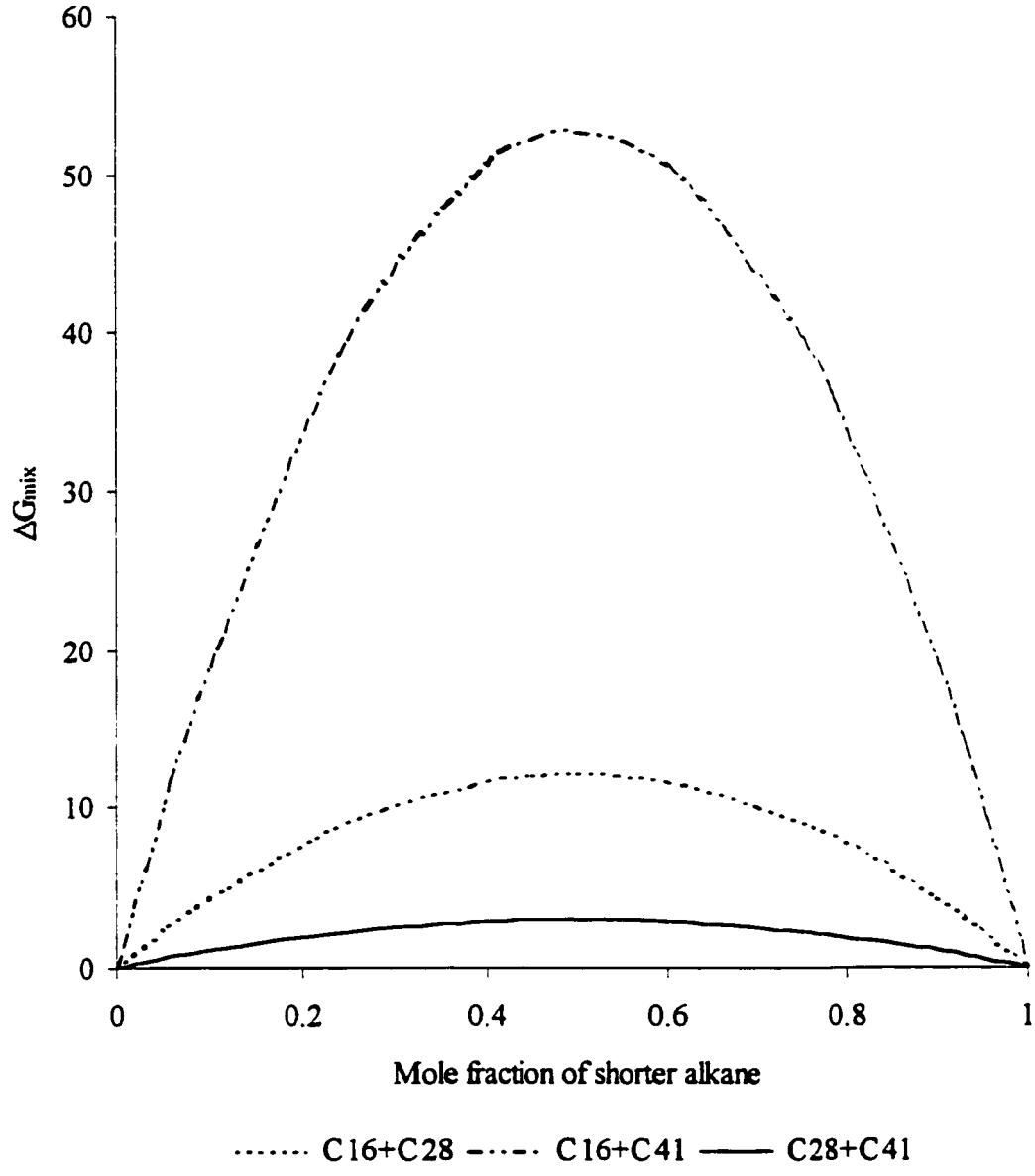

triacontane. At temperatures below the wax appearance temperature, liquid and solid phases in partially frozen mixtures were separated by isothermal filtration and analyzed by gas chromatography. Furthermore, the liquid-solid equilibrium data obtained were compared with the values predicted from several models, including Won (1986), Hansen et al.(1981), Pedersen et al. (1991), Coutinho et al. (1996) and Ungerer et al. (1995). Pauly et al. (1998) found that all activity coefficient models overestimate the solid appearance temperatures; nevertheless, this overestimation remained only slight. Unlike these models, the approach of Ungerer et al. (1995) was found to always underestimate the slope of solid deposition vs. temperature. The model predictions indicate that only the heaviest component precipitates at the solid appearance temperature and thus minimizes the amount of solid formed at the beginning.

4.2.3 Reproducibility of DSC Thermal Measurements

The reproducibility of the recordings is within 1% as proven by comparing two different recorded thermograms of the same sample. However, heating thermograms are not obtained with the same accuracy because the baseline is never precisely defined. Instead of being at the zero level as expected, the baseline always exhibits more or less positive or negative values. Good reproducibility of the measurement can be seen in the Figure 4.12. Figure 4.12 presents heating and cooling thermograms of duplicate runs for sample of C_{16} with the scan rate of 1°C/min.

Figure 4.12 Thermal traces of two runs for sample of C_{16} at the heating and cooling rate of 1°C/min

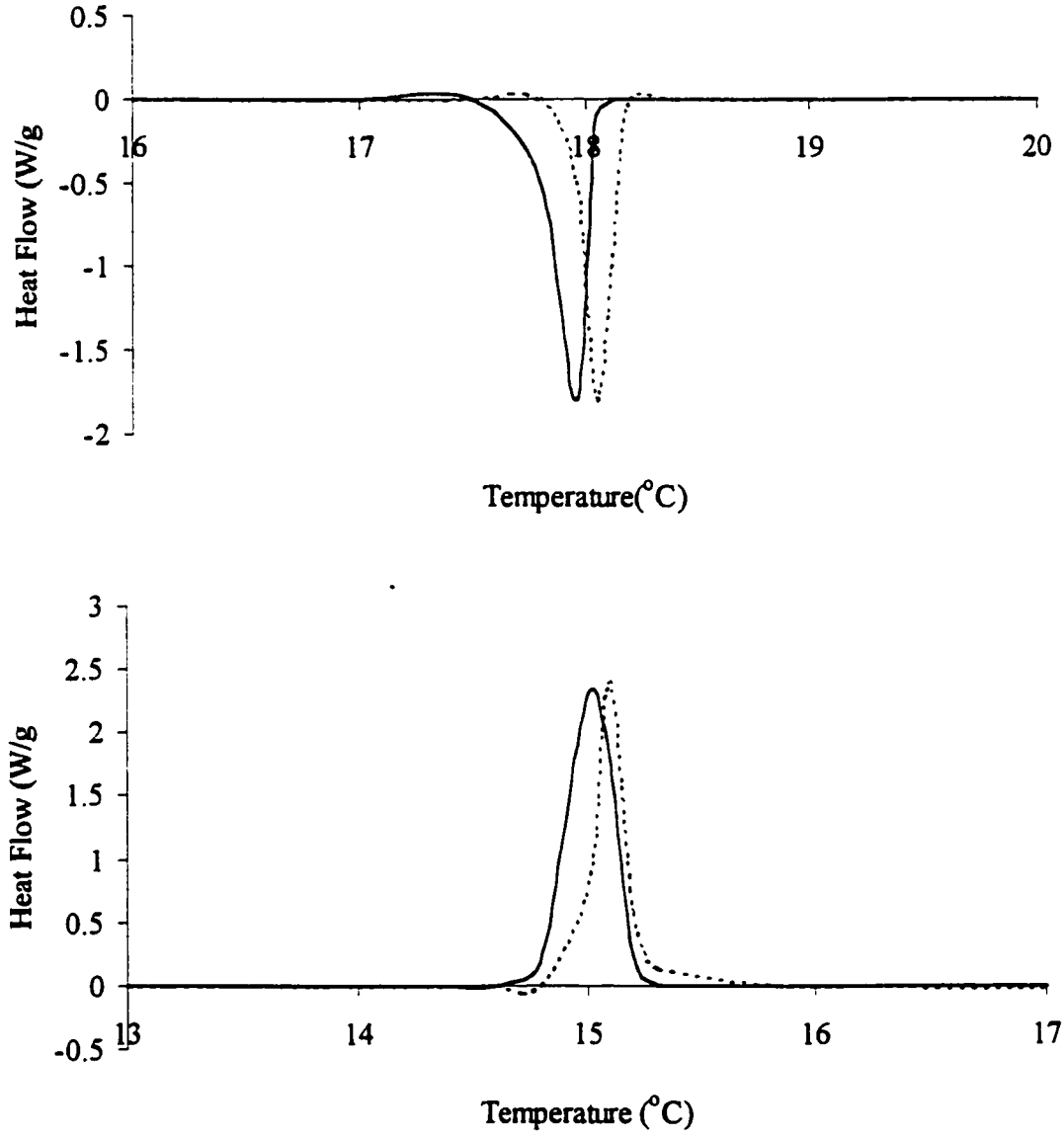

4.2.4 DSC Measurement of Binary Mixtures

As mentioned previously, DSC measurements were made on three binary *n*-alkane systems: C_{16}+C_{28}, C_{16}+C_{41} and C_{28}+C_{41} with the scan rate of 1°C/min. To illustrate the different interaction between two *n*-alkanes with a large difference in the chain length, the C_{16}+C_{28} system is chosen. Fifteen different concentrations of this system were investigated in this study; hence, it will be used as a basis of comparison for other binary mixtures.

To test the validity of existing models, it is useful to have experimental liquid-solid phase equilibrium data for system whose composition is precisely identified.

The data treatment for all binary mixtures involved the comparison of experimental phase diagrams with the ideal solution theory. To define the deviation from ideal eutectic, behavior, the regular solution theory, Won's model (1986) and Pedersen et al.'s model (1991) were used.

The phase diagrams have been constructed from DSC data and represent as a function of composition and temperature. All phase diagrams are constructed from DSC heating thermograms. To construct the phase diagrams the convention of Smith and Penning (1974), presented in the section 2.4.1.2, was used; i.e. the peak temperatures for the lower melting endotherms and the return to the baseline temperature for the higher melting endotherms. Phase diagrams plotted from DSC scans of all three *n*-alkane mixtures reveal a stable eutectic behavior.

In general, studies on binary eutectic mixtures of alkanes have indicated that the eutectic melts within one degree of the pure hydrocarbon of shorter chain length; the eutectic

mixtures usually contain 90-95% of the shorter paraffin (Mazee, 1949, 1957; Butler and MacLeod, 1961). An " ideal" eutectic mixture presupposes the existence of complete insolubility between the two components at all concentration. This seldom occurs in the strictest sense; the eutectics frequently are of the non-ideal type and show evidence of partial solubility in the solid state.

4.3.1 Analysis of DSC Thermograms for C_{16}+C_{28} Mixture

Figure 4.13 presents the thermal traces for binary mixture of C_{16}+C_{28} at the heating rate of 1°C/min. DSC thermograms of C_{16}+C_{28} mixture, arranged in the order of increasing mole fraction of C_{28}, are shown in the figure. A few important features can be pointed out for this plot. All mixtures (except for 95% of C_{16}) exhibit at least two peaks. The low temperature peak is independent of the mixture composition and appears at the constant temperature. From this diagram, it was inferred that the C_{16}+C_{28} system is a eutectic system with the eutectic temperature of 18.5°C and eutectic composition at 95% of C_{16} in the mixture.

Figure 4.14 presents the DSC traces of C_{16}+C_{28} binary mixture at the cooling rate of 1°C/min. Aside from normal, uniform undercooling of the specimens when crystallized from the melt, there is no difference in the DSC traces for heating and cooling. Beside undercooling, there is no difference in shape of the phase diagram constructed from cooling curves, compared to the one created from heating DSC curves.

From these plots we can see that at high concentrations of C_{28} all DSC thermograms exhibit three peaks. The high temperature peak represents liquid-solid transformation, the

Figure 4.13 DSC melting thermograms of C_{16}+C_{28} binary mixture (mole fraction of C_{16} are shown in the figure)

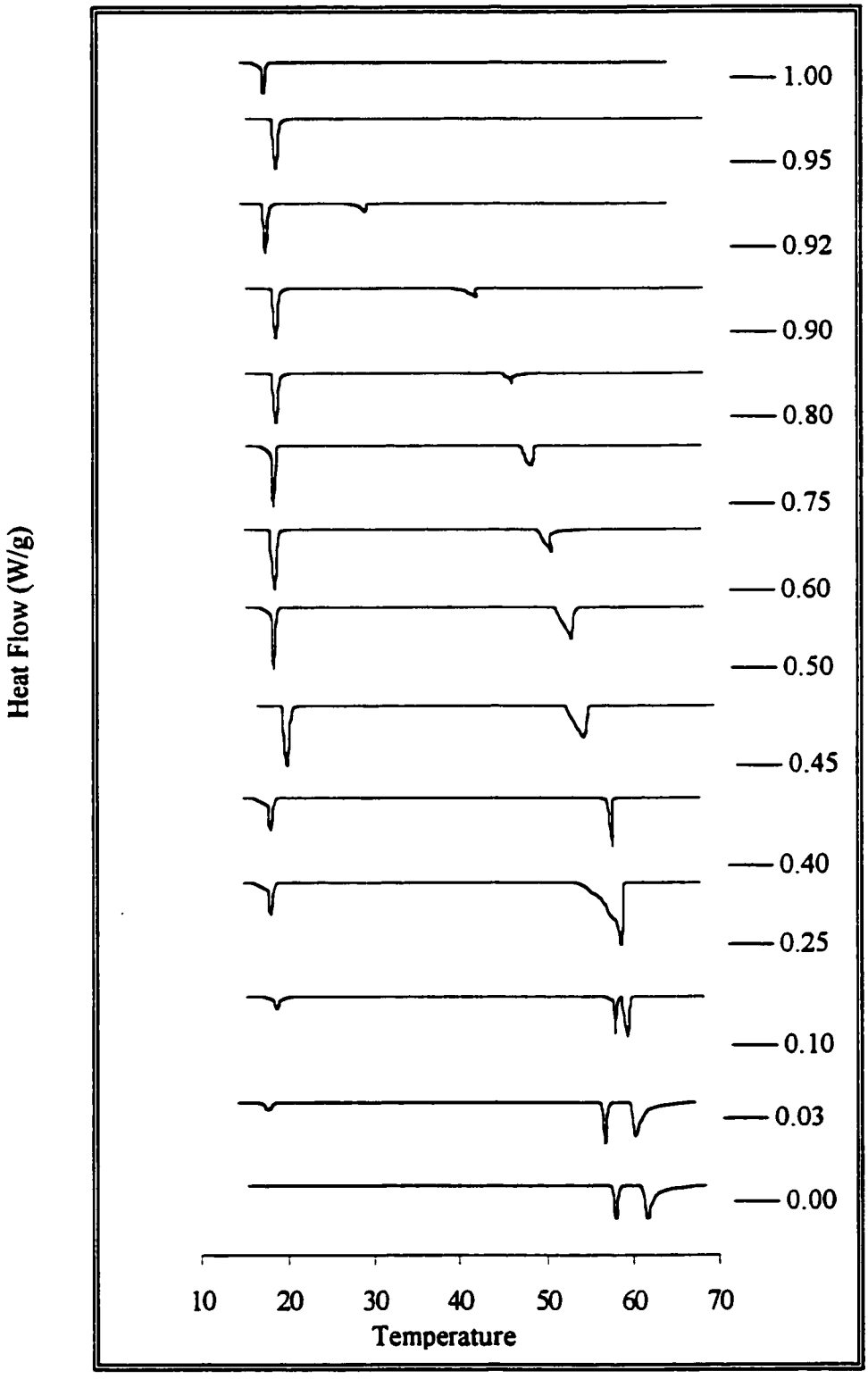

Figure 4.14 DSC cooling thermograms of C_{16}+C_{28} binary mixture (mole fraction of C_{16} are shown in the figure)

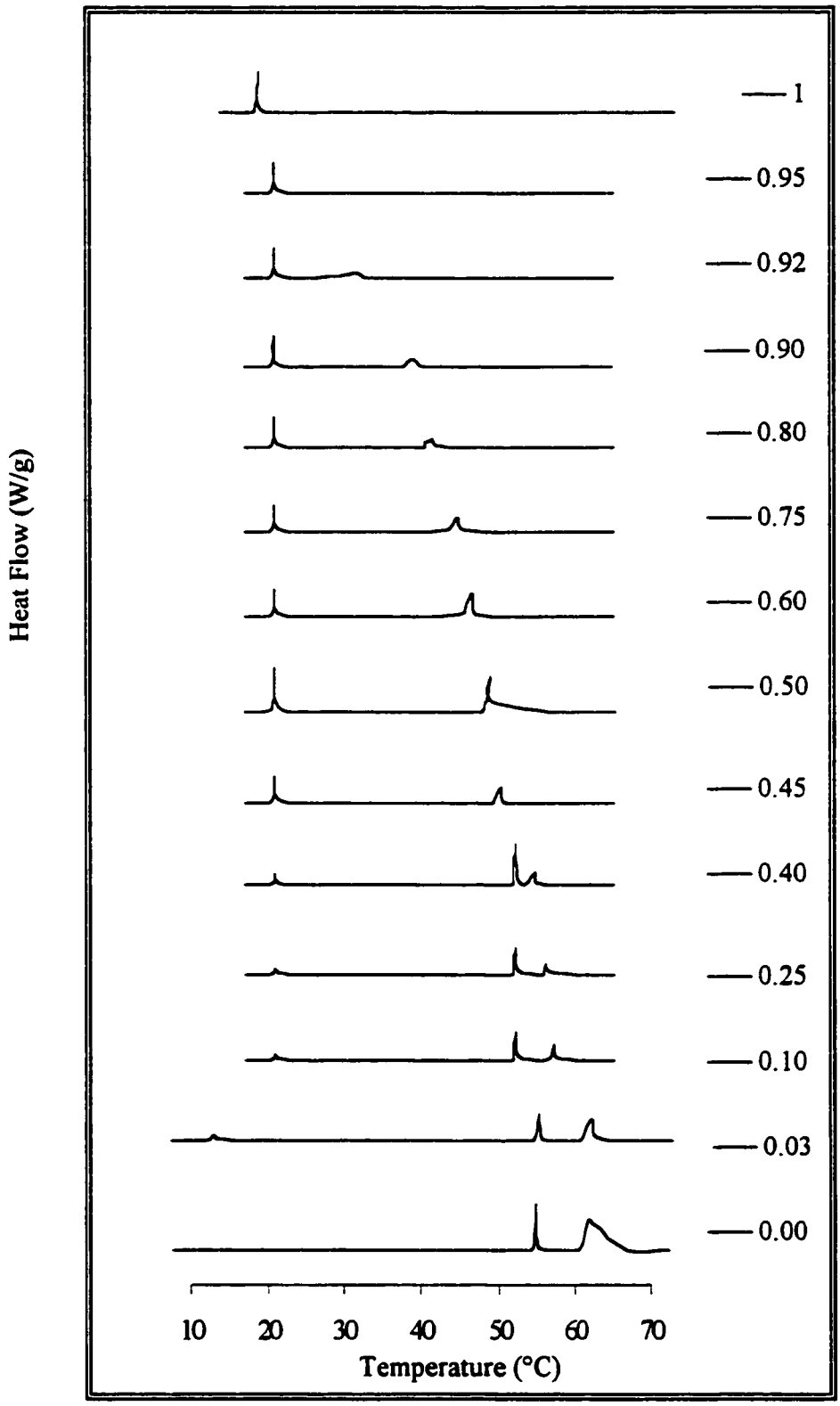

middle peak is for the solid-solid transformation, and the low temperature peak represents the eutectic temperature. The solid-solid transformation temperature as well as the melting temperature of C_{28} was systematically and progressively depressed by increasing the concentration of C_{16}.

As the percentage of C_{16} increases in the mixture, the melting peak tends to merge with solid-solid transition temperature peak. From Figure 4.14 we can see that the cooling exotherms exhibit the solid-solid transition peak up to 40% of C_{16} in the mixture, and from Figure 4.13, in the case of heating thermograms three peaks can be seen up to 25% of C_{16}.

The temperature for the solid-solid transition peak remains practically unchanged, until the solid-liquid temperature peak overlaps it. Even at the low scan rate of 1°C/min, the two peaks did not separate enough for an accurate trace to the base line. Over the concentration range of 40% to 60% of C_{16}, where the solid-liquid and solid-solid transition occur around the same temperature instead of the well-defined melting and transition point, the results show a very broad melting range. Experimental data for the solid-solid temperature from the heating and cooling experiments are presented in Table 4.4.

The solid-solid transition temperature for the binary mixture of C_{16}+C_{28}, for heating and cooling experiments appears to be independent of the composition. If we compare the solid-solid transition temperature with the transition temperature of pure C_{28}, there is practically no change of temperature where the solid-solid transition occurs. For pure C_{28}, the solid-solid transition occurs at 58.8 °C and for binary mixtures the temperature range is 58.9 ±0.1°C.

Table 4.4 Experimental data for solid-solid transition temperature for binary mixture of C_{16}+C_{28}

S_{16}	Heating	Cooling
0.0	58.8	53.5
0.03	59.0	53.5
0.10	58.9	53.6
0.25	-	53.5
0.40	-	53.8
0.45	-	-

From the evidence that the solid-solid transition temperature has practically not been changed, it can be concluded that the miscibility does not occur in the solid state over the concentration range of 0% up to 40% of C_{16}. Over this concentration range, formation of pure solid phase of C_{28} occurs.

The difference between crystallization and eutectic temperatures becomes smaller as the concentration of the C_{28} decreases. At low C_{28} concentrations, the melting range of C_{28} was broadened, and peak height decreased as well. A relatively small peak can be identified for concentration of 90% C_{16}, and the liquidus temperature becomes depressed by 20.2°C from to the melting temperature of pure C_{28}. At the concentration of 94.3% of C_{16}, the DSC thermogram exhibits just one peak, which appears at the eutectic temperature of 18.5°C.

4.3.2 Equilibrium Phase Diagrams and Equilibrium Calculation

4.3.2.1 Calculation Based on Ideal Solution

Initially the eutectic behaviour of C_{16}+C_{28} mixture was calculated assuming ideal eutectic behaviour i.e. Equation 2-19. As mentioned previously, this relationship is based on the assumption that no heat of mixing and no change of volume upon mixing. As reported in Table 4.5, the results based on the assumption of ideal solubility reasonably match the experimental data.

Before analyzing phase diagram, it will be useful to have a picture of the phenomena described in Figure 4.15. The curve represents the solid-liquid phase change curve for C_{28}. Consider a binary mixture with composition of 45% C_{28} and 55% C_{16} and initial

Table 4.5 Experimental and calculated equilibrium values of (T_m^E) and T_E for C_{16}+C_{28} eutectic mixture

S_{16}	(T_m^E) exp[1]	T_E exp[2]	(T_m^E) calc[3]	error[4] (°C)
0.00	63.0	-	63.0	0.0
0.03	62.9	18.3	60.9	2.3
0.10	61.8	18.3	60.5	1.3
0.25	60.5	18.4	59.2	1.3
0.40	59.1	18.5	57.6	1.5
0.45	54.4	18.5	56.9	-2.5
0.50	54.3	18.6	56.0	-1.7
0.60	51.9	18.6	54.2	-2.3
0.75	49.4	18.6	50.4	-1.0
0.80	47.1	18.5	48.8	-1.7
0.90	42.9	18.6	43.6	-0.7
0.92	32.6	18.5	41.0	-8.4
0.94	18.5	18.5	39.7	-20.8
1.00	18.8	-	18.8	-

[1] values corresponding to the return to the baseline of the high temperature exotherm

[2] values corresponding to the low temperature peak

[3] values calculated using Equation 2.19, assuming ideal behavior of the mixture

[4] difference between experimental and calculated (T_m^E) values

Figure 4.15 Phase diagram for C_{16}+C_{28} binary mixture; Comparison between experimental data and model assuming ideal behavior of the mixture

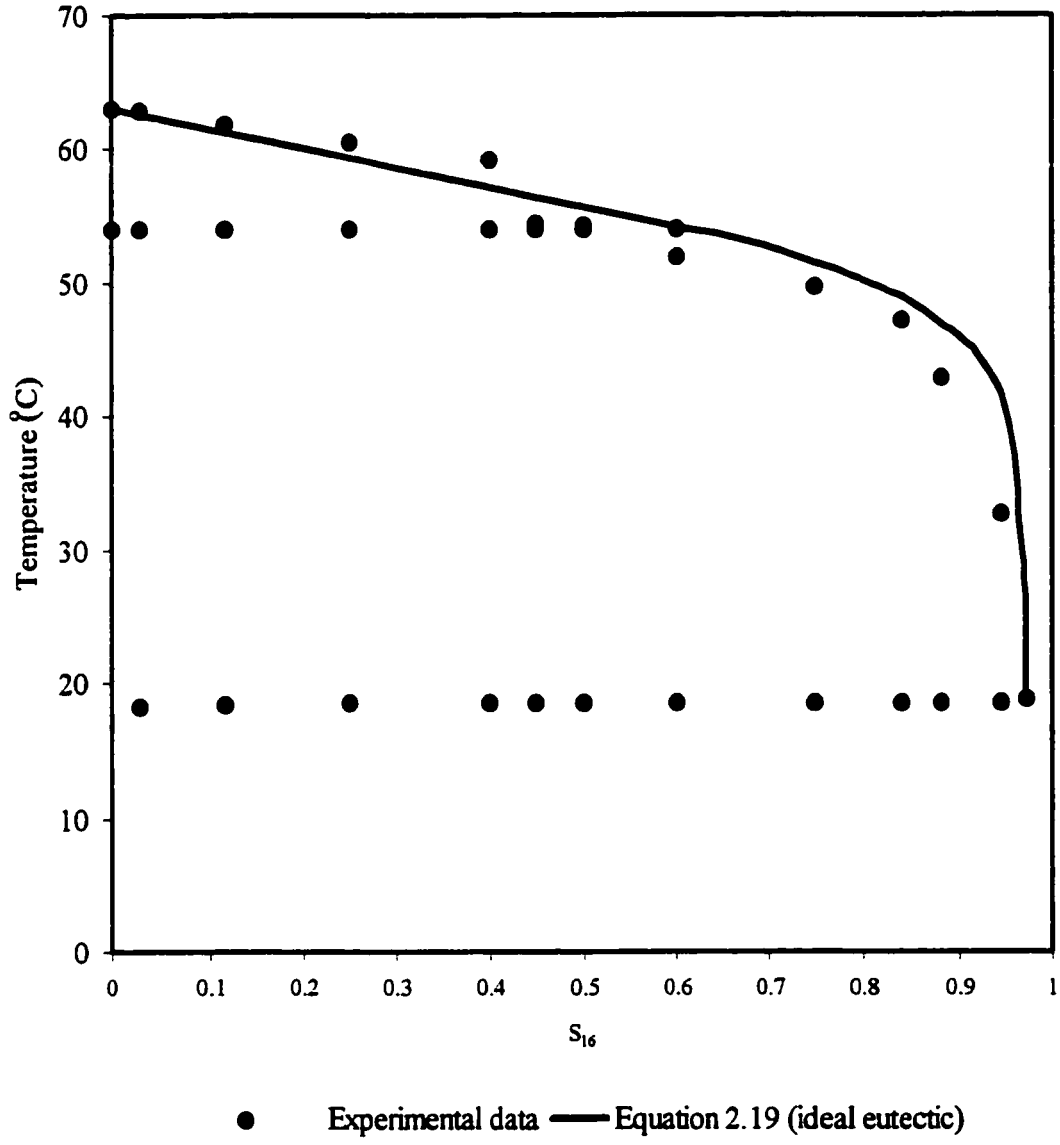

temperature of 65°C. As we start cooling the liquid, no change of phase occurs until the temperature of 57°C is reached. At this temperature, pure solid of C_{28} will just begin to crystallise. When this occurs, the liquid phase will become slightly leaner in C_{28}.

If the temperature is further lowered then more solid of C_{28} will separate, and so the proportion of C_{28} in the liquid phase will decrease; that is, the composition of the liquid phase moves along the liquidus curve. On further cooling down to 18.5°C, pure solid C_{28} continues to separate out and the composition of the liquid varies along the line. At this temperature, the eutectic temperature, pure solids of C_{28} and C_{16} coexist with a liquid of eutectic composition. Any attempt at further cooling will lead to complete crystallization; the temperature will remain constant at 18.5°C, while the liquid freezes with simultaneous formation of solid C_{28} and solid C_{16}. The presence of a peritectic point was observed around 50% of C_{16}.

The solid product is considered thermodynamically to be a mechanical mixture of pure solid of C_{28} and C_{16}, although it might microscopically consist of crystalline C_{28} and crystalline C_{16} at the eutectic composition (Lee, 1977).

An interesting feature can be observed in the concentration range of 40% to 45% of C_{16}. Although the increase in concentration is not significant, the decrease in the measuring temperature is remarkable, 4.7°C. Repeating measurements with different samples confirmed the results of this measurement, as well as others doubtful results. This peculiar behavior can be attributed to the fact that in this concentration range the solid-liquid and solid-solid peaks had merged.

The values of the melting temperature determined by DSC do not correspond very well to those predicted by ideal solution theory, especially for high value of percentage of C_{16}.

Using values of equilibrium melting temperatures and theoretical values of total enthalpy, all these equilibrium calculations were done. As mentioned earlier, this mixture exhibits a solid-solid transition up to 50% of C_{16} in the mixture and temperature of 54°C. A new calculation was completed using the value of enthalpy of fusion (Schaerer, et al., 1954) instead of value of total enthalpy (sum of enthalpy of fusion and transition enthalpy) for concentration range where mixture melts without any solid-solid transition. Although a value of enthalpy decreases by 33%, the difference in calculated equilibrium temperature is insignificant, less than 0.5°C or 1.5%.

It can be concluded as the concentration of C_{16} increases in the mixture, the corresponding temperature calculated from ideal behaviour theory more and more overpredicts the experimental value; a fact pointing to a non-ideal behaviour of mixture. Non-ideal behaviour increases by approaching the eutectic temperature and composition.

4.3.2.2 Calculation Based on Regular Solution Theory

To explain the non-ideality of the system, the regular solution theory was used, with ρ_o being an adjustable parameter that was proposed to account for non-zero heat of mixing (Lee, 1978). All the liquid temperature (T_m^E) were calculated using the Equation 2.20 with values of total transition enthalpy ΔH_{tot} estimated from theoretical equation of Dollhopf et al. (1981). The experimental results were fitted into Equation 2.20 and a satisfactory match between experimental and calculated values was obtained for value of ρ_o= 2.53 kJ/mol. The experimental results and predictions based on regular solution theory are compared in Table 4.6 and Figure 4.16.

Table 4.6 Experimental and calculated equilibrium values of (T_m^E) and T_E for C_{16}+C_{28} eutectic mixture

S_{16}	(T_m^E) exp[1]	T_E exp[2]	$(T_m^E)_j$ calc[4]	error[4] (°C)
0.00	63.0	-	-	-
0.03	62.9	18.3	62.8	-0.1
0.10	61.8	18.3	62.3	0.5
0.25	60.5	18.4	60. 6	0.1
0.40	59.1	18.5	58.4	-0.7
0.45	54.4	18.5	57.6	3.2
0.50	54.3	18.6	56.7	2.4
0.60	51.9	18.6	54.4	2.5
0.75	49.4	18.6	50.7	1.3
0.80	47.1	18.5	48.8	1.7
0.90	42.9	18.6	43.4	0.5
0.92	32.6	18.5	41.0	8.4
0.94	18.5	18.6	39.7	20.8
1.00	18.8	-	-	-

[1] values corresponding to the return to the baseline of the high temperature exotherm

[2] values corresponding to the low temperature peak

[3] values calculated using Equation 2.20 with ρ_o=2.53 kJ/mol

[4] difference between experimental and calculated (T_m^E) values

Figure 4.16 Phase diagram for C_{16}+C_{28} binary mixture; Comparison between experimental data and model assuming non-ideal behavior of the mixture

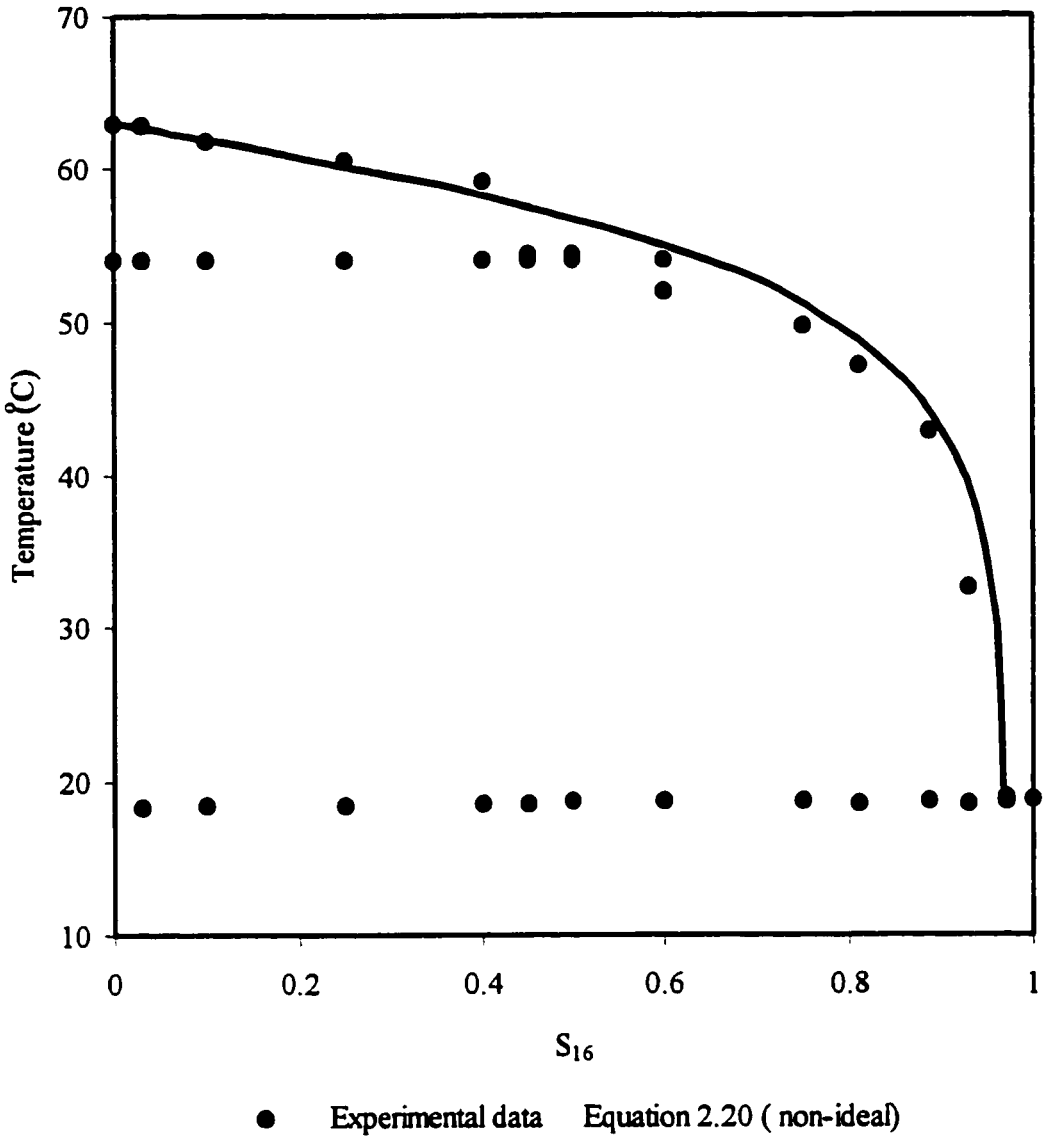

In order to indicate the sensitivity of calculated values of temperature on the different value of ρ_o, two different values of ρ_o were applied in the Equation 2.20. One of these values was 20% larger (ρ_o =3.04 kJ/mol) and the other one was 20% smaller (ρ_o =2.02 kJ/mol) than the "optimum" value of the ρ_o. The result of this calculation is shown at the Figure 4.17. As can be seen from the figure regardless of the value of ρ_o the calculated temperatures were similar with maximum difference of 0.3 °C.

The calculation and experimental temperatures are in a much better agreement. Experimental data agree very well with calculation up to a certain temperature and concentration (60% of C_{16} in the mixture and temperature of 53°C). Beyond that the mixture melts at a lower temperature than the calculation predicts. This discrepancy between the calculated values and experimental data could be due to the difficulty in separation melting and transition peaks, as the phase transition occurs in the same temperature range as the change in the crystalline structure.

4.3.2.3 Calculation Based on Won's (1986) and Pedersen et al. 's (1991) Models

The adequacy of Won's (1986) and Pedersen et al.'s (1991) models was tested for the binary mixture of C_{16}+C_{28}. All values were calculated using the Equation 2.38. The difference between these two methods is the values for solubility parameters in the liquid and in the solid phases. Both Won's and Pedersen et al.'s models give nearly the same values of solubility parameters in liquid phase throughout the range of carbon numbers. The variation is greater in the value of the solid phase solubility parameters predicted by

Figure 4.17 Sensitivity of the value of temperature on the different value of ρ_0

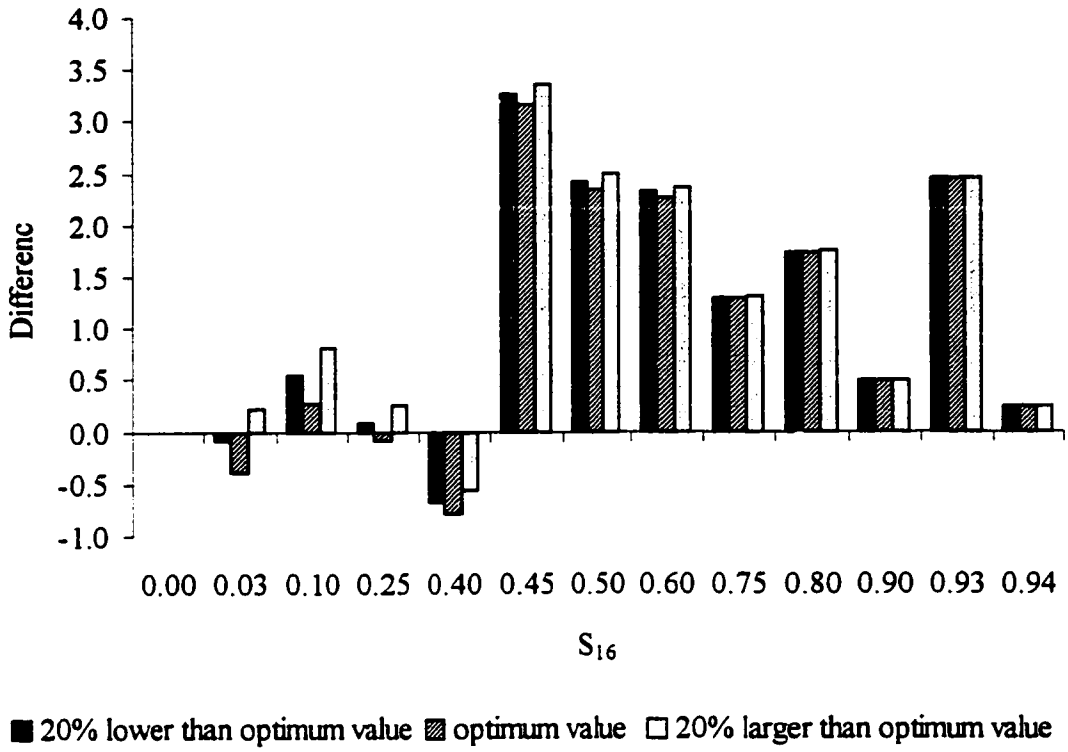

Won, and Pedersen. Pedersen's correlation gives 70% higher values for solid phase solubility, than those predicted by Won.

Results of calculation using parameters obtained with the Won's model are shown in Table 4.7. Figure 4.18 represents the corresponding phase diagram for the mixture, where solid-liquid equilibrium line on the diagram is calculated by using Won's model.

The Won's model prediction follows the experimental data accurately, especially for low concentration of C_{16}. The discrepancies between model prediction and the experimental data, in concentration range from 45% to 60% of C_{16}, can be attributed, again, to the fact that in this concentration range the solid-liquid and solid-solid peaks had merged. In the concentration range around eutectic composition, the predictions from Won's model are much better compared to the ideal behaviour and regular solution theory, although the model still over predicts the eutectic temperature and composition.

Results of calculation using parameters obtained with the Pedersen's correlation and measurements of equilibrium melting temperature are shown in the Table 4.8. Figure 4.19 represents the comparison between the experimental results and phase diagram obtained by using the model predictions.

Both models give about the same difference between experimental data and model prediction, as reported in the case of ideal and non-ideal solution theory for the range of compositions were melting peak overlaps solid-solid transition peak for the reason given above. Both models yield good prediction at low concentrations of C_{16} and give the best predictions at the region around the eutectic temperature and composition.

Results of calculation for ideal, non-ideal theory, Won's (1986) and Pedersen et al.'s (1991) model show the same trend, although the calculations usually over predict the

Table 4.7 Experimental and calculated equilibrium values of (T_m^E) and T_E for C_{16}+C_{28} eutectic mixture

S_{16}	(T_m^E) exp[1]	T_E exp[2]	(T_m^E) Won[3]	error[4] (°C)
0.00	63.0	-	63.0	-
0.03	62.9	18.3	62.8	0.1
0.10	61.8	18.3	62.2	-0.4
0.25	60.5	18.4	60.2	0.3
0.40	59.1	18.5	58.5	0.6
0.45	54.4	18.5	57.8	-3.4
0.50	54.3	18.6	56.9	-2.6
0.60	51.9	18.6	55.0	-3.1
0.75	49.4	18.6	51.1	-1.6
0.80	47.1	18.5	49.3	-2.2
0.90	42.9	18.6	43.8	-0.9
0.92	32.6	18.5	41.1	-8.4
0.94	18.5	18.5	37.2	-18.3
1.00	18.8	-	18.8	-

[1] values corresponding to the return to the baseline of the high temperature exotherm

[2] values corresponding to the low temperature peak

[3] values calculated using Equation 2.38 with solubility parameters from Won's (1986) model

[4] difference between experimental and calculated (T_m^E) values

Figure 4.18 Phase diagram for C_{16}+C_{28} binary mixture; Comparison between experimental data and Won's model (1986)

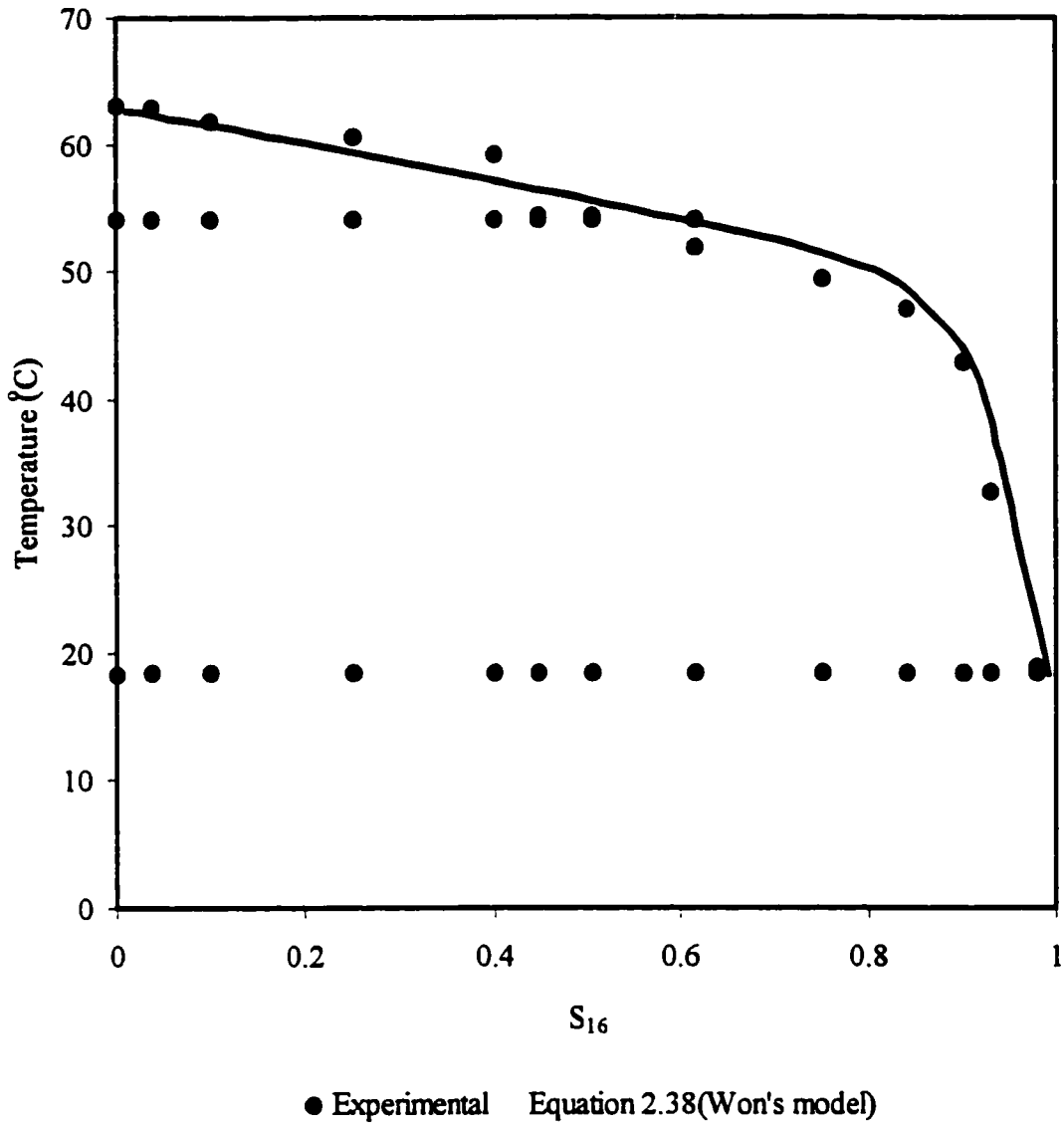

Table 4.8 Experimental and calculated equilibrium values of (T_m^E) and T_E for C_{16}+C_{28} eutectic mixture

S_{16}	(T_m^E) exp[1]	T_E exp[2]	(T_m^E) Pedersen[3]	error[4] (°C)
0.00	63.0	-	63.0	0.0
0.03	62.9	18.3	62.8	0.1
0.10	61.8	18.3	62.1	-0.3
0.25	60.5	18.4	60.3	0.2
0.40	59.1	18.5	58.2	0.9
0.45	54.4	18.5	57.4	-3.0
0.50	54.3	18.6	56.5	-2.2
0.60	51.9	18.6	54.5	-2.6
0.75	49.4	18.6	50.3	-0.9
0.80	47.1	18.5	48.4	-1.3
0.90	42.9	18.6	42.4	0.5
0.92	32.6	18.5	39.4	-6.8
0.94	18.5	18.5	35.5	-16.6
1.00	18.8	-	18.8	-

[1] values corresponding to the return to the baseline of the high temperature exotherm

[2] values corresponding to the low temperature peak

[3] values calculated using Equation 2.38 with solubility parameters from Pedersen et al.'s (1991) model

[4] difference between experimental and calculated (T_m^E) values

Figure 4.19 Phase diagram for C_{16}+C_{28} binary mixture; Comparison between experimental data and Pedersen et al.'s model (1991)

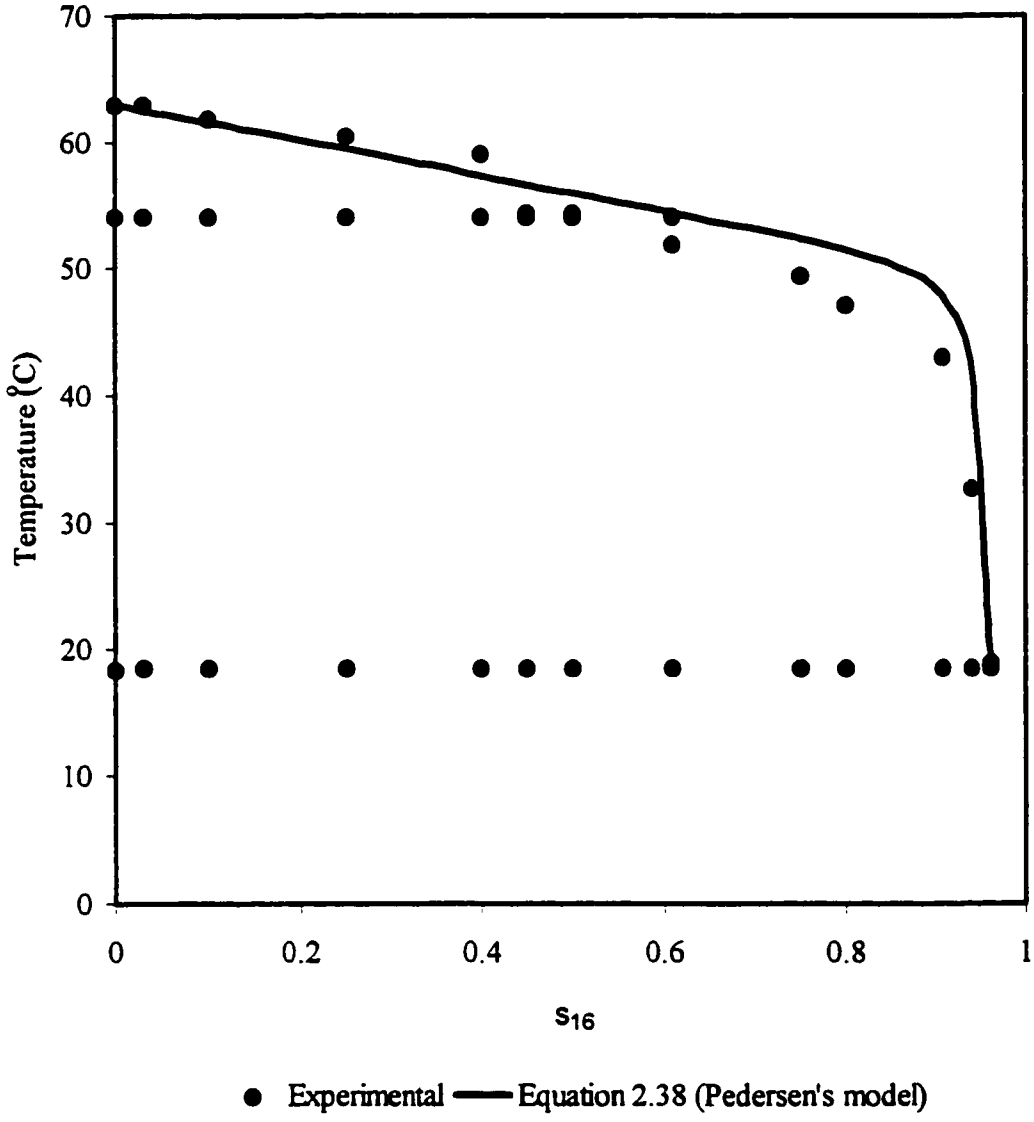

temperature around the eutectic point. In the concentration range where the melting peak overlaps the transition peak, dilemma exists in obtaining the experimental results correctly, and due to that uncertainty, all four models produce the similar mismatch of over predicting the melting temperature of the mixture.

4.3.3 Analysis of DSC Thermograms for C_{16}+C_{41} Mixture

The DSC thermograms for C_{16}+C_{41} mixture are presented in Figure 4.20. Unlike in the case of the pure components, where pure C_{16} and C_{41} exhibits just one peak, corresponding to the solid-liquid transformation, all mixtures (except for 95% and 96% of C_{16}) exhibit two peaks. The DSC thermograms are qualitatively similar to those observed with the C_{16}+C_{28} mixture. The low temperature peaks occurs at the same temperature despite of concentration. As the concentration of C_{16} increases the melting point depression of mixture increases. From this evidence, it can be concluded that the eutectic system is formed.

A lack of solid-solid transition peak in the mixture and the absence of composition range where that peak is overlapped with melting peak allowed measurement of smaller diversity of concentration in C_{16}+C_{41} mixture, than in case of C_{16}+C_{28} mixture.

Although the melting point depression was observed, no noticeable broadening of the peak occurred as the concentration of C_{41} increased in the mixture. Compared to the C_{16}+C_{28} mixture that difference can presumably be explained by the large peak height-width ratio.

Figure 4.20 DSC melting thermograms of C_{16}+C_{41} binary mixture (mole fraction of C_{16} are shown in the figure)

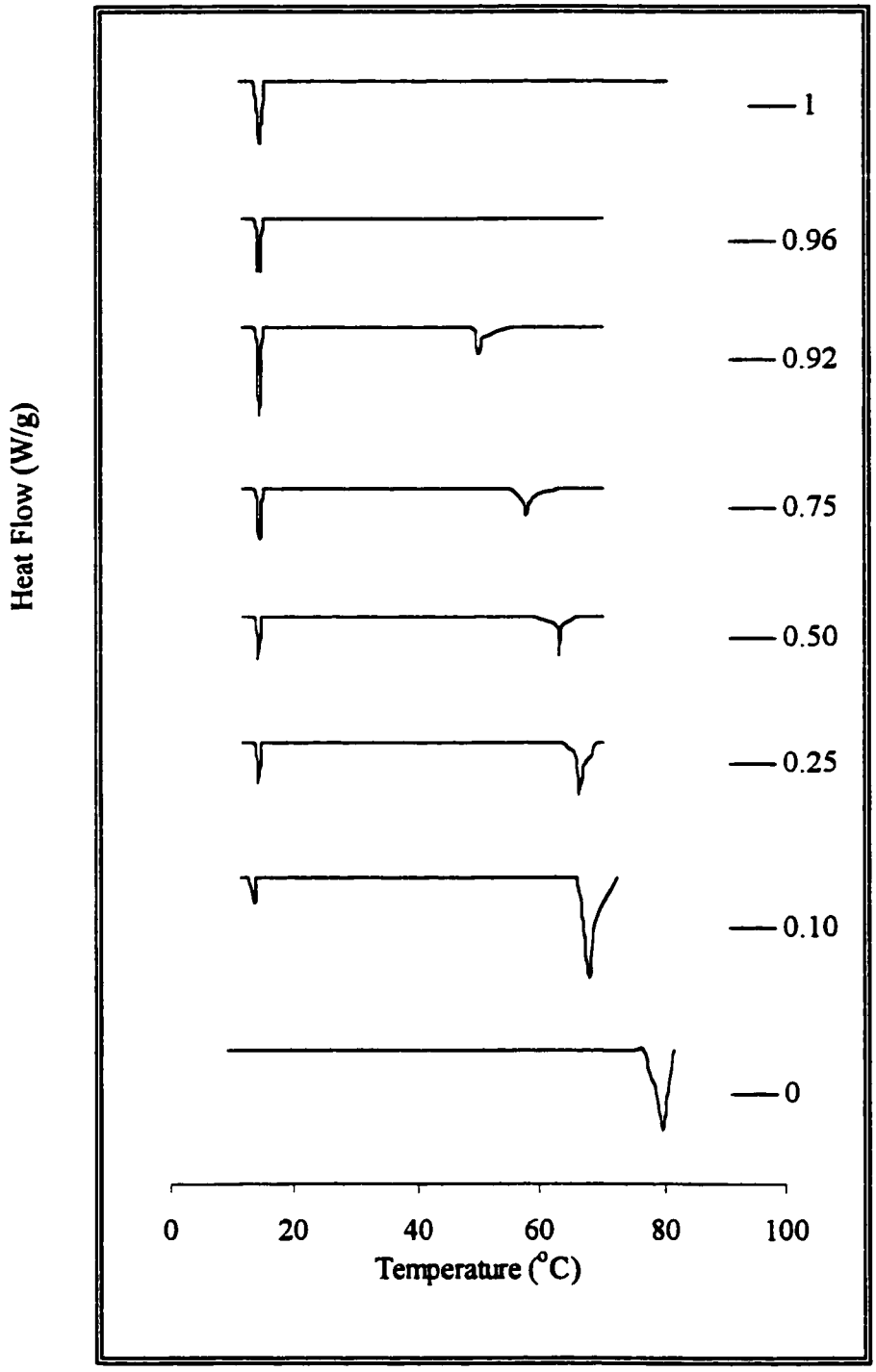

The difference between the melting temperature of the higher molecular weight component C_{41} and calculated melting temperature is the melting point depression. That lowering of the melting temperature is due to the diluent effect of the low molecular weight component in the mixture, C_{16}. The melting point depression for C_{41} is 32°C for the highest concentration of C_{16} in the mixture.

For comparison, calculations of liquidus temperature curve, based on ideal assumption, regular solution theory, Won's and Pedersen et al.'s models are presented in Table 4.9. These calculations are presented along with the mole fraction of C_{16} in the mixture and corresponding experimental melting temperatures.

Due to a large difference in the chain length between C_{16} and C_{41}, calculations based on the ideal solution theory produced the closest match with experimental data. The eutectic temperature is over predicted, but up to 92% (eutectic composition is at 96% of C_{16} in the mixture) of the C_{16} in the mixture the ideal solution theory gives a good estimation of the melting temperature. It can be concluded that since both C_{41} and C_{16} from the solid phase independently, each component has the crystalline form characteristics of its respecting pure component. The difference between experimental results and prediction of ideal solution theory around eutectic temperature can be probably explain by the fact that during the crystallization the small molecule of C_{16} is trapped by C_{41} during the simultaneous solidification.

The regular solution theory as well as Won's and Pedersen et al.'s model overpredict the temperature and produced the greater deviation from experimental data. The empirical parameter in regular solution theory, which takes in to account non-zero heat of mixing,

Table 4.9 Experimental and calculated equilibrium values of (T_m^E) and T_E for C_{16}+C_{41} eutectic mixture

S_{16}	(T_m^E) exp[1]	T_E exp[2]	(T_m^E) calc[3]	T_E calc[3]	(T_m^E) calc[4]	(T_m^E) calc[5]	(T_m^E) calc[6]
0.00	84.3	-	84.3	-	-	84.3	84.3
0.10	81.6	17.9	79.9	18.0	80.6	83.5	83.5
0.25	79.1	18.0	79.3	18.0	79.8	82.2	82.2
0.50	75.9	18.0	77.1	18.0	77.3	79.4	79.4
0.75	68.8	18.1	72.9	18.0	72.9	74.8	75.0
0.92	59.3	18.0	65.9	18.0	65.8	67.1	67.6
0.96	18.3	18.3	60.8	18.0	62.5	63.9	64.3
1.00	18.8	-	18.8	18.8	-	18.8	18.8

[1] values corresponding to the return to the baseline of the high temperature exotherm

[2] values corresponding to the low temperature peak

[3] values calculated using Equation 2.19

[4] values calculated using Equation 2.18 with ρ_o=1.54 kJ/mol

[5] values calculated using Equation 2.38 with solubility parameters from Won's (1986) model

[6] values calculated using Equation 2.38 with solubility parameters from Pedersen et al.'s (1991) model

was found to be ρ_o=1.54 kJ/mol. That value is the smallest value compared to the other two binary mixtures examined in this study, and to the values presented by Hammami (1994) for C_{44}+C_{50}, and Bhat (1996) for C_{37}+C_{41} mixture. The smallest value of empirical parameter shows that the mixture is nearly ideal due to the large difference in chain length of 25 carbon atoms.

The eutectic phase diagrams based on the calculations and DSC heating thermograms are shown in Figure 4.21. A comparison of the different phase diagrams presented in Figure 4.21 shows that the melting temperature predicted by the ideal behavior theory is the closest to the experimental curve, and that other theories have a greater discrepancy between the theoretical and experimental curves.

4.3.4 Analysis of DSC Thermograms for C_{28}+C_{41} Mixture

Figure 4.22 represents the heating DSC thermograms of C_{28}+C_{41} mixture. All thermograms are arranged in the order of decreasing C_{28} concentration in the mixture.

It can be seen that all thermograms (except for 90%, 92% and 95% of C_{28}) show appearance of the three peaks. The high temperature peak is the illustration of solid-liquid phase change. It represents the melting temperature of C_{41}. From the presented thermograms it can be seen that two lower temperature peaks occur at constant temperature regardless of concentration. The first of these peaks, one at the higher temperature, is for liquid-solid transitions of C_{28}, and temperature of that peak is eutectic temperature of binary mixture. The lowest temperature peak represents the solid-solid transformation of C_{28}.

Figure 4.21 Phase diagram for C_{16}+C_{41} binary mixture; Comparison between experimental data and predictions assuming ideal, non-ideal behavior, Won's (1986) and Pedersen et al.'s (1991) models

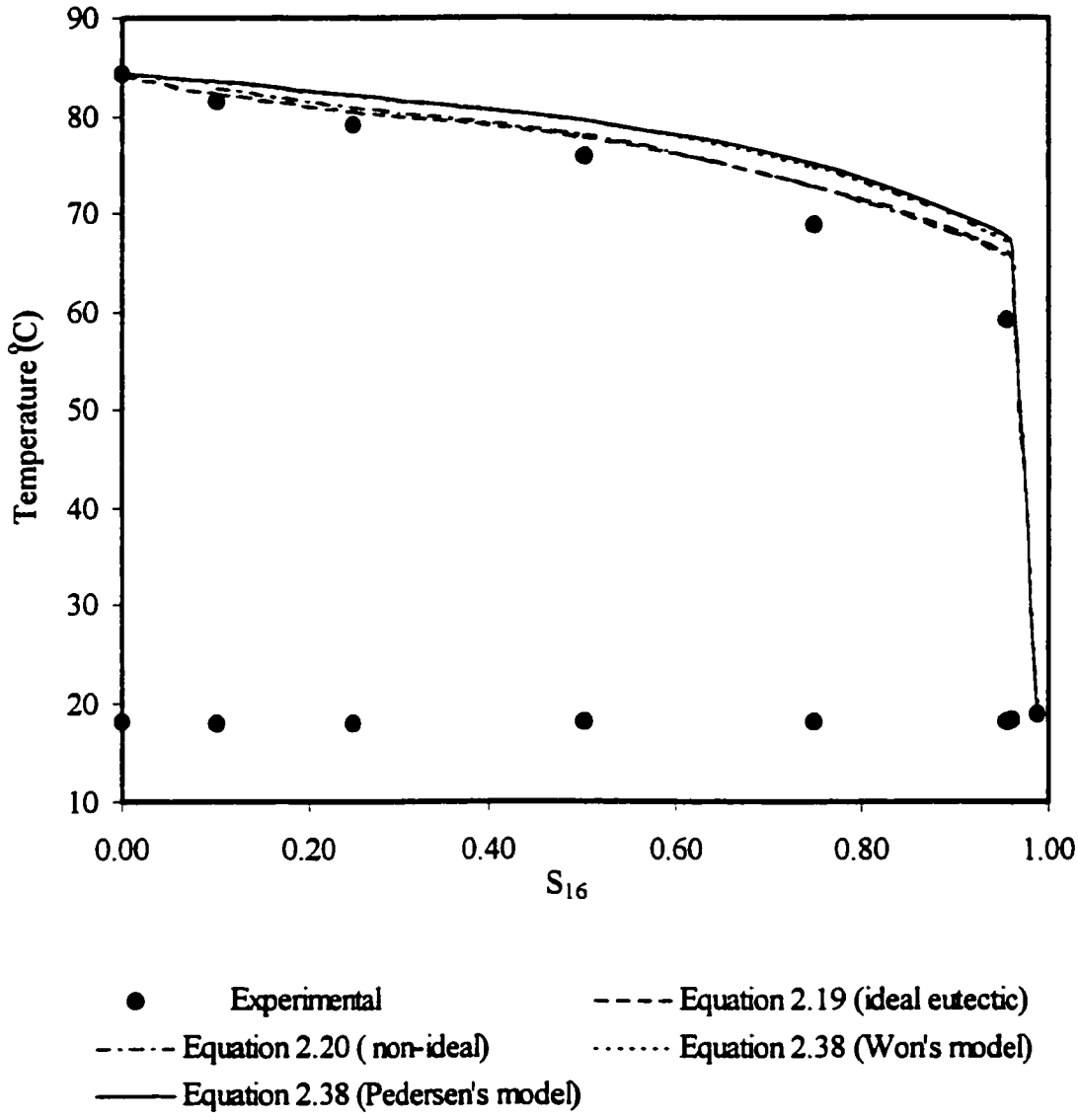

Figure 4.22 DSC melting thermograms of C_{28}+C_{41} binary mixture (mole fraction of C_{28} are shown in the figure)

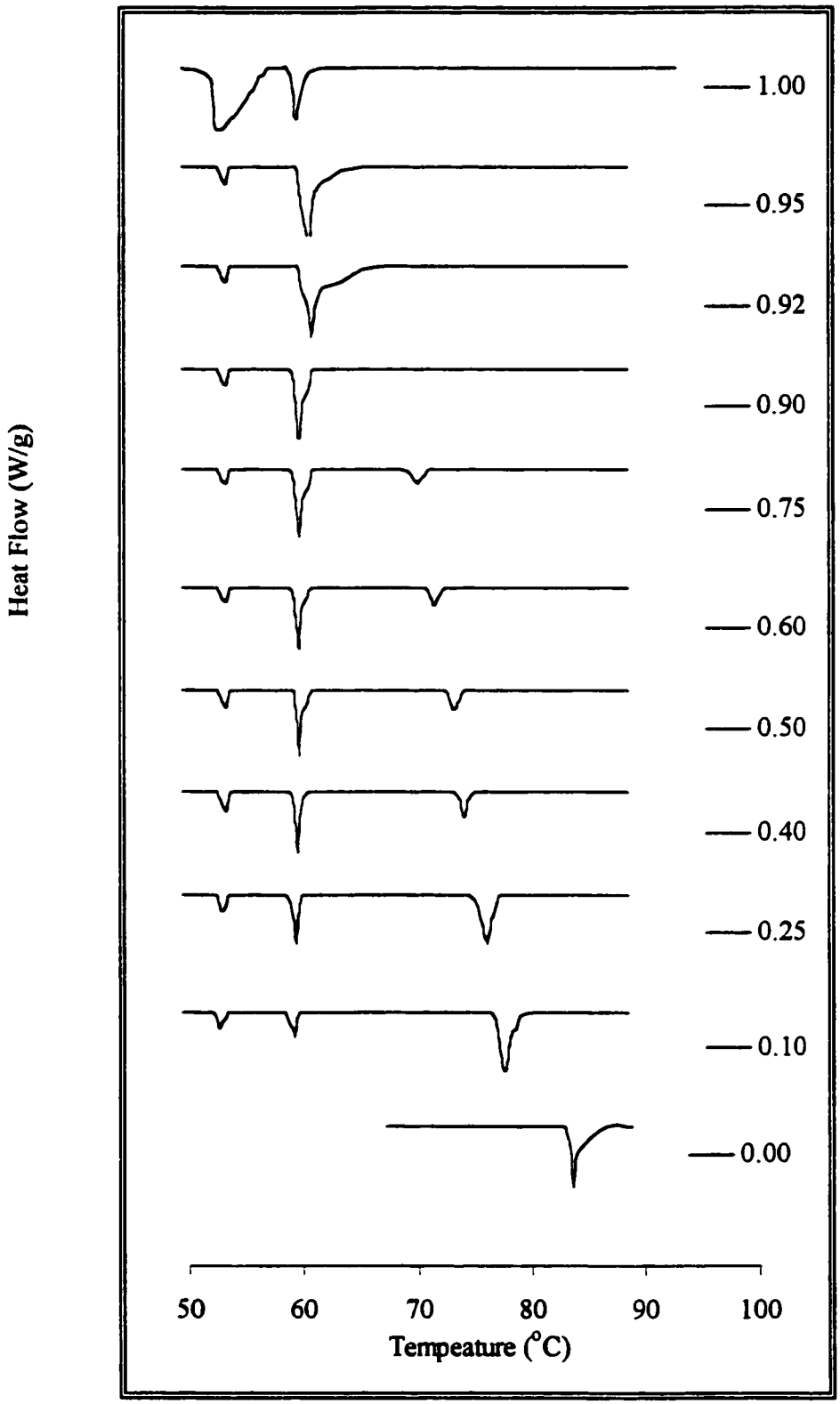

The pure C_{28} melts at 62.9°C and the temperature of 61.8°C± 0.5°C is the experimentally obtained eutectic temperature of the mixture. This result is in agreement with the other studies of *n*-alkane eutectic mixture, which show that eutectic mixture melts within one degree of the pure hydrocarbon of shorter chain length (Mazee, 1949, 1957; Butler and MacLeod, 1961; Hammami, 1994; Bhat, 1996).

Again, the melting point of the mixture was systematically and progressively depressed by increasing C_{41} concentration, and for the highest concentration of C_{28} depression is 21.5°C.

The Table 4.10 summarizes the solid-solid transition temperatures as well as the eutectic temperature for this mixture for heating and cooling experiments. From this table it can be seen that solid-solid transition temperature of pure C_{28} is 57.5°C and the same transition in the mixture occurs at the 54.3°C ± 0.8°C for heating experiments and 50.3°C ± 0.3°C for cooling ones. The value of standard deviation is greater for heating experiments because of slight broadening of the peak.

From other experimental studies of eutectic binary mixture (Hammami, 1994; Bhat, 1996) and C_{16}+C_{28} binary mixtures investigated in this study, it can be concluded that the solid-solid transition occurs at the same temperature for pure *n*-alkanes and the mixture. In the case of C_{28}+C_{41} mixture the transition occurs the temperature lower for 3.2°C. Lowering of the solid-solid transition temperature can be explained by formation of mixed crystal in the solid phase instead of eutectic-separate extension chains. A recent study done by Dirand el at. (1998), indicate that solid behavior of binary mixtures of *n*-alkanes is far more complicated that what is found in the literature. Findings from that study can explain the anomalies observed in this binary mixture.

Table 4.10 Experimental values of solid-solid transition peak and T_E for C_{28}+C_{41} eutectic mixture

	Heating thermograms		Cooling thermograms	
C_{28}	T_β(°C)	T_E (°C)	T_β (°C)	T_E (°C)
0.00	-	-	-	-
0.10	61.3	53.9	60.4	50.1
0.25	61.4	54.0	60.3	50.3
0.40	61.7	54.1	60.4	50.3
0.50	61.8	54.2	60.4	50.5
0.60	61.8	54.2	60.4	50.6
0.75	61.8	54.2	60.4	50.8
0.90	61.8	54.3	60.5	50.6
0.92	62.8	54.4	60.5	50.6
0.95	62.8	54.4	60.8	50.6
1.00	62.9	57.5	60.2	54.7

In the solid state according to this study instead of appearance of one solid-solid transition, many orthorhombic intermediate phases can be detected and formation of mixed crystals is possible. Mole fraction of C_{28} in the mixture, experimental melting points and models calculation prediction of depressing the liquid temperature are listed in Table 4.11. The predictions for the depression of the liquidus temperature are calculated from ideal, regular solution theory and Won's and Pedersen et al.'s models.

From the results presented in Table 4.11 we can see that the theory assumes the ideal mixture behavior and that Won's model overpredicts melting temperature of the mixture. The difference, error, observed in the calculated liquidus temperature of the mixture by ideal solution theory is possibly because, in spite of the great difference in chain length, the mixture is highly non-ideal and some mixing in the solid state occurs. The reason for temperature overprediction by Won' model is perhaps the small value for the solubility parameter in the solid state.

The results presented in the Table 4.11 show that both regular solution theory and Pedersen et al.' s model yield good results for the liquidus temperature, but at different concentration ranges. Up to 50% of C_{28} in the mixture melting points calculated based on non-ideal behavior of the mixture best fits experimental results. The empirical parameter used to produce the closest match to experimental results for C_{28}+C_{41} mixture was ρ_o=2.05 kJ/mol. The Pedersen et al.'s model over the same concentration region (from 0% up to 50% of C_{28}) overpredicts the melting temperature of the mixture, but as the concentration of C_{28} increases the prediction is much better and the model gives the best fitt to the experimental data. The eutectic temperature and composition predicted by Pedersen et al.'s model are in good agreement with experimental results.

Table 4.11 Experimental and calculated equilibrium values of (T_m^E) and T_E for C_{28}+C_{41} eutectic mixture

S_{28}	(T_m^E) exp[1]	(T_m^E) calc[2]	(T_m^E) calc[3]	(T_m^E) calc[4]	(T_m^E) calc[5]
0.00	84.3	84.3	-	84.3	84.3
0.10	82.4	81.1	81.6	83.6	83.5
0.25	80.8	80.6	80.9	82.5	82.2
0.40	78.3	79.6	79.8	81.1	80.6
0.50	77.3	78.7	78.8	79.9	79.3
0.60	75.3	77.6	77.7	78.6	77.8
0.75	73.8	75.3	75.3	75.9	74.5
0.90	68.8	71.1	71.2	71.4	68.4
0.92	63.0	69.9	69.9	70.1	66.5
0.95	62.8	68.5	68.5	69.2	63.9
1.00	63.0	62.9	-	63.0	63.0

[1] values corresponding to the return to the baseline of the high temperature exotherm

[2] values calculated using Equation 2.19

[3] values calculated using Equation 2.20 with ρ_o=2.05 kJ/mol

[4] values calculated using Equation 2.38 with solubility parameters from Won's (1986) model

[5] values calculated using Equation 2.38 with solubility parameters from Pedersen et al.'s (1991) model

The eutectic phase diagram for binary solids formed from C_{28}+C_{41}, constructed from experimental data and theoretical calculation, is presented in the Figure 4.23.

4.3.5 Analysis of the Value of Empirical Parameter in the Regular Solution Theory

The regular solution theory (Equation 2.20) describes deviation of mixture from the ideal behaviour. The non-ideality is caused mainly due to the non-zero heat of mixing. Empirical interaction parameter, ρ_o, is proposed to calculate the heat of mixing by using the relation $\Delta H_m = \rho_o x_1 x_2$.

In the present study, three binary mixtures of *n*-alkanes were studied. For each mixture the experimental results were compared with predictions of regular solution theory. The empirical, parameter ρ_o was proposed for each mixture. By adjusting values of the ρ_o the best fit of theory prediction and experimental data was achieved. Analysis of five values of empirical parameter, ρ_o, was done. Three of these values are from the present study and two of them were from the literature. Hammami (1994) for the C_{44}+C_{50} mixture proposed a value of ρ_o=3.86 kJ/mol, and Bhat (1996) determined the value of ρ_o for the C_{37}+C_{41} mixture to be 5.70 kJ/ mol. Binary mixture and corresponding values of the ρ_o, the difference in the chain length, Δn, were given in the Table 4.12. The table also contains the value of the ±20% "optimum" values of ρ_o, hence there is no strong dependence of the values of calculated temperature and values of the ρ_o (Figure 4.17).

The empirical parameters were fitted to an equation. Figure 4.24 contains values of ρ_o versus difference in the chain length Δn. A adequate representation (R^2=0.992) of the

Figure 4.23 Phase diagram for C_{28}+C_{41} binary mixture; Comparison between experimental data and predictions assuming ideal, non-ideal behavior, Won's (1986) and Pedersen et al.'s (1991) models

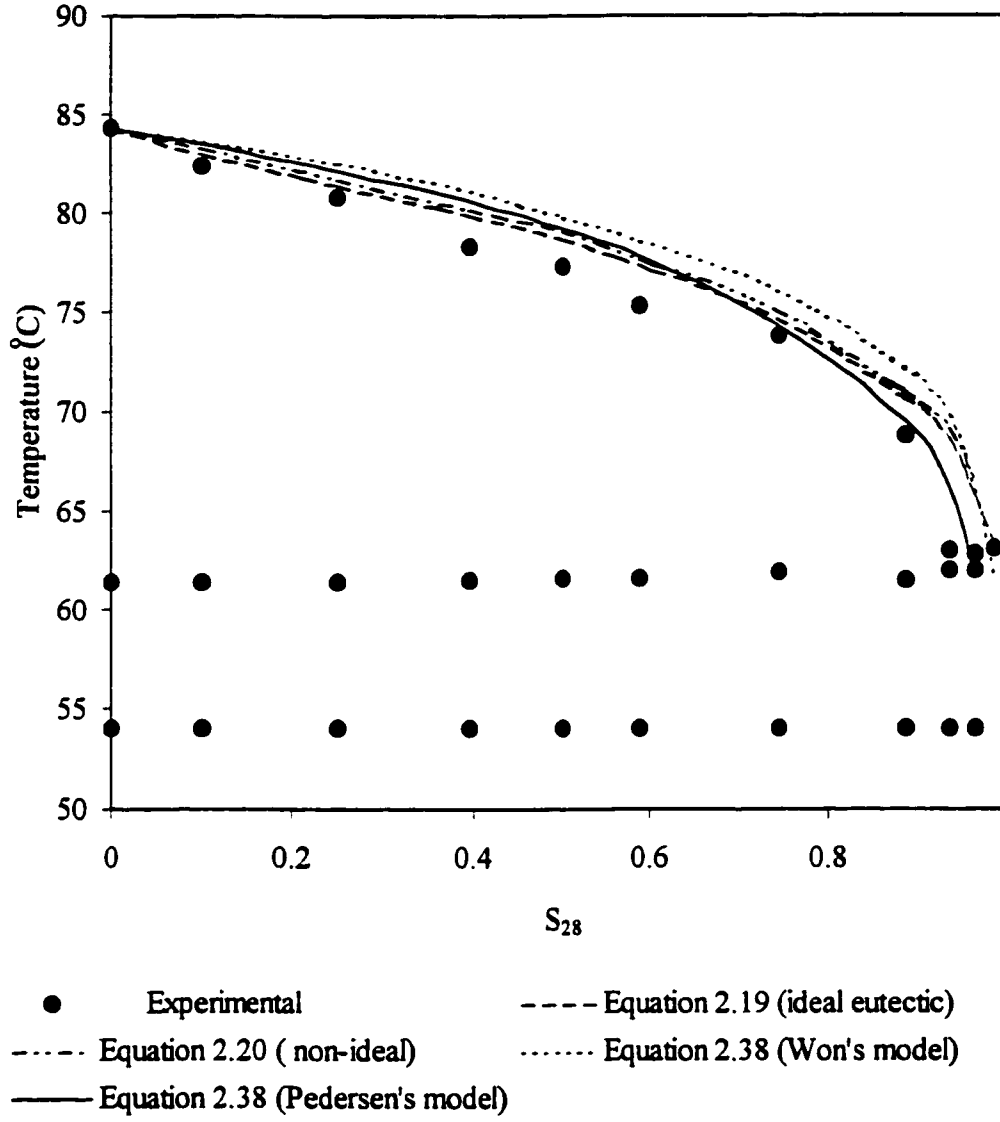

Table 4.12 Binary mixture and corresponding values of the empirical coefficients, ρ_o (kJ/mol)

n1	n2	Δn	ρ_0 (kJ/mol)[1]	ρ_0 (kJ/mol)[2]	ρ_0 (kJ/mol)[3]
37	41	4	5.70	6.84	4.56
44	50	6	3.86	4.63	3.09
16	28	12	2.53	3.04	2.02
28	41	13	2.05	2.46	1.64
16	41	25	1.54	1.85	1.23

[1] optimum values of ρ_0 (kJ/mol)

[2] 20% larger value than optimum

[3] 20% smaller value than optimum

Figure 4.24 Values of empirical coefficient ρ_0 (kJ/mol) versus the difference in the chain length of *n*-alkanes forming binary mixture

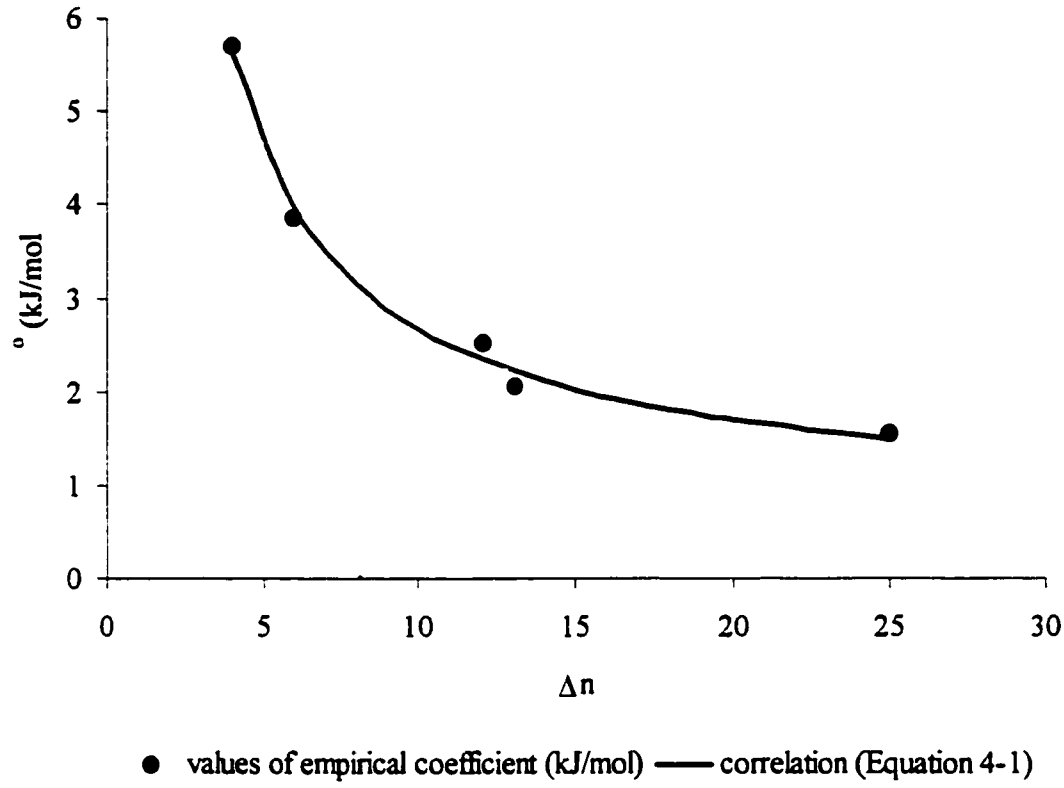

results is given by the following correlation:

$$\rho_0 = 0.706 + \frac{19.70}{\Delta n} \qquad 4\text{-}1$$

It is important to note that Equation 4-1 should be used only for eutectic mixtures. If the difference in chain length is outside of boundary conditions for the formation of solid solution according to Equation 2-10 (Matheson and Smith, 1985) or Equation 2-11 (Bhat, 1996), the Equation 4-1 can be used for the estimation of ρ_o. Equation 4-1 is in agreement with the theory of binary mixtures of *n*-alkanes. In case of broad range in chain length difference between *n*-alkanes forming the binary mixture, the value of the parameter ρ_o would be smaller and smaller as the difference increases; the larger the difference between two paraffins the smaller the effect of heat of mixing would be.

Table 4.13 contains binary mixture values of the ρ_o and prediction of the empirical parameter ρ_o calculated by using Equation 4.1. The values predicted by Equation 4.1 are in good agreement with values of ρ_o found in this study and literature.

Table 4.13 Comparison of empirical determined values of parameter ρ_o and values calculated by proposed equation

n1	n2	Δn	ρ_0 (kJ/mol)[1]	ρ_0 (kJ/mol)[2]
37	41	4	5.70	5.63
44	50	6	3.86	3.99
16	28	12	2.53	2.35
28	41	13	2.05	2.22
16	41	25	1.54	1.49

[1] actual values of ρ_0 (kJ/mol)

[2] value calculated by Equation 4.1

CHAPTER 5

TERNARY MIXTURE

Attempts have been made to explain all interactions between *n*-alkanes in order to create a model, which would describe solid deposition in crude oil.

In the present study examination of the pure *n*-alkanes and their binary mixtures were done. Four samples of ternary mixture were studied to investigate the presence and importance of interaction between paraffins; to compare the effect of *n*-alkane interactions in their binary and ternary mixtures; to determine the ability of the existing models to describe the ternary system.

The melting DSC curve for the ternary mixture is presented in the Figure 5.1. All thermograms exhibit three peaks. The thermograms of the C_{16}+C_{28}+C_{41} mixture retained practically all-general characteristics of the pure *n*-alkanes and appear to be superposition of thermogram of pure alkanes forming the ternary mixture. All thermograms exhibit a low temperature peak whose position is independent of the mixture composition. Thus it can be concluded that ternary mixture of C_{16}+C_{28}+C_{41} form immiscible system.

5.1 Analysis of DSC Thermograms of Ternary Mixture

From these DSC thermograms, experimental equilibrium melting temperatures as well as mixture compositions are presented in the Figure 5.1. No noticeable broadening of the

Figure 5.1 DSC melting thermograms of C_{16}+C_{28}+C_{41} ternary mixture (mole percents of C_{16}, C_{28}, C_{41} are shown in the figure, respectively)

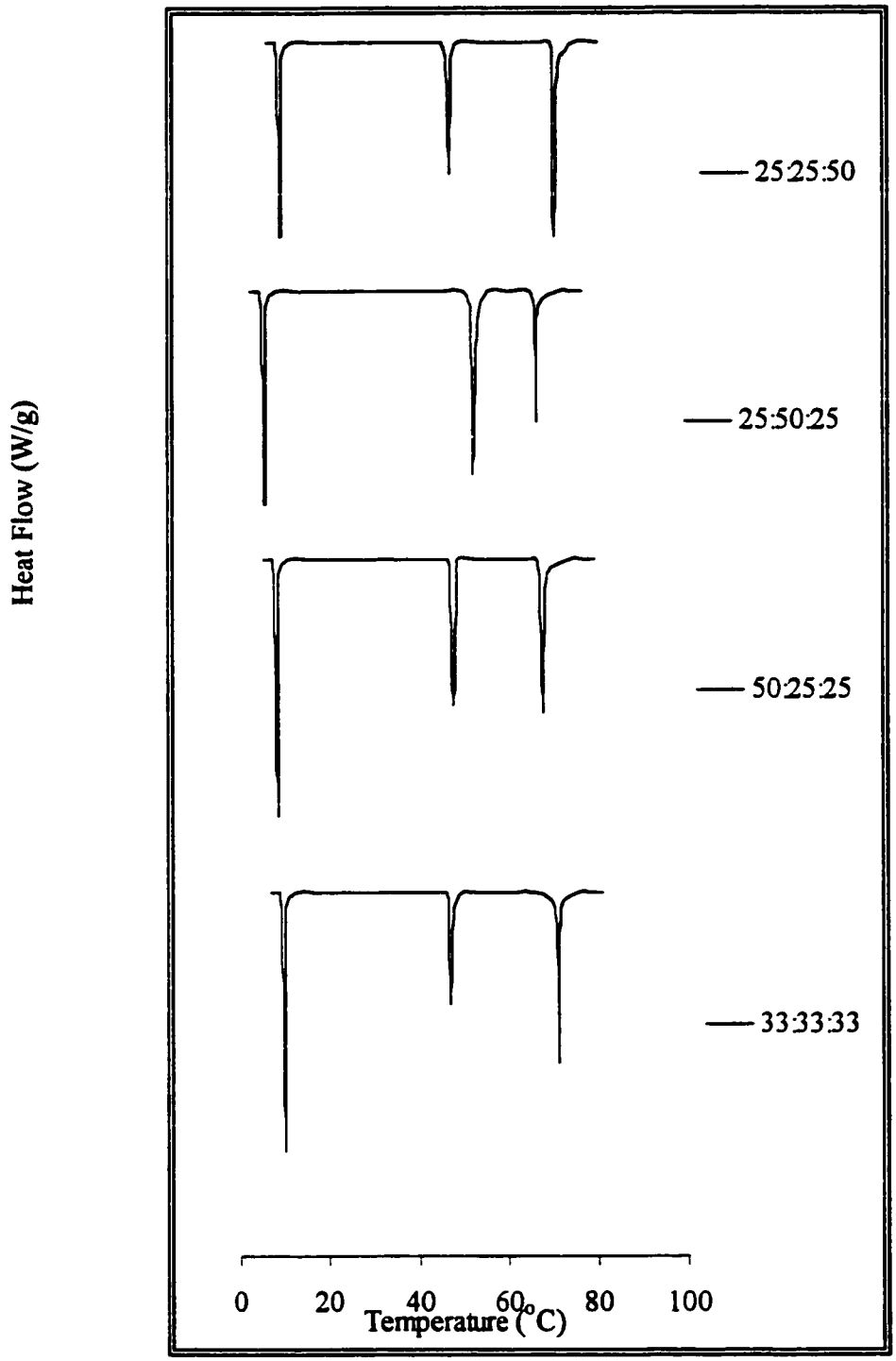

melting range was observed. Broadening of the low temperature peak is observed as the concentration of the high molecular component in the mixture increased. The height of that peak is constant through the range of concentrations.

Return to the base line of the high temperature peak, α peak, is presented as the melting temperature of this ternary system. The high temperature peak represents the solid-liquid transitions of C_{41}. Although the concentration of C_{41} in the mixture changed from 25% up to 50%, the melting temperature regardless of concentration remained almost the same, with the value of 75.3°C ± 0.7°C. Figure 5.2 represents the melting temperature of C_{41} as a function of concentration. The highest temperature of the melting peak was, as expected, observed for the highest concentration of C_{41} in the mixture. Although the concentration of C_{41} is the same for two samples of the mixture, 25%, different melting temperatures were measured for these two samples. The origin of this discrepancy lies in different concentration of C_{28} and C_{16} in the mixtures. Higher value of melting temperature was recorded for higher concentration of C_{28} in the mixture. Clarification of this can be found in capability of C_{41} to form mixed crystals with C_{28}.

The low temperature peak represents the eutectic temperature of this ternary mixture. This temperature is at the constant position on DSC thermograms regardless of the concentration. The temperature where the eutectic composition of the mixture started to form is 18.0°C ± 0.3°C. Figure 5.3 represents values of the low temperature peak as a function of concentration. The value of the eutectic temperate is 1°C lower than the melting temperature of the pure hydrocarbon of the shortest chain length, like the value of the binary eutectic temperature.

Figure 5.2 Melting temperature of C_{41} as a function of concentration of ternary mixture

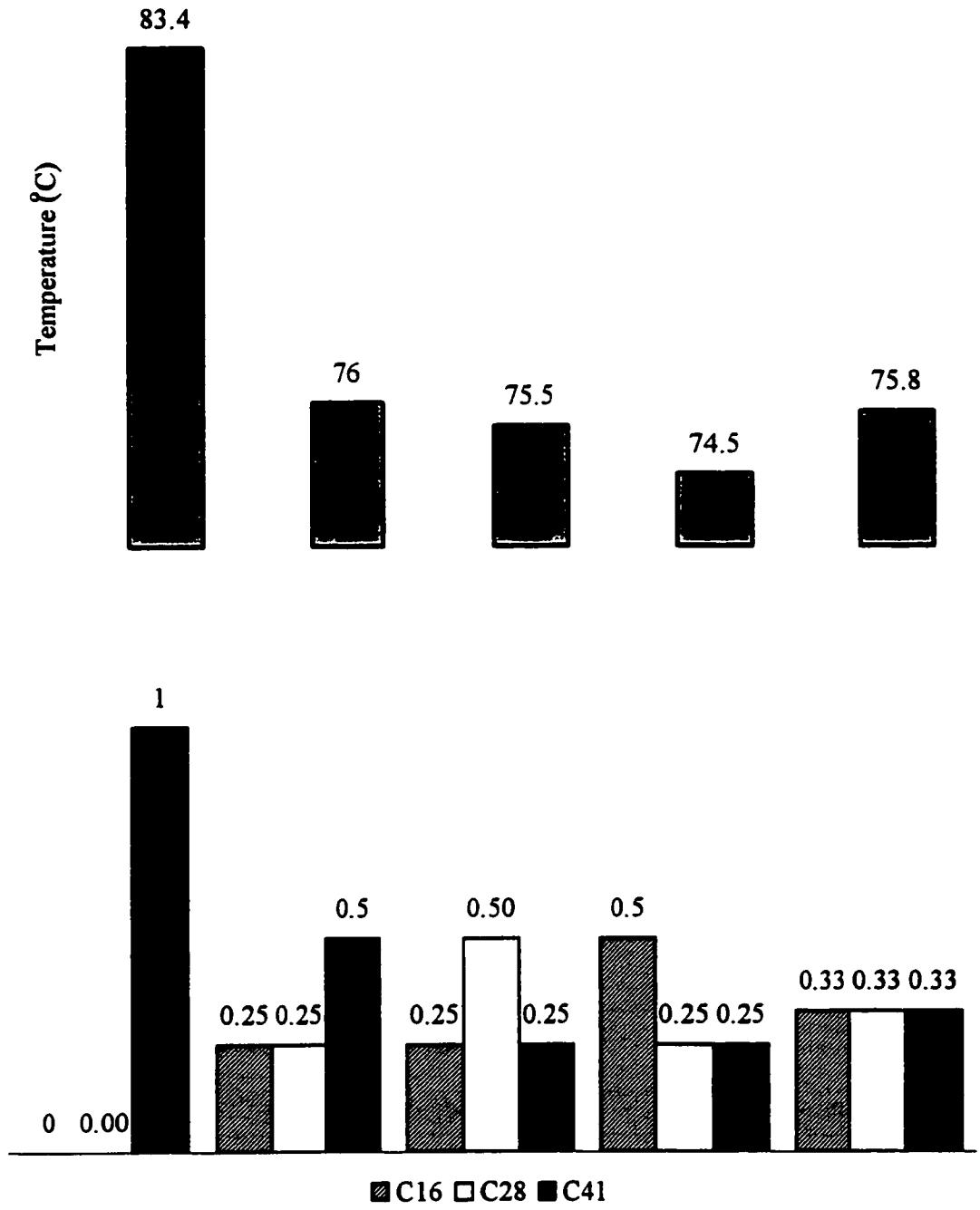

Figure 5.3 Melting temperature of C_{16} as a function of concentration of ternary mixture

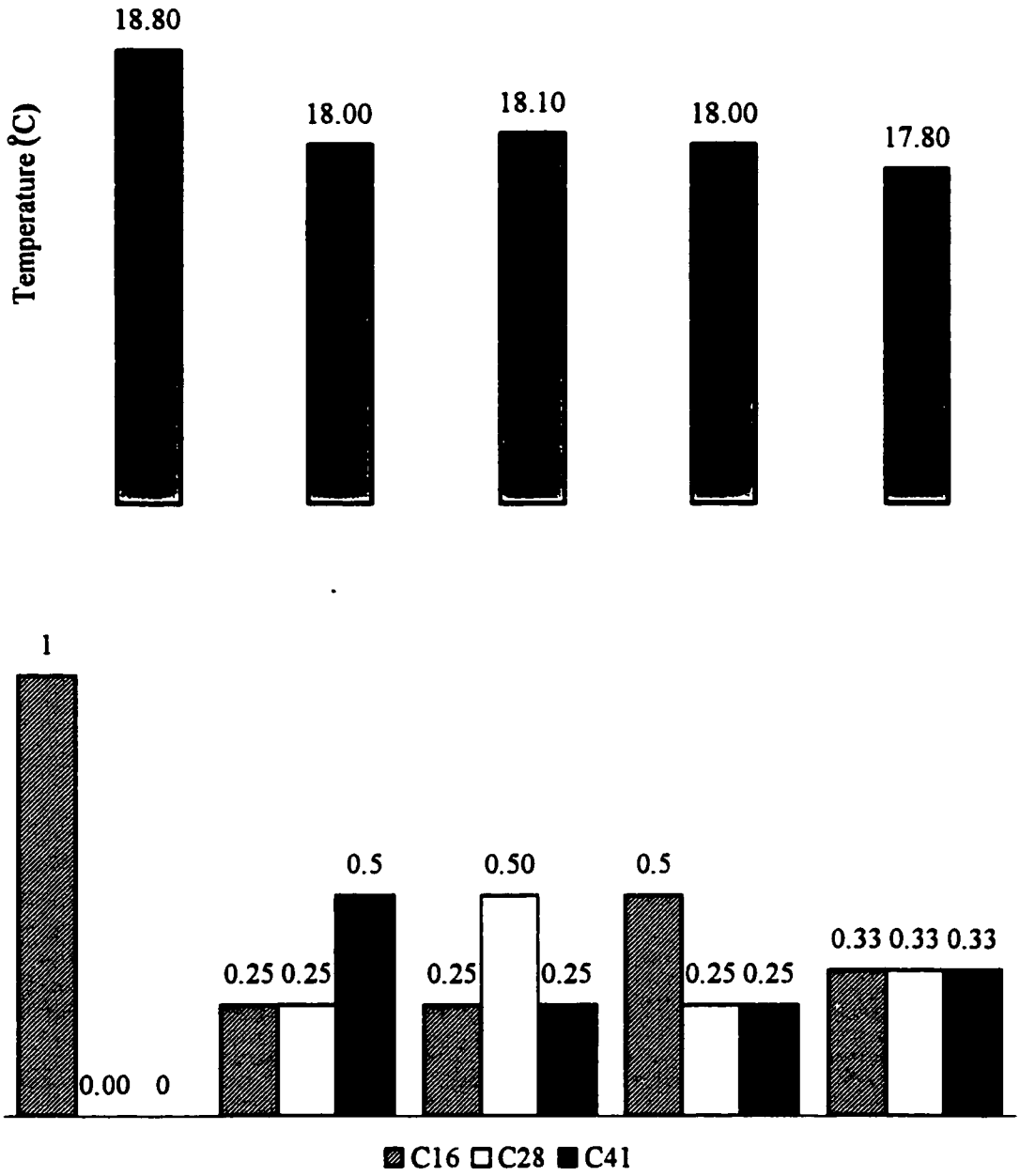

The second temperature peak, β peak, is the result of the presence of C_{28} in the mixture. The value of temperature of that peak shows the strongest dependence on the concentration of the mixture. Figure 5.4 presents the value of the second temperature peak associated with concentrations. The highest value of that peak is observed for the highest value of concentration of C_{28} in the mixture. As can be seen from Table 5.1 and Figure 5.4, the value of the second temperature peak depends not only on C_{28} concentrations but also on C_{16} and C_{41} concentrations. Similar to the case of C_{41}, there are two samples of C_{28} of the same concentrations, but different corresponding temperatures. Comparison of these two temperatures shows that a higher value was measured for the sample which had higher concentration of C_{41}. As mentioned earlier, the source of different temperature values for the sample of the same concentration of C_{28} rests in the formation of mixed crystals.

The difference between these two values is 4.5°C, a difference more significant than in the case of C_{41}, where the difference was 1°C. A larger difference is caused by the ability of C_{28} to form a mixed crystals both with C_{16} and C_{41}.

All these measurements of ternary mixtures support the conclusions from binary mixture measurements, formation of eutectic mixture, but also prove the existence of mixed crystals and some solubility in the solid state.

5.2 Experimental Phase Diagrams

The phase behaviour of the ternary mixture is presented on an equilateral triangular

Table 5.1 DSC experimental values of (T_m^E), T_β and T_E for C_{16}+C_{28}+C_{41} eutectic mixture obtained for heating rate of 1°C/min

S_{16}	S_{28}	S_{41}	$(T_m^E)^1$	T_β^2	T_E^3
1.00	0.00	0.00	18.8	-	-
0.00	1.00	0.00	62.9	57.7	-
0.00	0.00	1.00	84.3	-	-
0.24	0.25	0.51	76.0	53.4	18.0
0.25	0.49	0.26	75.5	62.0	18.3
0.50	0.24	0.26	74.5	49.0	18.0
0.34	0.32	0.34	75.8	52.6	18.0

[1] values corresponding to the return to the baseline of the high temperature exotherm

[2] value corresponding to the return to the base line of the second temperature exotherm

[3] values corresponding to the low temperature peak

Figure 5.4 Melting temperature of C_{28} as a function of concentration of ternary mixture

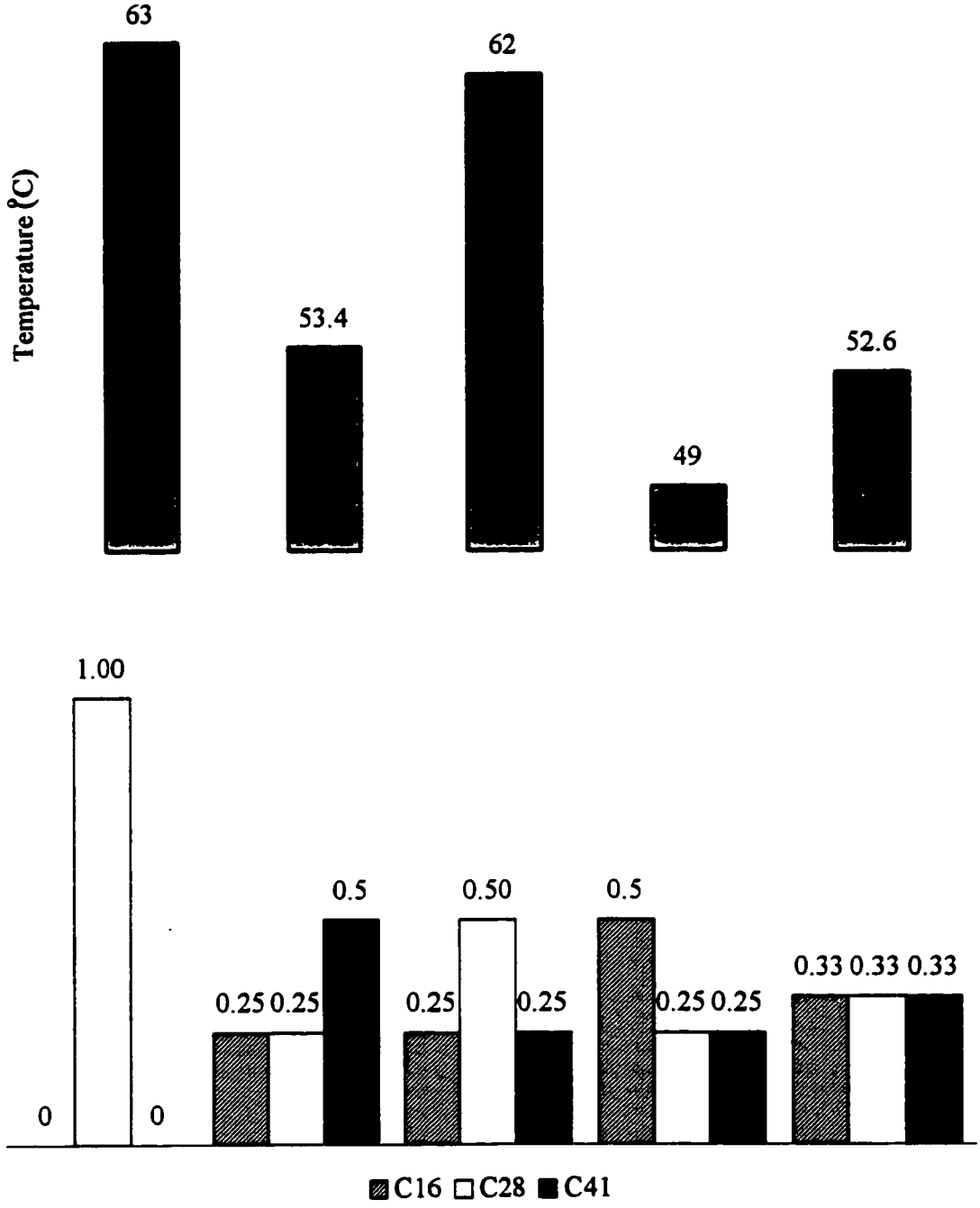

diagram. In general, the ternary phases diagrams apply to mixture of different components, but in this study they will be presenting one mixture at different temperatures. this approach is chosen in order to explain changes in the solid-liquid equilibrium. Figure 5.5 shows an effect of changing the temperature on the solid-liquid equilibrium in the mixture of C_{16}+C_{28}+C_{41}. All compositions plotted are mole fractions of C_{41} in the case of representing mixtures of C_{16}+C_{41} and C_{28}+C_{41}, and mole fractions of C_{28} in representation of C_{16}+C_{28} mixtures.

The phase diagram is based on the four different concentrations measured for ternary mixture and all measurements of binary mixtures.

First, we considered mixtures at 84.3°C, which is shown in Figure 5.5. Under these conditions there is no solid phase. This point is above the solidification temperature of all three components.

There is single liquid phase at all compositions at 76°C binary mixtures of C_{28} with C_{16}, but binary mixtures of C_{16} with C_{41} and of C_{28} with C_{41} exhibit solid-liquid equilibrium. The triangular diagram has solid region shade in the Figure 5.5. In all cases, the liquid phase is rich in C_{16} and C_{28}.

Figure 5.5 illustrates that at the higher temperatures, the shapes of the two-phase regions can change drastically in response to a relatively minor change of temperature. Between the temperatures 75.8°C and 75.5°C the amount of solid phase changes drastically although the temperature changes by just 0.2 °C or 0.5°C respectively.

However, if the temperature falls to 62°C, then the C_{41} and C_{28} binary mixture is a single-phase solid at all concentrations, while the C_{41}+C_{16} and C_{16}+C_{28} binary mixtures can still exhibit solid-liquid equilibrium. At this lower temperature, the ternary mixtures now

Figure 5.5 Effect of a change of temperature on the solid-liquid equilibrium in the mixture of C_{16}+C_{28}+C_{41}-experimental results

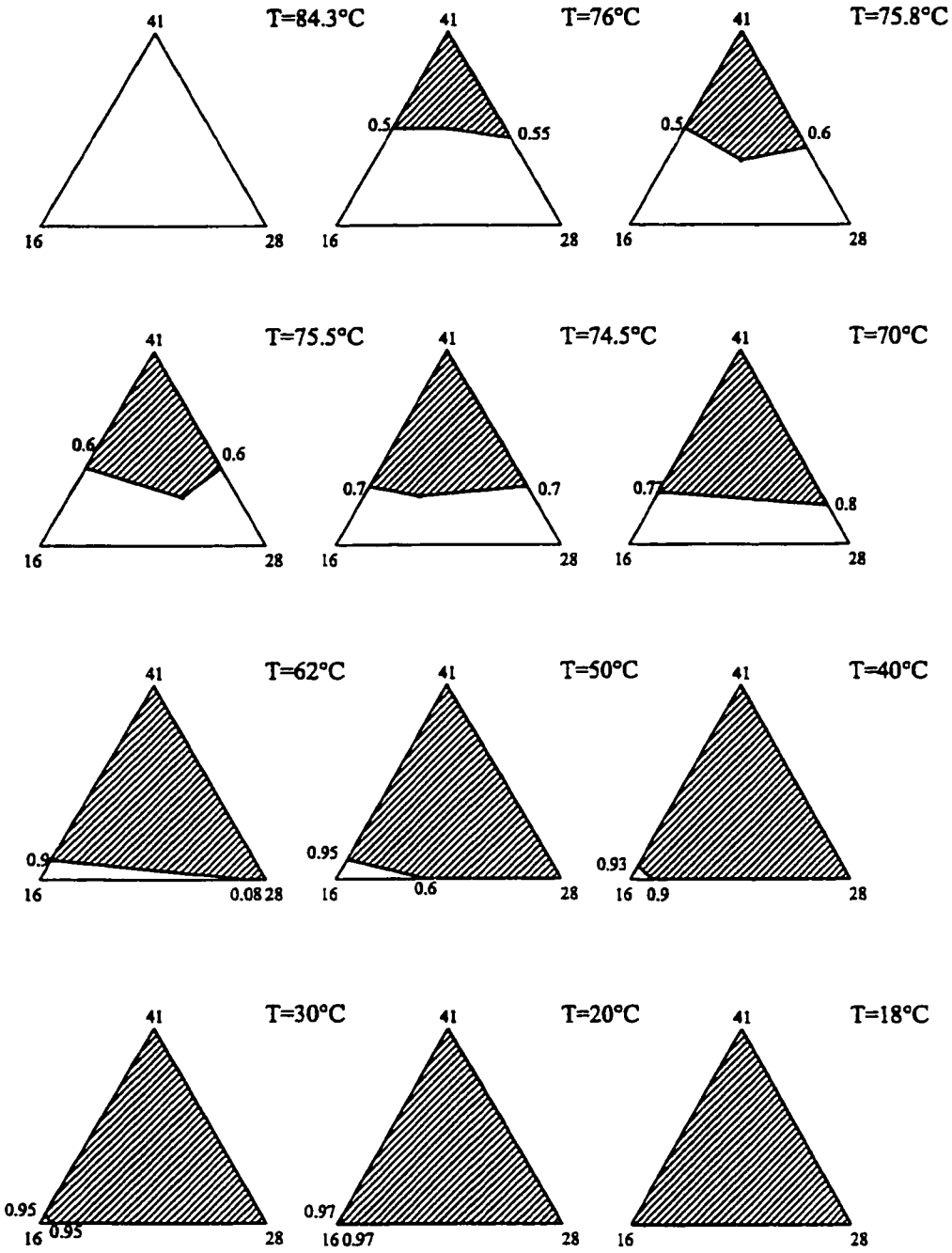

undergo solid-liquid phase transition over a larger region of the triangular diagram than they do at 76°C.

If we further consider decrease of temperature, at all temperatures below 62°C, the ternary diagram takes the simple form. A major temperature change produces limited change in the amount of solid formed and generally in solid-liquid equilibrium, as opposed to the high temperature region. Liquid phase is rich in C_{16} and it occurs until temperature reaches 18°C, at which all components appear in the solid phase.

5.3 Calculation based on the Ideal Solution Theory, Won's (1986) and Pedersen et al's (1991) Models

The methods of analysing the ternary immiscible system are practically the same as for the binary mixtures. The results of the thermodynamic calculations made on the ternary systems are tabulated in Table 5.2. Figure 5.6 shows the schematic representation of differences between the experimental value of temperature and temperature values predicted by models.

As can be seen from the all three models calculated the correct value of the temperature for pure alkanes. All models have the same trend in temperature prediction and overpredict the values of temperature. The temperature predictions from the ideal solution theory match the best in all cases except for the highest concentration of C_{41}

Table 5.2 Experimental and calculated equilibrium values of (T_m^E) for C_{16}+C_{28}+C_{41} eutectic mixture

S_{16}	S_{28}	S_{41}	$(T_m^E)^1$	$(T_m^E)_j$ calc[2]	Error[5] (°C)	$(T_m^E)_j$ calc[3]	Error[5] (°C)	$(T_m^E)_j$ calc[3]	Error[5] (°C)
1.00	0.00	0.00	18.8	18.8	0.0	18.8	0.0	18.8	0.0
0.00	1.00	0.00	62.9	62.9	0.0	62.9	0.0	62.9	0.0
0.00	0.00	1.00	84.3	84.3	0.0	84.3	0.0	84.3	0.0
0.24	0.25	0.51	76.0	79.8	3.8	79.4	3.4	80.1	4.1
0.25	0.49	0.26	75.5	75.7	0.2	75.8	0.3	78.6	3.1
0.50	0.24	0.26	74.5	75.3	0.8	75.5	1.0	78.4	3.9
0.34	0.32	0.34	75.8	77.4	1.6	79.0	3.2	79.4	3.6

[1] values corresponding to the return to the baseline of the high temperature exotherm

[2] values calculated using Equation 2.19

[3] values calculated using Equation 2.38 with solubility parameters from Won's (1986) model

[4] values calculated using Equation 2.38 with solubility parameters from Pedersen et al.'s (1991) model

[5] difference between experimental and calculated (T_m^E) values

Figure 5.6 Schematic representation of differences between the experimental value of temperature and temperature values predicted by models

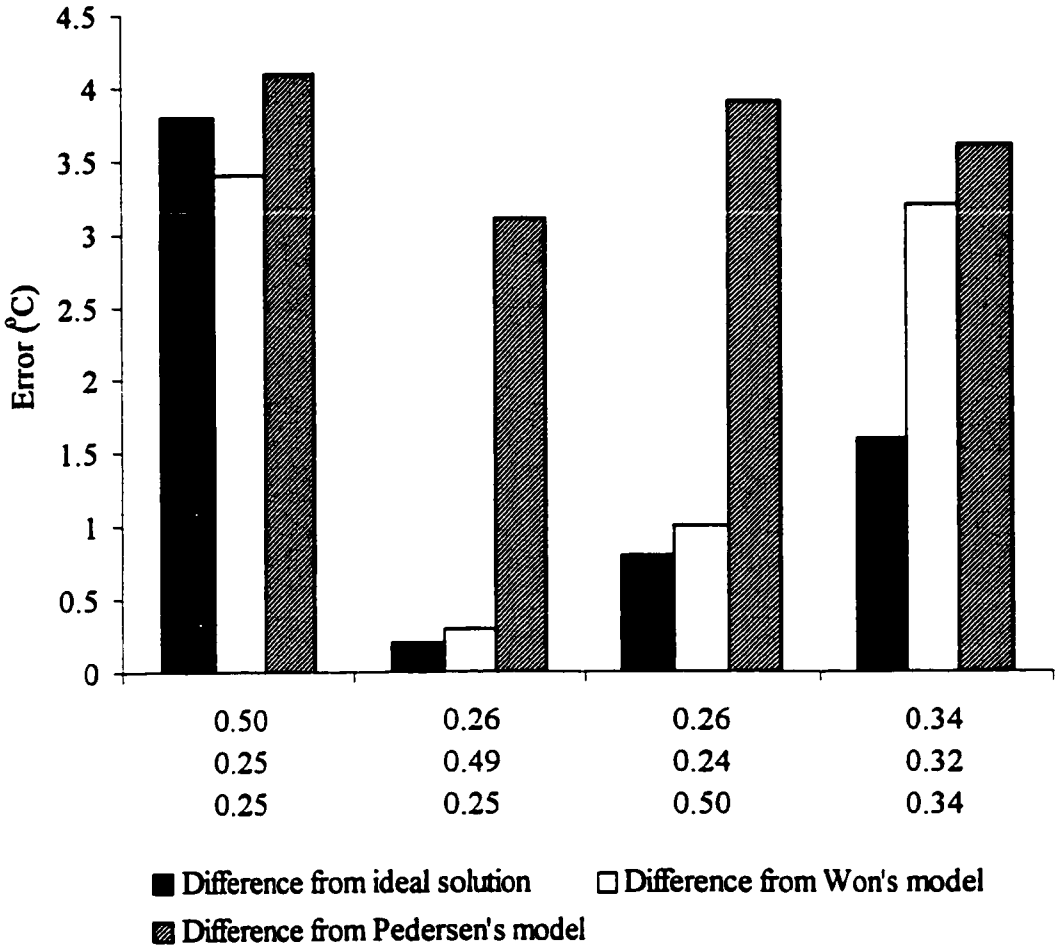

For that sample, Won's model gives better prediction, but the difference between these two is only 0.2°C. It can be concluded that the ideal solution theory gives overall the best estimation of the liquidus temperatures (within 3°C). As was indicated in Chapter 4 for binary mixtures, and supported the findings of Pauly et al. (1998), all models overestimate the solid appearance temperatures; nevertheless, this overestimation is only slight.

Figure 5.7 shows the effect of a change in temperature on the solid-liquid equilibrium calculated from ideal solution theory for mixtures of C_{16}+C_{28}+C_{41}. To show differences between the experimental value of solid-liquid equilibrium and values predicted by models, the same set of temperatures values was used as in Figure 5.5.

As can be seen the predictions of the model are as sensitive to temperature change as experimental results. Since the prediction of the model overestimate the appearance of the solid phase below 40°C the model predicts only small amount of liquid phase. The liquid phase exit but once presented in the diagram it is hardly noticeable.

From the presented result it can be concluded that the experimental result of binary mixture should be enough for modelling the thermodynamically behaviour of multicomponent mixture of paraffins.

Figure 5.7 Effect of a change of temperature on the solid-liquid equilibrium in mixture of C_{16}+C_{28}+C_{41} predicted by ideal solution theory

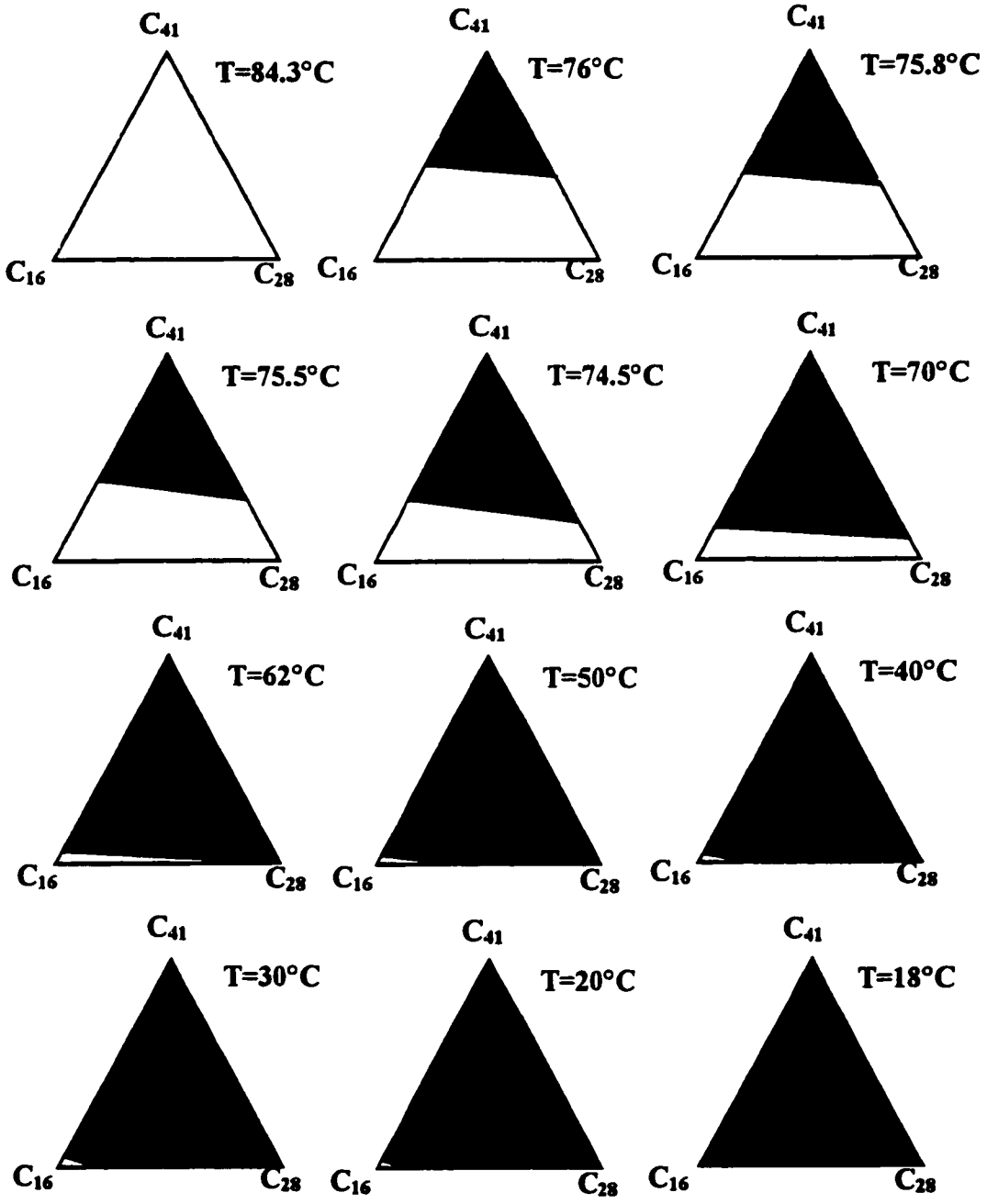

CHAPTER 6

SUMMARY OF RESULTS

There has been considerable interest in study of crystallization habits and thermal behavior of *n*-alkanes during the past decades. The studies of the nature and magnitude of the interaction between *n*-alkanes are both theoretical and practical.

The emphasis in this work was the examination of the effect of broad range in chain length difference between *n*-alkane forming the binary and ternary mixtures and obtaining more experimental points of various concentrations of the mixtures and to construct phase diagrams.

Differential scanning calorimetry measurements were completed in this study on three pure *n*-alkanes, their binary and ternary mixtures. The reproducibility of the recordings is within 1% as proved by comparing two different recorded thermograms of the same sample.

All DSC peaks for the low scan rate are small, but sharp. The melting or crystallization range for the scan rate of 1°C/min, is found to be very narrow, less than 1°C. An increase in the scan rate brings about an increase in the peak height, accompanied with an enlargement of the temperature range over which the peak occur, due to a deviation from thermodynamic solid-liquid equilibrium.

6.1 Pure n-Alkanes

The DSC thermograms of C_{28} exhibits two peaks, since all *n*-alkanes with the chain length between 20 and 40 are polymorphic. The high temperature peak represents the solid-liquid phase change. A solid-solid transition peak appears to be immediately below the melting point. C_{16} and C_{41} melt directly from the orthorhombic structure and transition is not seen.

The effect of the scan rate was measured on the identical samples of C_{16}, C_{41} and C_{28} at heating and cooling rates of 1, 3, 5, and 7°C/min, respectively. The DSC thermograms show shifts to the higher temperature as the heating rate increases. Effect of supercooling can be seen as the temperature peaks shift noticeably to lower temperature as the cooling rate increases. The solid-solid transitions were found to occur without much supercooling or superheating.

The experimental melting temperatures versus scan rate were examined. The linear trend was found to correspond to the given set of experimental data. An interesting feature is that the melting and cooling curves when extrapolated to the zero cooling or heating rate were found to not correspond to the same temperature for each *n*-alkane. This conclusion is in agreement with Gimzewski and Audley (1993) who found that at a scan rate lower than 1°C/min the curve rises steeply for cooling experiments, and falls steeply for heating runs. Because of that phenomenon, equilibrium condition can not be reached even at the scan rate of 0.01°C/min.

A conclusion from Hammami's study was confirmed that the peak difference between melting and solid-solid transition peak is constant for particular paraffins as a function of the number of carbon atoms in the molecules, but not on the scan rate.

6.2 Binary Mixtures

When *n*-alkanes are mixed together they can form three different systems; solid solution, partially miscible, or eutectic systems. The tendency to form a particular type of mixture was shown by Hammami (1994) to depend not only on the disparity in their chain length between two *n*-alkanes and crystal structure similarity of the pure components, but also on the thermal method of sample preparation and preconditioning.

The difference between the chain length of *n*-alkanes forming the binary mixtures examined in this work was too immense; therefore the chain length difference was the dominant factor compared to the other two factors governing the formation of immiscible system.

DSC measurements were made on three binary *n*-alkane systems: C_{16}+C_{28}, C_{16}+C_{41} and C_{28}+C_{41} with the scan rate of 1°C/min.

The phase diagrams have been constructed from DSC heating thermograms. To construct the phase diagrams the convention of Smith and Penning (1974) was used, i.e. the peak temperatures for the lower melting endotherms and the return to the baseline temperature for the higher melting endotherms. All phase diagrams plotted from DSC scans of all three *n*-alkane mixtures reveal a stable eutectic behavior. This study confirms that all eutectic mixtures studied melt within one degree of the pure hydrocarbon of shorter chain length; the eutectic mixtures usually contain about 95% of the shorter paraffin (Mazee, 1949, 1957; Butler and MacLeod, 1961).

Experimental results of all DSC measurements were compared with existing thermodynamically models; ideal behavior theory, regular solution theory, Won's model (1986), Pedersen et al's model (1991).

An " ideal" eutectic mixture presupposes the existence of complete insolubility between the two components at all concentration. Two out of three binary mixtures (C_{28}+C_{16} and C_{28}+C_{41}) were found to be non-ideal type and show evidence of partial solubility in the solid state and formation of mixed crystals.

In the C_{16}+C_{28} mixture, the temperature for the solid-solid transition peak remains practically unchanged, appears to be independent of the composition, and remains the same value as for pure C_{28}. From this evidence it can be concluded that the miscibility does not occur in the solid state over the concentration range of 0% up to 40% of C_{16}. At higher concentrations of C_{16}, solubility in the solid state occurs.

It can be concluded that since both C_{41} and C_{16} form the solid phase independently, each component has the crystalline form characteristic of its behavior as a pure component. Because a large difference in the chain length between C_{16} and C_{41}, the mixture are ideal eutectic. The difference between experimental results and prediction of ideal solution theory around eutectic temperature can be probably explained by the fact that during the crystallization, the small molecule of C_{16} is trapped by C_{41} during the simultaneous solidification.

The regular solution theory describes deviation of the mixture from the ideal behaviour. The non-ideality is caused mainly due to the non-zero heat of mixing. Empirical interaction parameter, ρ_o, is proposed to calculate the heat of mixing; however the calculated temperatures are not very sensitive to the adjustable parameter. This conclusion is based on the calculation in which two different values of ρ_o were applied; 20% larger and smaller than the optimum value of the ρ_o.

Both Won's and Pedersen et al.'s model are based on regular solution theory of mixtures as well on equation on state. Both models give nearly the same values of solubility parameters in liquid phase throughout the range of carbon numbers. The variation is greater in the value of the solid phase solubility parameters predicted by Won, and Pedersen. Pedersen's correlation gives 70% higher values for solid phase solubility, than those predicted by Won.

All models overestimate the solid appearance temperatures; nevertheless, this overestimation remained only slight.

From calculation and comparison between experimental date and models predictions for the eutectic systems done in this study, the following can be concluded:

All models are found to be highly responsive to the change of components forming the mixture and predict the melting temperature accurately for at least one particular mixture. One single model that would be suitable for prediction of the phase change temperature for any eutectic mixture can not be recommended.

Equilibrium calculation of eutectic systems selected in this study indicates the presence of non-ideal behavior for these systems. The non-ideality is particularly significant around the eutectic composition and temperature, where instead of the formation of two separate solid systems, formation of mixed crystals occurs.

In the present study three binary mixtures of *n*-alkanes were studied. For each mixture the experimental results were compared with predictions from regular solution theory. The empirical parameter, ρ_o, was proposed for each mixture. By adjusting the value of ρ_o the best fit of theory prediction and experimental data was achieved. Analysis of five values

of empirical parameter, ρ_o, was done. The empirical parameters were fitted to the following correlation:

$$\rho_0 = 0.706 + \frac{19.70}{\Delta n}$$

6.3 Ternary Mixture

Four samples of ternary mixture were studied. All thermograms exhibit three peaks. The thermograms of the C_{16}+C_{28}+C_{41} mixture retained practically all general characteristics of pure *n*-alkanes and look like superposition of thermogram of pure alkanes forming the ternary mixture.

The value of temperature peaks of C_{28} and C_{41} depend not only on their concentrations but also on the concentration of the two remaining *n*-alkanes in the mixture. There were two samples with the same C_{28} and C_{41} concentrations, which yielded different corresponding temperatures. Comparison of these two temperatures shows that a higher value measured for sample with a higher concentration of *n*-alkane with higher melting temperature. The source of different temperature values for the sample of the same concentration is the formation of mixed crystals. The difference between these two values is 4.5°C for C_{28}, a difference much larger than in case of C_{41} where difference was 1°C. A larger difference is caused by the ability of C_{28} to form mixed crystals both with C_{16} and C_{41}.

All the measurements with ternary mixtures support the conclusions from binary mixture measurements, i.e. formation of eutectic mixture, but existence of mixed crystals and some solubility in the solid state.

Measurement of four different concentrations of ternary mixtures allowed analysis of immisciblity. The solid-liquid equilibrium at high temperatures can change drastic ally response to a relatively minor change of temperature, and in the low temperature range major temperature change produces limited response in amount of formed solid.

Comparison between experimental data and prediction from thermodynamic model were done in this study for ternary mixture forming eutectic system. All models overestimate the solid appearance temperatures. The predicted values from ideal solution theory meets values of temperate the best.

From the results presented it can be concluded that the interaction between n-alkanes are the same in the binary compared to the ternary mixture. Hence the experimental result of binary mixture should be enough for modelling the thermodynamically behaviour of multicomponent mixture of paraffins.

CHAPTER 7

CONCLUSION AND RECOMMENDATION FOR FUTURE WORK

7.1 Conclusions

Results obtained by DSC verify that the technique, as a method of thermal analysis, is a sufficiently accurate tool for investigating *n*-alkanes interaction. Although the melting points determined by the DSC technique may deviate slightly from the equilibrium values, good agreement in obtained between the experimentally determined melting point of the binary and ternary mixtures of *n*-alkanes and values calculated from thermodynamic equations.

Repeatability of the DSC measurements was very good in terms of the heat flow amounts, shape, size, and location of the peak for cooling and heating thermograms. It can be concluded that the analysis of DSC heat flow rate measurements is a useful tool to support phase diagram investigation in complex systems.

The present study of thermal behavior of three different *n*-alkanes allowed the conformation of different phase transitions presented in earlier studies (Hammami, 1994; Turner, 1971; Broadhurst, 1962b, Srivastava et al., 1993). Pure normal alkanes with chain length between 20 and 40 carbon atoms are known to exhibit a transition from orthorhombic to hexagonal crystal structure upon heating, while *n*-alkanes with chain length outside this range melt directly from the orthorhombic structure (i.e. a transition is not seen).

The effect of scan rate on the peak temperature was studied. The DSC thermograms show shifts to the higher temperature as the heating rate increases. Effect of supercooling can be seen as the temperature peaks noticeably shift to lower temperature, as the cooling rate increases. Solid-solid transition was found to occur without much supercooling or superheating.

The results of various temperature scan rates on the melting and crystallization temperatures show that a linear trend is obtained in both cases. This conclusion is in agreement with the work of Gimzewski and Audley (1993) where at the scan rate lower than 1°C/min the curve rises steeply for cooling experiments, and decline steeply for heating runs. Due to that phenomenon and apparatus limitation, with the lowest scan rate of 1°C/min, extrapolating the melting temperature to the zero scan rate could result in inaccurate values.

The peak-to-peak temperature difference, in the case of C_{28}, is independent of the cooling or heating rate. This conclusion is supported by Hammami's study (1994) where he discovered that the peak to peak difference between melting and solid-solid transition peak is constant for a particular paraffin; it varies as a function of the number of carbon atoms in molecules, but not with the scan rate.

The tendency to form a particular type of mixture was shown by Hammami (1994) to depend not only on the disparity in their chain length between two *n*-alkanes and crystal structure similarity of the pure components, but also on the thermal method of sample preparation and preconditioning.

The analysis of binary mixtures examined, prepared from *n*-alkanes with large differences in chain length, showed that all three mixtures form eutectic systems. This

observation led to the conclusion that a large difference in chain length is the governing factor for forming immiscible system.

In cases where C_{28} was one of the components of the binary mixture, there was an appearance of the solid-solid transition peak. The location of those temperature peaks remained constant regardless of the mixture composition. This indicates that over the concentration range, where solid-solid transition is detected, the miscibility does not occur in the solid state at all. For the specific case of C_{28}+C_{16} mixture, increasing the concentration of C_{16} significantly reduced the melting temperature of the mixture; the melting peak overlaps the solid-solid transition peak, making it difficult to obtain the correct value of the onset temperature.

Results of prediction of melting temperature obtained from ideal, regular solution theory and the models of Won (1986) and Pedersen et al. (1991) show the same trend. All activity coefficient models overestimate the solid appearance temperature; nevertheless, this overestimation is only slight. Agreement between experimental data and model predictions is not always very good, especially around the eutectic composition and temperature; a fact pointing to a complex non-ideal behavior of mixtures, where instead of the formation of two separate solid phases, formation of mixed crystals occurs.

The study of solidification curves shows that Won's model and ideal solution model lead to similar prediction. These results come from the values of regular activity coefficients, which are nearly similar in both phases. Actually, all these models, which are based on the assumption that heavy components precipitate in one solid solution, predict that all components are presented in the solid bulk, whereas the measurements show that light components do not precipitate at the solid appearance temperature.

For the binary mixture C_{16}+C_{28}, Pedersen et al.'s model gives the best prediction, for the C_{16}+C_{41} mixture ideal solution theory matches the experimental results the best, and for the C_{28}+C_{41} mixture in different concentration ranges the regular solution theory and Pedersen et al.'s model fit experimental data well.

From all this evidence, recommendation of one convenient thermodynamic model for predicting value of the solid formation temperature for eutectic mixture would not be appropriate.

Four different mixture compositions were examined for the ternary mixture. The behavior of the mixture is found to be eutectic and all DSC thermograms show the presence of three peaks. All thermograms appear to be superposition of the thermogram of pure *n*-alkanes forming the ternary mixture. The values of high temperature peak do not depend only on concentration of C_{41}, but also on concentration of two other alkanes in the mixture, a fact pointing to formation of mixed crystals. The largest variation in temperature is observed for the middle temperature peak, that appeared as a result of the presence of C_{28} in the mixture, because C_{28} can form mixed crystals both with C_{16} and C_{41}.

As was indicated for binary mixture and supported by finding of Pauly et al. (1998, all models overestimate the solid appearance temperatures. Ideal solution theory gives the best estimation of the liquidus temperatures (±3°C) of the tested mixtures.

7.2 Recommendation For Future Work

Most crude oils and even some gas condensates have an amount of heavy paraffinic molecules dissolved under reservoir, production and pipeline transport conditions. Project which would be investigate the effect of pressure on precipitation of solid *n*-alkanes, would be useful because the pressure effects increase as drilling and production advance. A way to getting an understanding of the conditions leading to the precipitation of solid paraffins study where the construction of the *p-T* diagram of mixtures under operating conditions would be major element. Beside the effect of pressure, the effect of shear rate and temperature should be explored on wax formation in crude oils.

In order to extend this thermal behavior study, it is important to continue to collect the experimental data for mixtures containing methane and heavy components like polyaromatics, polynaphtenics and naphteno-aromatics. These data would be useful for comparison of some available models to calculate solid-liquid-vapor equilibrium.

Studies of thermal behavior of typical commercial waxes would be beneficial from a practical point, because the first thing that a consumer does after receiving a shipment of waxy materials is to melt them. After processing, the final product is cooled and allowed to crystallize.

A study of the solubility of binary multicomponent mixtures of *n*-alkanes in different organic solvents would also be important from practical and theoretical point. The data could be useful for thermodynamic modeling of wax deposition in pipelines and reservoirs.

Studies for the effects various additives and inhibitors (called the pour point depressants), on wax formation and deposition under typical processing conditions will be very important from industrial operating standpoint.

Studies of three-phase behavior of *n*-alkanes with the broad range of the chain length would be interesting as theoretical perspective not only for oil industry but also for polymer productions.

CHAPTER 8

REFERENCE

Asbach, G. I., Kilian, H.G., Stacke, F., *Coll. Polym. Sci, 260*, 151 (1982)

Asbach, G. I., Kilian, H.G., *Polymer, 32*, 3006 (1991)

Askeland, D.R., *"The Science and Engineering of Materials"*, Wadsworth Inc., Belmont, CA (1984)

Bhat, N., V., *"Phase Transformation and Crystallization of Paraffin mixtures under Non-Isothermal Condition"*, MSc Thesis, Univ. of Calgary, Calgary, Alberta (1996).

Broadhurst, M. G., *J. Res. Natl. Bur. Stand. Sec. A, 66*, 241, (1962a)

Bucaram, S. M., *J. Pet. Tech., 19*,150, (1967)

Butler, R. M., MacLeod, D. M., *Can. J. Chem. Eng., 39*, 53, (1961)

Carnahan, N. F., *SPE Technol. Today, 1024* (1989)

Chevallier, V., Petitjean, D., Bouroukba, M., Dirand, M., *Polymer, 40*, 2129 (1999)

Countinho, J. A. P., Andersen, S. I., Stenby, E. H., *Fluid Phase Equlibria., 117*, 138 (1996)

Countinho, J. A. P., Meray, V., *Fluid Phase Equlibria., 148*, 147 (1998)

Daniel, V., *Advan. Phys., 2*, 450, (1953)

Denicolo, I., Craievich, A. F., Doucet, J., *J. Chem. Phys., 80*, 12 (1984)

Dirand, M., Achour, Z., Jouti, B., Sabour, A., Gachon, J.C., *Mol. Crys. Liq. Cryst., 275*, 293 (1996)

Dirand, M., Chevallier, V., Provost, E., Bouroukba, M., Petitijean, D., *Fuel, 77*, 12

(1998)

Dollhoph, W., Grossmann, H. P., Leute, U., *Coll. Polym. Sci., 259*, 267, (1981)

Dorset, D. L., *Macromolecules, 18*, 2158 (1985)

Dorset, D. L., *Macromolecules, 19*, 2965 (1986)

Dorset, D. L., *Macromolecules, 20*, 2782 (1987)

Dorset, D. L., Hanlon, J., Karet, G., *Macromolecules, 22*, 2169 (1989)

Espeau, P., Robles, L., Cuevas-Dirate, M. A., Mondieig, D., Haget, Y., *Material Research Bulletin, 31*, 10, (1996)

Etessam, A. H., Sawyer, M. F., *J. Inst. Petrol., 25*, 253, (1939)

Evans, U. R., *Trans. Faraday Soc., 41*, 365, (1945)

Faust, H. R., *Thermochimica Acta, 26*, 383, (1978)

Flory, P. J., *"Principles of Polymer Chemistry"*, Cornell University Press, New York (1953)

Flory, P. J., Vrij, A., *J. Am. Chem. Soc., 85*, 3548, (1963)

Garner, W. E., Madden, F. C., Rushbrooke, J. E., *J. Chem. Soc.*, 2491, (1924)

Garner, W. E., Bibber, K. V., King, A. M., *J. Chem. Soc.*, 1533, (1931)

Giavani, C., Pochetti, F., *J. Therm. Anal., 5*, 83, (1983)

Gimzewski, E., Audley, G., *Thermochim. Acta., 214*, 149, (1993)

Gugenheim, E. A., " *Mixture*", Oxfor University Press, New York (1952)

Hammami, A., Mehrotra, A. K., *CSChE Annual Meeting*, Toronto, (1992a)

Hammami, A., Mehrotra, A. K., *Thermochimica Acta, 211*, 137 (1992b)

Hammami, A., Mehrotra, A. K., *Thermochimica Acta, 215*, 197 (1993)

Hammami, A., Mehrotra, A. K., *Fuel, 74*, 96 (1995a)

Hammami, A., Mehrotra, A. K., *Fluid Phase Equilib., 111*, 253 (1995b)

Hammami, A., Mehrotra, A. K., *Fuel., 75*, 4 (1996)

Hammami, A., "*Thermal Behavior and Non-Isothermal Crystallization Kinetics of Normal Alkanes and Their Waxy Mixtures Under Quiescent Conditions*", Ph.D. dissertation, University of Calgary, Calgary, Alberta (1994)

Hsu, E. C. H., Jonson, J. F., *Mol. Cryst. Liq. Cryst., 27*, 95 (1974)

Kitaigorskii, A. I., "*Organic Chemical Crystallography*" Consultants Bureau, New York (1961)

Kitaigorskii, A. I., Mnyunkh, Y. V., Asadov, Y. G., J. *Phys. Chem. Solids, 26*, 463 (1965)

Letoffe, J. M., Claudy, P., Kok, M. V., Garcin, M., Volle, J. L., *Fuel, 74*, 6 (1995)

Lee, A. G., *Biochim. Biophys. Acta, 472*, 285 (1977)

Lee, A. G., *Biochim. Biophys. Acta, 507*, 433 (1978)

Mandelkern, L., Flory, P. *J., J. Am. Chem. Soc., 73*, 3206 (1951)

Marconnelli, M. Q. S. P., Strauss, H. L., Snyder, R. G., *J. Am. Chem. Soc., 104*, 6237 (1985)

Marconnelli, M. Q. S. P., Strauss, H. L., Snyder, R. G., *J. Phys. Chem., 89*, 5260 (1985)

Matlach, W. J., Newberry, M. E., *SPE 1151, Rocky Mounting Regional Meeting*, Salt Lake City, UT, (1983)

Matheson, R. R., Smith. P., *Polymer, 26*, 288 (1985)

Mazee, W. M., *Recueil, 67*, 197 (1948)

Mazee, W. M., *J. Inst. Petrol., 35*, 97 (1949)

Mazee, W. M., *Anal. Chim. Acata, 17*, 97 (1957)

Mnyukh, Y. V., *Zh. Struct. Chem., 1*, 370 (1960a)

Nechitailo, N. A., Topshiev, A. V., Rosenberg, L. M., Terentiva, E. M., *Zh. Fiz. Khim., 34*, 1268 (1960)

Onoe, K., Hoshi, A., Shimazaki, T., Yamaguchi, T., Toyokura, K., *Acta Polytechnic. Scandinavica, 244*, 114 (1997)

Pauly, J., Dauphin, C., Daridon, J. L., *Fluid Phase Equilibria, 149, 191 (1998)*

Pechold, W., Dollhopf, W., Engel, A., *Acustica, 17*, 61 (1966)

Pedersen, K.S., Skovborg, P., Rønningsen, H. P., *Energy & Fuels, 5*, 924 (1991)

Phipps, L. W., *Trans. Farsday Soc., 60*, 1873 (1964)

Piper, S. N., Chinall, A. C., Hopkins, S. J., Pollard, A., Smith, J. A. B., *Biochem. J. 25*, 2072 (1931)

Prime, R., Wunderlich, B., *J. Plym. Sci.*, A-2, 7, 2073 (1969)

Reid, R. C., Prausnitz, J. M., Sherwood, T. K., " *The Properties of gases and Liquids*" 3rd Ed., Mc Graw-Hill Book Company, New York (1977)

Roberts, D. E., Mandelkern, L., *J. Am. Chem. Soc., 77*, 781 (1955)

Royaud, I. A. M., Hendra, P. J., Maddams, W., Passingham, C., Willis. H. A., *J. Mol. Struct., 239*, 83 (1990)

Scahaerer, A. A., Busso, C. J., Smith. A. E., Skinner, L. B., *J. Am. Chem. Soc., 77*, 2017 (1955)

Seyer, W. F., Patterson, R. F., Keays, J. L., *J. Am. Chem. Soc., 66*, 179 (1944)

Smith, J. C., *J. Chem. Soc., 732* (1932)

Smith, H. M., Bureau of Mines, (1968)

Smith, P., Pennings, A. J., *Polymer, 15*, 413 (1974)

Smith, P., Pennings, A. J., *J. Mater. Sci., 11*, 1450 (1976)

Smith, P., Pennings, A. J., *J. Polym. Sci. Polym.Phys. Ed., 15*, 523 (1977)

Srivastava, S. P., Handoo, J., Agrawal. K. M., Joshi, G. C., *J. Phys. Chem. Solids, 54*, 639 (1993)

Srivastava, S. P., Saxena, A. K., Tandon, R. S., Shekher, V., *Fuel, 76*, 625 (1997)

Stolk, R., Rajabalee, F., Jacobs, M. H. G., Espeau, P., Mondieig, D., Oonk, H. A. J., Haget, Y. *Calphad, 3*, 401 (1997)

Turner, W. R., *Ind. Eng. Chem. Prod. Res. Dev., 10*, 238 (1971)

Ungar, G., *J. Phys. Chem., 87*, 689 (1983)

Ungar, G., J. Masic, N., *J. Phys. Chem., 89*, 1036 (1985)

Uneger, P., Faissat, B., Leibovici, C., Zhou, H., Behar, E., Moracchini, G., Courcy, J. P. *Fluid Phase Equilib.*, 111, 287 (1995)

Wesolowski, M., *Themochim. Acta., 46*, 21 (1981)

Won, K. W., *AIChE Spring National Meeting, Houston*, TX, Paper 27A (1985)

Won, K. W., *Fluid Phase Equilib., 30*, 265 (1986)

Won, K. W., *Fluid Phase Equilib., 53*, 377 (1989)

Wunderlich, B., "*Macromolecular Physics*" vol.3, Academic Press, New York (1980)

Wunderlich, B., *Thermochimica Act 212*, 131 (1992)

APPENDIX

CALCULATION FOR DATA PROCESSING

A.1 Calculation

Differential scanning calorimetry (DSC) is a thermal analysis technique in which a sample and reference are both maintained at the temperature pre-determined by the program even during a thermal event in the sample. The amount of energy that has to be supplied to or withdrawn from the sample to maintain zero temperature differential between the sample and the reference is an experimental parameter displayed as the ordinate of the thermal analysis curve.

The measurement signal, U, is recorded in μV. The calorimetric constant, sensitivity $E(T)$ is determined by calibration with standard material, indium, undergoing a known enthalpy change. The unit for $E(T)$ is μV/ mW. It is a measure of the number of μV required for a heat flow to the sample of 1mW. Therefore, the heat flow per unit mass to the sample Q at any time can be calculated by:

$$Q = \frac{U}{E(T) \cdot m} \qquad \text{A.1}$$

where m is the sample mass (in mg) and T is temperature (°C).

By integration, the enthalpy change of sample can be calculated from:

$$\Delta H = \frac{\int U dt}{E(T) \cdot m} \qquad \text{A.2}$$

where ΔH is the enthalpy change of the sample (in mJ) and t is time. $E(T)$ can be resolved into a temperature dependent and temperature independent component according to:

$$E(T) = E_{\ln} \cdot E_{rel} \qquad \text{A.3}$$

where E_{ln} is value of E at 156.6 °C, the melting point of indium, and dertermined durring calibration. E_{rel} is function of temperature and is determined by the material and design of apparatus. E_{rel} can be detremined using equqtion:

$$E_{rel} = A + BT \qquad \text{A.4}$$

where A is 1.078 and B is -5.12×10^{-4}.

After E_{ln} is found thruogh calibration, the haet flow in mW/mg can be calculating using:

$$Q = \frac{U}{E_{rel} \cdot E_{\ln} \cdot m} \qquad \text{A.5}$$

A.2 Data Processing

The apparatus software presents the data in the graphical form, and data files are in machine language format. Each measurement file contains information about the mass of the sample, calorimetric sensitivity, temperature and measured signal. The following procedure written in Basic program was used to convert data from calorimetric measurements to Excel spreadsheet.

Every line of the data contains four entrees. Line from 1 to 37 contains three entrees of zero and the constant occurs in just one of the four columns. Calorimetric sensitivity occurs in the third line, and mass of the sample in the fourth line.

The experimental values of temperature and measurement signal are obtained from line 38. These two values are always recorded consecutively. Two other columns are zero, and measurement values were extracted by identification of non-zero product value.

Some data files obtained from measurements were very large and selecting each n^{th} does reduction, where n is an integer number.